

Materials Reliability Program Crack Growth Rates for Evaluating Primary Water Stress Corrosion Cracking (PWSCC) of Alloy 82, 182, and 132 Welds (MRP-115NP)

1006696

Final Report, November 2004

NON-PROPRIETARY INFORMATION

NOTICE: This report contains the non-proprietary information that is included in the proprietary version of this report. The proprietary version of this report contains proprietary information that is the intellectual property of MRP utility members and EPRI. Accordingly, the proprietary versions are only available under license from EPRI and may not be reproduced or disclosed, wholly or in part, by any Licensee to any other person or organization.

**EPRI Project Manager
J. Hickling**

DISCLAIMER OF WARRANTIES AND LIMITATION OF LIABILITIES

THIS DOCUMENT WAS PREPARED BY THE ORGANIZATION(S) NAMED BELOW AS AN ACCOUNT OF WORK SPONSORED OR COSPONSORED BY THE ELECTRIC POWER RESEARCH INSTITUTE, INC. (EPRI). NEITHER EPRI, ANY MEMBER OF EPRI, ANY COSPONSOR, THE ORGANIZATION(S) BELOW, NOR ANY PERSON ACTING ON BEHALF OF ANY OF THEM:

(A) MAKES ANY WARRANTY OR REPRESENTATION WHATSOEVER, EXPRESS OR IMPLIED, (I) WITH RESPECT TO THE USE OF ANY INFORMATION, APPARATUS, METHOD, PROCESS, OR SIMILAR ITEM DISCLOSED IN THIS DOCUMENT, INCLUDING MERCHANTABILITY AND FITNESS FOR A PARTICULAR PURPOSE, OR (II) THAT SUCH USE DOES NOT INFRINGE ON OR INTERFERE WITH PRIVATELY OWNED RIGHTS, INCLUDING ANY PARTY'S INTELLECTUAL PROPERTY, OR (III) THAT THIS DOCUMENT IS SUITABLE TO ANY PARTICULAR USER'S CIRCUMSTANCE; OR

(B) ASSUMES RESPONSIBILITY FOR ANY DAMAGES OR OTHER LIABILITY WHATSOEVER (INCLUDING ANY CONSEQUENTIAL DAMAGES, EVEN IF EPRI OR ANY EPRI REPRESENTATIVE HAS BEEN ADVISED OF THE POSSIBILITY OF SUCH DAMAGES) RESULTING FROM YOUR SELECTION OR USE OF THIS DOCUMENT OR ANY INFORMATION, APPARATUS, METHOD, PROCESS, OR SIMILAR ITEM DISCLOSED IN THIS DOCUMENT.

ORGANIZATION(S) THAT PREPARED THIS DOCUMENT

Dominion Engineering, Inc.

ORDERING INFORMATION

Requests for copies of this report should be directed to EPRI Orders and Conferences, 1355 Willow Way, Suite 278, Concord, CA 94520, (800) 313-3774, press 2 or internally x5379, (925) 609-9169, (925) 609-1310 (fax).

Electric Power Research Institute and EPRI are registered service marks of the Electric Power Research Institute, Inc. EPRI. ELECTRIFY THE WORLD is a service mark of the Electric Power Research Institute, Inc.

Copyright © 2004 Electric Power Research Institute, Inc. All rights reserved.

CITATIONS

This report was prepared for the PWR Materials Reliability Program by

Dominion Engineering, Inc.
11730 Plaza America Drive
Suite 310
Reston, VA 20190

Principal Investigator
G. White

Contributors
J. Gorman
N. Nordmann
P. Jones
M. Kreider

Valuable input and review comments were received from many sources, in particular from the following core members of the EPRI-MRP Expert Panel on PWSCC:

P. Andresen (GE GRC), S. Attanasio (KAPL), W. Bamford (Westinghouse), W. Cullen (NRC Research), J. Daret (Corrodys), P. Efsing (Barsebäck), S. Fyfitch (Framatome-ANP), R. Jacko (Westinghouse), C. Jansson (SwedPower), A. Jenssen (Studsvik), A. McIlree (EPRI), W. Mills (Bettis), R. Pathania (EPRI), P. Scott (Framatome-ANP), W. Shack (ANL), T. Yonezawa (MHI), K. Yoon (Framatome-ANP), together with the EPRI Project Manager.

It should be noted that not all sections of this report reflect the views of each member of the crack growth rate review team.

This report describes research sponsored by EPRI.

The report is a corporate document that should be cited in the literature in the following manner:

Materials Reliability Program Crack Growth Rates for Evaluating Primary Water Stress Corrosion Cracking (PWSCC) of Alloy 82, 182, and 132 Welds (MRP-115NP), EPRI, Palo Alto, CA: 2004. 1006696.

REPORT SUMMARY

The Materials Reliability Program (MRP) has developed crack growth rate (CGR) curves for the weld metals selected for use with Alloy 600 base material (Alloy 82, 182, and 132), which are used as “J-groove” welds in various nozzle penetrations and in the piping butt welds to be found at numerous locations in the pressurized water reactor (PWR) primary circuit. An earlier curve for Alloy 182, published in 2000 in EPRI report 1000037, was based on a smaller set of data available at the time and did not result from a systematic statistical assessment.

Background

Recent incidents of PWSCC of Alloy 600 components other than steam generator tubes in the primary circuits of PWRs have highlighted the need for qualified equations for crack growth rates to evaluate flaws found by in-service inspection of thick-walled parts, including weldments. In 2002, the MRP developed a recommended CGR curve for primary water stress corrosion cracking (PWSCC) of thick-wall components fabricated from Alloy 600 base material, such as reactor vessel head nozzles (MRP-55, EPRI report 1006695). The recommended “MRP-55” curve, which was subsequently incorporated into the ASME Section XI Code for flaw evaluation, can be applied directly to disposition many detected PWSCC flaws so as to provide guidance on inspection intervals and repair or mitigation options. This report extends the MRP-55 work to cover Alloy 82/182/132 weldments following observations of cracking in primary circuit welds with high residual stresses and in some J-groove welds attaching control rod drive mechanism (CRDM) nozzles to the reactor upper head.

Objectives

To provide the PWR industry with additional tools to assess the progress of cracking detected in thick-walled Alloy 600 components including deterministic evaluations of real or hypothetical flaws and data that can be used as input to probabilistic assessments.

Approach

The work began with a detailed assessment of all available CGR data for Alloys 82, 182 and 132 in simulated PWR primary water environments. Investigators also paid close attention to the specific properties of the weld metal “cast” microstructure, which can lead to more complex cracking behavior than that seen in Alloy 600 base metal. The EPRI MRP CGR review team, an international panel of experts in the area of PWSCC, provided input to the MRP in evaluation and screening of data, as well as in development of the recommended CGR curves.

Results

Evaluation of the screened laboratory data on a “weld-by-weld” basis, using a linearized multiple regression model, resulted in a log-normal distribution of CGR curves that describes both the observed variability in crack growth rates and the effect of alloy type and dendrite orientation. The MRP recommended CGR curves correspond to the 75th percentile level of this distribution and may be interpreted as the mean of the upper half of the distribution describing the variability in CGR due to material heat. For Alloy 82, the relevant curve is 2.6 times lower than the curve for Alloy 182/132. For crack propagation that is clearly perpendicular to the dendrite solidification direction, a factor of 2.0 lowering the CGR may be applied to the separate curves for Alloy 182/132 and Alloy 82. Comparison with other laboratory data not used directly to develop the curves and with limited field data from repeat inspections of a cracked butt weld supports the validity of the derived CGR curves.

If the operating temperature of the cracked component is taken into account, the MRP recommended curves can be applied directly to disposition detected PWSCC flaws in Alloy 82/182/132. Example calculations are provided for a hot-leg outlet nozzle-to-safe-end weld.

EPRI Perspective

PWSCC has been extensively investigated for many years in connection with the primary-side cracking observed in steam generator tubing. However, studies of the behavior of thick-walled material have been much more limited and the CGR data available worldwide from these exhibit a large amount of scatter, even for wrought base metal. For weld metals, the situation is more complex still, owing both to the variety of microstructures that can be produced and to the less tangible effects of welding procedures, such as the influence of weld restraint on residual stress. In addition to mechanical loading, both temperature and material condition are known to be key variables but quantitative assessment of their influence has often been hindered by deficiencies in test procedures. Input from the MRP Expert Panel on PWSCC was invaluable in assembling and screening the available database so as to de-convolute, as far as possible, the known dependencies. The procedures adopted permitted a statistical approach, which takes into account the strong influence of individual material heats on the expected CGR. The resulting disposition curves are considered to provide a sound basis for engineering calculations and should also be a valuable input into current ASME Code deliberations on this subject. In addition, the screened MRP database is being used directly in probabilistic assessments of risk from butt weld cracking.

Keywords

PWSCC

Alloy 82, 182, 132

Crack Growth Rate

Disposition Curve

Expert Panel

ABSTRACT

Nickel-based austenitic alloys, including wrought Alloy 600 and its weld metals, are used extensively in pressurized water reactor (PWR) applications. Recent incidents of primary water stress corrosion cracking (PWSCC) of Alloy 600 components other than steam generator tubes in the primary circuits of PWRs have highlighted the need for a qualified equation for crack growth rates to evaluate flaws found by in-service inspection. This requirement was fulfilled for the wrought Alloy 600 base material by the issuance in 2002 of the Materials Reliability Program (MRP) MRP-55 report (EPRI report 1006695). The disposition curve established in that work has since been incorporated into the ASME Section XI Code for flaw evaluation.

A similar requirement has also been identified for Alloy 82/182/132 weldments following observations of cracking in primary circuit welds with high residual stresses and in some J-groove welds attaching control rod drive mechanism (CRDM) nozzles to the reactor upper head. A preliminary MRP crack growth rate (CGR) curve for Alloy 182 material was published in 2000 (EPRI report 1000037), but this rate was based on a fairly limited experimental database and simplifying assumptions. Weld metals are by definition “as-cast” structures and, as such, are much more inhomogeneous than wrought materials. The scatter introduced by the inhomogeneous nature of weld metals necessitated the development of a more sophisticated approach.

The present report describes key metallurgical aspects of Alloys 82, 182 and 132, as well as the laboratory testing techniques that have been used to generate CGR data in simulated PWR primary water environments. The report details the screening procedures that were applied to produce the final MRP database and the data reduction methodology used to derive separate CGR curves as a function of the stress intensity factor K_I for Alloy 82/182/132 weld metals, including consideration of the effects of dendrite orientation. Comparisons are made with other laboratory data not used in derivation of the new MRP lines, with limited field data available from repeat non-destructive examination (NDE) inspections of a cracked primary circuit butt weld at the Ringhals PWR in Sweden, and with the CGR disposition curves that have been proposed by other workers. Finally, an example is provided of the way in which the curves can be applied to the assessment of further growth through PWSCC of weld flaws that might be detected in service.

NOMENCLATURE

Symbols

The following symbols are used in this report:

a	crack extent or depth
\dot{a}	crack growth rate
Δa_{ave}	crack growth averaged across the specimen width
Δa_{max}	maximum crack growth across the specimen width
B	compact tension specimen thickness
B_{sg}	compact tension specimen thickness at side groove
f	fugacity
f_{alloy}	crack growth rate factor to account for effect of alloy composition
f_{orient}	crack growth rate factor to account for crack orientation relative to the dendrite direction
f_{temp}	crack growth rate factor to account for temperature
f_{weld}	crack growth rate factor to account for heat of weld material and welding process
K	crack tip stress intensity factor
K_I	crack tip stress intensity factor for opening mode
ΔK	cyclic change in crack tip stress intensity factor
K_{max}	maximum crack tip stress intensity factor
K_{th}	threshold crack tip stress intensity factor
p	pressure
Q_g	thermal activation energy for crack growth
R	universal gas constant, or
R	ratio of minimum load to maximum load
T	absolute operating temperature at location of crack
T_{ref}	absolute reference temperature used to normalize crack growth rate data
\bar{V}	aqueous phase molal volume
W	compact tension specimen width
α	crack growth rate power-law constant
β	crack growth rate power-law exponent
σ_{YS}	yield strength
σ_{UTS}	ultimate tensile strength

Acronyms

The following acronyms are used in this report:

1TCT	one inch thick compact tension
AWS	American Welding Society
BMI	(reactor vessel) bottom mounted instrumentation
BWR	boiling water reactor
CEDM	control element drive mechanism
CGR	crack growth rate
CRDM	control rod drive mechanism
CT	compact tension specimen
CV	crack velocity
DCPD	direct current potential drop
ECP	electrochemical potential
HAZ	heat affected zone
IG	intergranular
IGSCC	intergranular stress corrosion cracking
LEFM	linear elastic fracture mechanics
LS	weld CGR sample orientation (see Figure 3-5)
LT	weld CGR sample orientation (see Figure 3-5)
MC	metal carbide
MGB	migrated grain boundary
MIG	metal inert gas
MRP	Materials Reliability Program
NDE	non-destructive examination
NWC	normal water chemistry
OD	outside diameter
PWHT	post-welding heat treatment
PWR	pressurized water reactor
PWSCC	primary water stress corrosion cracking
RPV	reactor pressure vessel
RVON	reactor vessel outlet nozzle
SCC	stress corrosion cracking
SEM	scanning electron microscopy
SGB	solidification grain boundary
SL	weld CGR sample orientation (see Figure 3-5)
SSGB	solidification subgrain boundary
ST	weld CGR sample orientation (see Figure 3-5)
STP	standard temperature and pressure
TG	transgranular
TIG	tungsten inert gas
TL	weld CGR sample orientation (see Figure 3-5)
TOC	total organic carbon
TS	weld CGR sample orientation (see Figure 3-5)
UT	ultrasonic testing

CONTENTS

1 INTRODUCTION	1-1
1.1 Introduction	1-1
2 EVALUATION OF NICKEL-BASED WELD METAL PROPERTIES ON CRACK GROWTH RATE.....	2-1
2.1 Macrostructural and Microstructural Features of Nickel-Based Weld Metals.....	2-1
2.2 Effects of Chemical Composition on Crack Growth Rate.....	2-4
2.3 Effect of Weld Design and Fabrication on Crack Growth Rate	2-5
3 CRACK GROWTH RATE TESTING TECHNIQUES AND DATA SCREENING.....	3-1
3.1 Specimen Manufacture	3-1
3.1.1 Simulated Weld Joint Design.....	3-2
3.1.2 Weld Chemical Composition	3-3
3.1.3 Solidification Direction and Weld Dendrite Direction	3-3
3.1.4 Convention Used for Identifying Crack Orientation	3-7
3.1.5 Restraint	3-7
3.1.6 In-Process NDE	3-8
3.1.7 Weld Defects	3-9
3.1.8 Post-Welding Heat Treatment	3-10
3.1.9 Crack Front Patterns	3-11
3.2 Specimen Loading.....	3-13
3.2.1 Specimen Loading Considerations.....	3-13
3.2.2 Fatigue Precracking.....	3-13
3.2.3 On-line Crack Monitoring.....	3-14
3.2.4 Other Testing Factors.....	3-14
3.3 Test Environment	3-14
3.4 Derivation of Crack Growth Rate Considering Uneven Crack Fronts	3-15
3.5 Screening Criteria.....	3-16

4 MRP DATABASE AND DERIVATION OF CGR CURVES	4-1
4.1 Development of MRP Database for Alloy 82/182/132.....	4-1
4.2 Data Reduction.....	4-2
4.3 MRP Disposition Curves	4-4
5 COMPARISON OF MRP DISPOSITION CURVES WITH OTHER DATA	5-1
5.1 Comparison With Other Laboratory Data	5-1
5.1.1 Comparison With Laboratory Data Generated for Removed Plant Weld Material.....	5-1
5.1.2 Comparison With Additional Westinghouse Data Investigating the Potential Effect of pH.....	5-3
5.1.3 Comparison With Average Crack Growth Data That Were Screened Out from the MRP Database	5-5
5.1.4 Comparison With Maximum Crack Growth Data That Were Screened Out From the MRP Database.....	5-6
5.1.5 Investigation of Effect of Periodic Unloading and Hold Time.....	5-7
5.2 Comparison With Other Field Data	5-8
5.3 Comparison With Other Deterministic Curves for Alloy 182.....	5-10
6 EXAMPLE APPLICATION	6-1
6.1 Example Application: PWR Piping Butt Welds.....	6-2
6.1.1 Example Geometry.....	6-2
6.1.2 Loadings	6-2
6.1.3 Welding Residual Stresses.....	6-2
6.1.4 Operating Stresses.....	6-2
6.1.5 Results.....	6-3
6.2 Effects of a Stress Intensity Factor Threshold Assumption.....	6-3
7 CONCLUSIONS	7-1
8 REFERENCES	8-1
A METALLURGICAL ASPECTS OF NICKEL-BASED WELD MATERIALS AND THEIR EFFECTS ON CRACK GROWTH RATES.....	A-1
A.1 Microstructure of Alloy 182 and 82H Welds.....	A-1
A.2 SCC Fracture Surface Appearance for Alloy 82H, 182, and 132 Welds.....	A-3
A.3 Effect of Chemical Composition and Post-Weld Heat Treatment on Crack Growth Rate.....	A-7

A.3.1 Effect of Chromium and Post-Weld Heat Treatments	A-7
A.3.2 Effect of Carbon	A-10
A.3.3 Effect of Manganese	A-10
A.3.4 Effect of Niobium (a.k.a. Columbium) and Titanium.....	A-10
A.3.5 Effect of Impurities (e.g., Si, P, and S)	A-11
A.3.6 Summary of Chemical Composition Effects.....	A-11
A.4 Effect of Welding Condition on Crack Growth Rate.....	A-12
A.5 Effect of Strength Level on Crack Growth Rate.....	A-13
A.6 Effect of Microstructure on Crack Growth Rate	A-13
A.7 Effect of Weld Defects on Crack Growth Rate.....	A-14
A.7.1 Fundamentals of Hot Cracking and Ductility-Dip Cracking	A-14
A.7.2 Current Understanding Regarding Influence of Weld Defects on PWSCC.....	A-15
B RECOMMENDATIONS REGARDING SPECIMEN LOADING PROCEDURE.....	B-1
B.1 Specimen Loading Considerations	B-1
B.2 Fatigue Precracking and Transitioning	B-2
B.3 Continuous Crack Monitoring and Effects of Crack Front Unevenness.....	B-3
C EFFECTS OF DISSOLVED HYDROGEN CONCENTRATION AND TEMPERATURE.....	C-1
C.1 Electrochemical Considerations of SCC.....	C-1
C.1.1 Introduction	C-1
C.1.2 Corrosion Potential and the Nernst Equation.....	C-1
C.1.3 Hydrogen Fugacity	C-2
C.1.4 Contact Electrical Resistance Measurement of Ni-NiO Transition.....	C-2
C.1.5 Effect of Proximity of the Corrosion Potential to the Ni-NiO Transition on SCC Growth Rate.....	C-2
C.2 Examination of MRP CGR Database After Screening in Context of Reported Dissolved Hydrogen Concentrations.....	C-4
D DERIVATION OF CRACK GROWTH RATES GIVEN INCOMPLETE ENGAGEMENT TO INTERGRANULAR CRACKING	D-1
D.1 Incomplete Engagement as an Artifact of Test-Specific Conditions	D-1
D.2 Incomplete Engagement as a Result of Spatial Variations in Cracking Susceptibility	D-9
D.2.1 Nature of Intergranular Stress Corrosion Cracks in Alloy 82/182/132 Welds	D-9
D.2.2 Discussion of Options of Section D.1 for Resolving Incomplete Engagement Issue	D-10

D.2.3 Alternate Methods for Addressing the Incomplete Engagement Issue	D-10
D.3 Treatment of Crack Front Engagement Used to Develop the MRP-115	
Deterministic CGR Model.....	D-11
 E CONCEPT AND SIGNIFICANCE OF A STRESS INTENSITY FACTOR THRESHOLD	
FOR PWSCC	E-1
 F LABORATORY ALLOY 82/182 CGR DATA EXCLUDED IN THE DEVELOPMENT	
OF MRP CGR DISPOSITION CURVES	F-1
 G COMPARISON WITH EXCLUDED DATA FOR WHICH AVERAGE CGRS WERE	
REPORTED	G-1
 H COMPARISON WITH EXCLUDED DATA FOR WHICH ONLY MAXIMUM CGRS	
WERE REPORTED	H-1
 I EVALUATION OF EFFECT OF PERIODIC UNLOADING AND HOLD TIME	I-1

LIST OF FIGURES

Figure 2-1 Transverse Section of Alloy 82H Weld Showing Columnar Grain Structure [8]	2-2
Figure 2-2 Light Optical Micrographs Showing Columnar Grains: (a) Alloy 182 Weld [9] and (b) Alloy 82H Weld [10]	2-3
Figure 2-3 Micrograph Showing Various Kinds of Grain Boundaries in Weld Metals (Courtesy of Ohio State University [11]).....	2-3
Figure 3-1 Example of an Alloy 182 Test Weld Block Made With Two Plates and a Backing Strip [6]	3-2
Figure 3-2 Example of an Alloy 182 Test Weld Block Made With a V-groove in a Single Plate [6]	3-3
Figure 3-3 Sketch Showing Various Kinds of Grain Boundaries in Weld Metals [11]	3-6
Figure 3-4 Micrograph Showing Various Kinds of Grain Boundaries in Weld Metals (Courtesy of Ohio State University [11]).....	3-6
Figure 3-5 Terminology Used for Orientations of Cracks in Test Specimen With Respect to Welds [6]	3-7
Figure 3-6 Example of a Fracture Surface of Alloy 182 Weld Metal With Moderately Uniform Crack Front.....	3-11
Figure 3-7 Example of a Fracture Surface of Alloy 182 Weld Metal With Irregular Crack Front.....	3-12
Figure 3-8 Example of a Fracture Surface of Alloy 182 Weld Metal With Highly Irregular Crack Front	3-12
Figure 4-1 Complete Set of Worldwide Alloy 82/182/132 Average CGR Data Before Screening Process (144 points)	4-12
Figure 4-2 Complete Set of Worldwide Alloy 82/182/132 Maximum CGR Data Before Screening Process (158 points)	4-12
Figure 4-3 Average CGR Data for Alloys 182 and 132 After MRP Screening (43 Points).....	4-13
Figure 4-4 Average CGR Data for Alloy 82 After MRP Screening (34 Points).....	4-13
Figure 4-5 Log-Normal Fit to 19 Weld Factors for Screened MRP Database of CGR Data for Alloy 82/182/132	4-14
Figure 4-6 MRP-115 Deterministic Curves for Alloy 182/132 and Alloy 82 Weld Materials.....	4-14
Figure 4-7 Average CGR Data for Alloys 182 and 132 After MRP Screening (43 Points) Normalized to a Crack Orientation Parallel to the Weld Dendrites with MRP-115 Curve for Alloy 182/132.....	4-15
Figure 4-8 Average CGR Data for Alloy 82 After MRP Screening (34 Points) Normalized to a Crack Orientation Parallel to the Weld Dendrites with MRP-115 Curve for Alloy 82	4-15

Figure 5-1 Comparison of MRP-115 Curves for Alloys 182/132 and 82 With Westinghouse CGR Data for Weld Material Removed From VC Summer Reactor Hot Leg Safe End Butt Weld [52,65]	5-3
Figure 5-2 Additional Westinghouse Crack Growth Data Gathered to Investigate the Potential Effect of pH for Alloy 182	5-4
Figure 5-3 Average Crack Growth Rate Versus Stress Intensity Factor for Data Screened Out Because $\Delta a_{ave} < 0.5$ mm.....	5-5
Figure 5-4 Comparison of Cumulative Distribution Function for Maximum Measured CGR Normalized by the CGR Predicted by the MRP-115 Deterministic Model.....	5-6
Figure 5-5 Average Crack Growth Rates Normalized by the CGR Predicted by the MRP-115 Deterministic Model Plotted as a Function of Hold Time (Bettis Lab Test Data—Heat C-4).....	5-7
Figure 5-6 Field Crack Growth Data for Ringhals Unit 3 Hot Leg Safe End Alloy 182 Weld	5-9
Figure 5-7 Comparison of MRP-115 Curve for Alloy 182 Weld Metal With Other Disposition Curves	5-12
Figure 6-1 Geometry of the Weld Region Used for the Crack Growth Illustrations (Reactor Vessel Outlet Nozzle and Pressurizer Safety and Relief Nozzle-to-Safe-End Welds).....	6-4
Figure 6-2 Standard Residual Stress Distributions Applied to Piping Butt Welds [77].....	6-5
Figure 6-3 Results of Sample Calculations for a Range of Flaw Shapes: Time for Through-Wall Growth for a Part-Depth Circumferential Flaw at a Reactor Vessel Outlet Nozzle (RVON) Safe End Region (Incl. Residual Stress).....	6-5
Figure 6-4 Results of Sample Calculations for a Range of Flaw Shapes: Time for Through-Wall Growth for a Part-Depth Circumferential Flaw at a Pressurizer (PZR) Safety and Relief Nozzle Safe End Region (Incl. Residual Stress).....	6-6
Figure 6-5 Results of Sample Calculations Showing the Effect of a Stress Intensity Factor Threshold: Circumferential Flaw at a Pressurizer Safety and Relief Nozzle Safe End Region; Time for Through-Wall Growth for a Part-Depth Circumferential Flaw (top) and Subsequent Time for Growth in the Circumferential Direction of a Through-Wall Circumferential Flaw (Bottom)	6-7
Figure 6-6 Results of Sample Calculations Showing the Effect of a Stress Intensity Factor Threshold: Circumferential Flaw at a Pressurizer Surge Nozzle Safe End Region; Time for Through-Wall Growth for a Part-Depth Circumferential Flaw (top) and Subsequent Time for Growth in the Circumferential Direction of a Through-Wall Circumferential Flaw (Bottom).....	6-8
Figure 6-7 Results of Sample Calculations Showing the Effect of a Stress Intensity Factor Threshold: Circumferential Flaw at a Core Flood Nozzle Safe End Region; Time for Through-Wall Growth for a Part-Depth Circumferential Flaw (top) and Subsequent Time for Growth in the Circumferential Direction of a Through-Wall Circumferential Flaw (Bottom).....	6-9
Figure 6-8 Results of Sample Calculations Showing the Effect of a Stress Intensity Factor Threshold: Circumferential Flaw at a Decay Heat Nozzle Safe End Region; Time for Through-Wall Growth for a Part-Depth Circumferential Flaw (top) and Subsequent Time for Growth in the Circumferential Direction of a Through-Wall Circumferential Flaw (Bottom).....	6-10

Figure A-1 Transverse Section of Alloy 82H Weld Showing Columnar Grain Structure [8].....	A-2
Figure A-2 Light Optical Micrographs Showing Columnar Grains: (a) Alloy 182 weld [9] and (b) Alloy 82H Weld [10]	A-2
Figure A-3 Scanning Electron Microscopy (SEM) Micrographs Showing the Convolutd Nature of Dendritic Grain Boundaries: (a) Alloy 182 Weld [20], and (b) Alloy 82H Weld [125].....	A-3
Figure A-4 SEM Fractographs Showing Intergranular SCC: (a) T-S oriented Alloy 182 Specimen 9], (b) T-S Oriented Alloy 82H Specimen [10], and (c) T-L Oriented Alloy 82H Specimen [10].....	A-5
Figure A-5 Nature of Intergranular SCC in a Nozzle to Safe-End Alloy 182 Weld in Ringhals Unit 4 [70]: (a) SEM Fractograph and (b) Metallographic Section.....	A-6
Figure A-6 SEM Fractographs Showing Nature of Intergranular SCC in an Alloy 132 Weld [28]: (a) Crack Propagation Along Convolutd Grain Boundaries (b) Fingers of SCC That Extend Beyond the Fatigue Precrack.....	A-6
Figure A-7 Macroscopic Fracture Surface Morphology for T-S Oriented Alloy 82H Specimens [10]: (a) Uneven Cracking Proceeding Along Susceptible Grain Boundaries and (b) Large Unbroken Ligaments (Denoted by Arrows) in Wake of Crack Front	A-7
Figure A-8 Effect of Chromium Content on the Stress Corrosion Cracking Resistance of Solution Annealed Ni-Cr-Fe Alloys 13].....	A-8
Figure A-9 Effect of Niobium Addition on the Stress Corrosion Cracking Resistance of Annealed Alloy 600 in 360°C High Temperature Water [86].....	A-11
Figure A-10 Schematic Diagram Showing the Temperature Ranges in Which Ductility- Dip Cracking (Type 2) and Solidification Cracking or Liquation Cracking (Type 1) Occur [94].....	A-15
Figure C-1 Pourbaix (Potential-pH) Diagram for the Ni-H ₂ O Using 10 ⁻³ N Ionic Species [102]	C-5
Figure C-2 H ₂ Fugacity vs. Temperature in Water at Saturation Pressure [104]	C-6
Figure C-3 Effect of Temperature on the Dissolved H ₂ Required to Cross the Ni / NiO Phase Transition [106]	C-6
Figure C-4 CGR of Alloy 600 vs. Dissolved H ₂ at 338°C [108]	C-7
Figure C-5 CGR of Alloy 600 vs. Corrosion Potential (Controlled by Dissolved H ₂) at 338°C [108]	C-7
Figure C-6 CGR of Alloy 600 vs. Corrosion Potential (Controlled by Dissolved H ₂) [106].....	C-8
Figure C-7 CGR of Alloy 600 CT Specimens From the Base Metal or Aligned Along the Weld Heat Affected Zone vs. Temperature [109].....	C-8
Figure C-8 CGR vs. Corrosion Potential Relative to the Ni / NiO Transition (Controlled by H ₂ Fugacity) of Alloy 600 [109].....	C-9
Figure C-9 Apparent Activation Energy for Alloy 600 Base Metal or Heat Affected Zone Material [109]	C-9
Figure C-10 CGR vs. Corrosion Potential Relative to the Ni / NiO Transition (Controlled by H ₂ Fugacity) of Alloy 600 and Alloy X-750 HTH [108]	C-10
Figure C-11 CGR of Alloy X-750 vs. Dissolved H ₂ at 360°C and 49.4 MPa√m [108,37]	C-10

Figure C-12 CGR vs. Corrosion Potential Relative to the Ni / NiO Transition (Controlled by H ₂ Fugacity) of Alloy X-750 in the HTH Heat Treatment Condition [108]	C-11
Figure C-13 CGR vs. Corrosion Potential Relative to the Ni / NiO Transition (Controlled by H ₂ Fugacity) of Alloy X-750 in the AH Heat Treatment Condition [106]	C-11
Figure C-14 CGR vs. H ₂ Concentration for CT Specimens Alloy EN82H Weld Metal Tested at 338°C at 39 MPa√m [106].....	C-12
Figure C-15 Dissolved Hydrogen Level and Temperature Environmental Conditions for Data in the MRP Database After Screening in Comparison to the Reported Ni-NiO Transition Line.....	C-12
Figure C-16 Average Crack Growth Rates Normalized by the CGR Predicted by the MRP-115 Deterministic Model Plotted as a Function of Temperature and Grouped by Hydrogen Level	C-13
Figure C-17 Average Crack Growth Rates Normalized by the CGR Predicted by the MRP-115 Deterministic Model Plotted as a Function of Hydrogen Level and Grouped by Temperature	C-13
Figure C-18 Inverse Temperature Plot for Average CGRs Adjusted for Alloy Type, Crack Orientation, and Stress Intensity Factor.....	C-14
Figure D-1 Schematic of One Origin of the Problem of Transitioning From a Transgranular Crack to an Intergranular Crack.....	D-2
Figure D-2 Schematic of the Evolution of a Transgranular Fatigue Precrack to an Intergranular Stress Corrosion Crack, and its Effect on Estimated Crack Growth Rates.....	D-3
Figure D-3 Correlations Developed by Lockheed Martin Based on Their Extensive Testing of Alloys 182 and 82 [37].....	D-4
Figure D-4 Correlation Between Maximum and Average Crack Length [37]	D-5
Figure D-5 Fracture Surface for Cold Worked Stainless Steel Test Specimen	D-5
Figure D-6 Fracture Surface for Cold Worked Stainless Steel Test Specimen	D-6
Figure D-7 Fracture Surface for Alloy 182 Weld Metal Test Specimen	D-7
Figure D-8 Fracture Surface for Alloy 182 Weld Metal Test Specimen	D-7
Figure D-9 Fracture Surface for Alloy 182 Weld Metal Test Specimen	D-8
Figure D-10 Fracture Surface for Alloy 182 Weld Metal Test Specimen	D-8
Figure D-11 Fracture Surface for Alloy 82 Weld Metal Test Specimen	D-9
Figure E-1 Schematic Illustration of the Relation Between Exposure Time and IGSCC Crack Velocity (CV) of Pipeline Steels Exposed to Carbonate-Bicarbonate Solution (After [118]).	E-3
Figure E-2 Crack Growth Per Reactor Cycle as a Function of Crack Length in Roll Transition Zones of Steam Generator Tubes (After Scott [119]).....	E-4
Figure G-1 Average Crack Growth Rate Versus Stress Intensity Factor for Data Screened Out Because $\Delta a_{avg} < 0.5$ mm.....	G-2
Figure G-2 Average Crack Growth Rates Normalized by the CGR Predicted by the MRP-115 Deterministic Model Plotted as a Function of Average Crack Increment Δa_{avg} (Including Data Screened Out Because $\Delta a_{avg} < 0.5$ mm)	G-3

Figure G-3 Average Crack Growth Rate Versus Stress Intensity Factor for Data Screened Out Because Hold Time < 1 hour	G-3
Figure G-4 Average Crack Growth Rate Versus Stress Intensity Factor for Data Screened Out Because of a High Dissolved Hydrogen Concentration (150 cc/kg)	G-4
Figure G-5 Average Crack Growth Rate Versus Stress Intensity Factor for Data Screened Out Because of Violation of LEFM Validity Criterion.....	G-4
Figure G-6 Average Crack Growth Rate Versus Stress Intensity Factor for Data Screened Out Because Crack Engagement < 50%	G-5
Figure H-1 Maximum Crack Increment Δa_{max} Versus Average Crack Increment Δa_{ave} for All Such Available Data	H-4
Figure H-2 Maximum Crack Increment Δa_{max} Versus Average Crack Increment Δa_{ave} for Bettis Alloy 82H Data	H-5
Figure H-3 Maximum Crack Growth Rate Versus Stress Intensity Factor for Weld D545/D582	H-6
Figure H-4 Maximum Crack Growth Rate Versus Stress Intensity Factor for Data Excluded From the MRP Database Because Only CGR_{max} Is Available.....	H-6
Figure H-5 Maximum Crack Growth Rate Versus Stress Intensity Factor for Data in MRP Database After Screening	H-7
Figure H-6 Maximum Crack Growth Rate Versus Stress Intensity Factor for Data Excluded From the MRP Database Only Because $\Delta a_{ave} < 0.5$ mm	H-7
Figure H-7 Comparison of Cumulative Distribution Function for Maximum Measured CGR Normalized by the CGR Predicted by the MRP-115 Deterministic Model.....	H-8
Figure H-8 Maximum Measured CGR Normalized by the CGR Predicted by the MRP- 115 Deterministic Model as a Function of Δa_{max}	H-8
Figure I-1 Average Crack Growth Rates Normalized by the CGR Predicted by the MRP- 115 Deterministic Model Plotted as a Function of Hold Time (Including Hold Time < 1 hour).....	I-3
Figure I-2 Average Crack Growth Rates Normalized by the CGR Predicted by the MRP- 115 Deterministic Model Plotted as a Function of Hold Time (Including $\Delta a_{ave} < 0.5$ mm or Hold Time < 1 hour)	I-3
Figure I-3 Average Crack Growth Rates Normalized by the CGR Predicted by the MRP- 115 Deterministic Model Plotted as a Function of Hold Time (Welds With Multiple Hold Times).....	I-4
Figure I-4 Maximum Crack Growth Rates Normalized by the CGR Predicted by the MRP-115 Deterministic Model Plotted as a Function of Hold Time	I-4
Figure I-5 Average Crack Growth Rates Normalized by the CGR Predicted by the MRP- 115 Deterministic Model Plotted as a Function of Hold Time (Bettis Lab Test Data— All Specimens)	I-5
Figure I-6 Average Crack Growth Rates Normalized by the CGR Predicted by the MRP- 115 Deterministic Model Plotted as a Function of Hold Time (Bettis Lab Test Data— Heat C-4).....	I-5
Figure I-7 Average Crack Growth Rates Normalized by the CGR Predicted by the MRP- 115 Deterministic Model Plotted as a Function of Hold Time (Bettis Lab Test Data— Heat A-1).....	I-6

LIST OF TABLES

Table 2-1 Nominal Chemical Composition for Alloy 82, 182, and 132 Weld Metal.....	2-4
Table 3-1 Compositions of the Test Materials Used for Crack Growth Rate Tests (MRP Database After Screening).....	3-5
Table 3-2 Environments Used for Crack Growth Rate Tests (MRP Database After Screening).....	3-15
Table 3-3 Key Factors for Consideration in CGR Testing and Data Reporting	3-17
Table 4-1 Summary of Data Sources for CGR Testing of Alloy 82, 182, and 132 Welds	4-6
Table 4-2 Laboratory Alloy 82/182/132 CGR Data in the Screened MRP Database ¹	4-7
Table 4-3 Calculated Normalization Factors for Alloy Type (82/182/132) and Weld Heat/Processing	4-11
Table 5-1 Data Reported for Ringhals Unit 3 Hot Leg Safe End Nozzle Weld Cracks	5-8
Table A-1 Nominal Chemical Composition for Alloy 82, 182, and 132 Weld Metal	A-11
Table F-1 Laboratory Alloy 82/182/132 CGR Data Excluded in the Development of the MRP Disposition Curve ^{1,2}	F-2
Table H-1 Statistical Comparison of Maximum CGR Data for Data Included in the Development of the MRP-115 CGR Model With Data Excluded Because Only Maximum CGR Data Were Available (See Figure H-7)	H-3

1

INTRODUCTION

1.1 Introduction

Nickel-based austenitic alloys, including wrought Alloy 600 and weld metals Alloy 82, 182 and 132, are used extensively in pressurized water reactor (PWR) applications. These materials offer a useful combination of good mechanical properties and fracture toughness, compatibility with other vessel or piping materials, and corrosion resistance. However, recent incidents of primary water stress corrosion cracking (PWSCC) of Alloy 600 components other than steam generator tubes in the primary circuits of PWRs [1,2] have highlighted the need for a qualified equation for crack growth rates (CGRs) to evaluate flaws found by in-service inspection. This requirement was fulfilled for the wrought Alloy 600 base material, after much deliberation involving an international panel of PWSCC experts, by the issuance in 2002 of the Materials Reliability Program (MRP) MRP-55 report [3]. The disposition curve established in that work has since been incorporated into the ASME Section XI Code for flaw evaluation [4].

A similar requirement has also been identified for Alloy 82/182/132 weldments following observations of cracking in primary circuit welds with high residual stresses and in some J-groove welds attaching control rod drive mechanism (CRDM) and bottom mounted instrumentation (BMI) nozzles to the reactor upper head [5]. A preliminary MRP CGR curve for Alloy 182 material was published in 2000 [6], but this was based on a fairly limited experimental database and an assumption that the results could be described by application of a simple multiplication factor to the then current Scott model for base metal, which had been derived from field data on thin-walled steam generator tubing [7]. Weld metals are by definition “as-cast” structures and, as such, are much more inhomogeneous than wrought materials. The scatter introduced by the inhomogeneous nature on a microscopic scale of weld metals makes the simple multiplication factor approach not suitable for extensive use, and necessitated the development of a more sophisticated methodology.

The approach taken here to deriving a more appropriate model for nickel-based weld metals was analogous to that used to establish the MRP-55 curve for thick-walled wrought Alloy 600, namely detailed consideration and screening by the MRP PWSCC Expert Panel of all available laboratory data from relevant CGR tests in simulated PWR water and statistical derivation of best-fit curves, taking into account, as far as possible, the particular nature of PWSCC in weld material and its possible influence on the experimental results that had been obtained. The present report starts by describing key metallurgical aspects of Alloys 82, 182, and 132. It continues with a description of the laboratory testing techniques that have been used and details the screening procedures that were applied to produce the final MRP database. After setting out the data reduction methodology used to derive separate CGR curves as a function of the stress intensity factor K_I for nickel-based weld metals, comparisons are made with other laboratory data

Introduction

not used in derivation of the new CGR lines, the limited field data available from repeat non-destructive examination (NDE) inspections of a cracked primary circuit butt weld at the Ringhals PWR in Sweden, and with the CGR disposition curves that have been proposed by other workers. Finally, an example is provided of the way in which the curves can be applied to the assessment of further growth of cracks by PWSCC which might be detected in service.

2

EVALUATION OF NICKEL-BASED WELD METAL PROPERTIES ON CRACK GROWTH RATE

This section briefly reviews the effects of metallurgical factors on the crack growth rate observed in Alloys 82, 182 and 132. Additional details are provided in Appendix A regarding weld metallurgy and its possible effects on CGR. The incentive for covering metallurgical aspects is that high variability is observed in the measured CGRs of Alloys 82, 182 and 132, and it is therefore important to understand how metallurgical factors contribute to this variability. However, while discussion of these factors provides useful background information, firm correlations between metallurgical factors and CGR are not available except for differences in CGR between Alloys 182/132 and Alloy 82. For this reason, the CGRs for different weld alloys need to be addressed on a statistical basis, and not by correlation with specific metallurgical features.

2.1 Macrostructural and Microstructural Features of Nickel-Based Weld Metals

The CGR in Alloy 82/182/132 is strongly affected by the microstructure of the weld and by the orientation of the crack growth with respect to the microstructure. For this reason, it is important to develop an understanding of the main features of Alloy 82/182/132 microstructure.

Weld metal forms by solidification from a molten state, which leads to the formation of dendrites growing in the direction of the heat flow, i.e., perpendicular to the solid material on which the weld is deposited. Most welds are made with multiple passes. The grain structure of dendrites in subsequent passes is normally related to that of previous passes as a result of epitaxy, i.e., by the tendency of a crystal forming on a substrate to have the same structural orientation as the substrate. This results in the dendrites persisting through several or many weld passes. The macrostructure of a typical weld is shown in Figure 2-1 [8]. The weld shown in Figure 2-1 was made with Alloy 82H (Alloy 82H is essentially the same as Alloy 82, as discussed in Appendix A). Features to note regarding Figure 2-1 include:

- The weld was made with over 30 weld passes.
- There is a strong pattern of columnar grains formed by dendrites, and the pattern persists through many weld passes.
- The dendrites tend to be perpendicular to the base material at the weld-base material interface, and tend to become vertical (root to crown direction) as the weld thickness increases. The dendrites are mainly vertical in the central region of the weld.

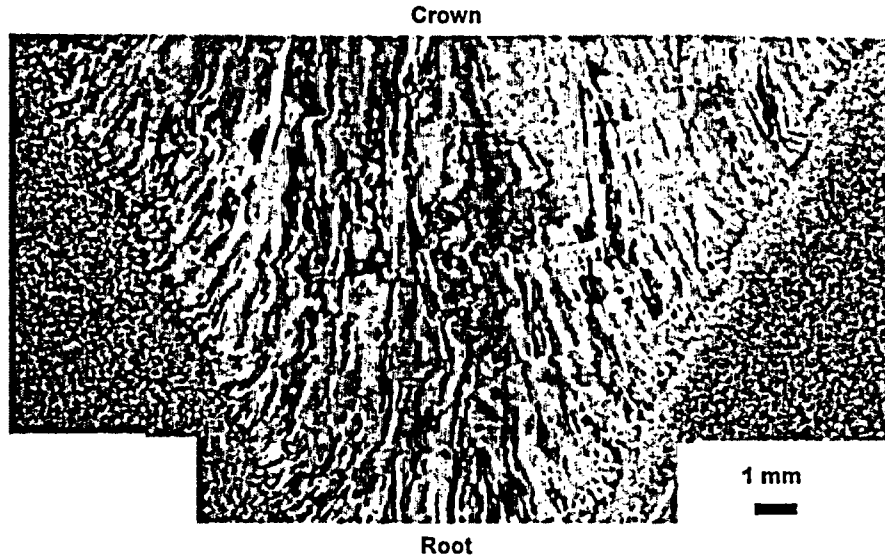


Figure 2-1
Transverse Section of Alloy 82H Weld Showing Columnar Grain Structure [8]

As the weld metal forms, parallel bundles of dendrites with nearly identical crystallographic orientation form and grow into the melt. The boundaries between these similarly oriented dendrites tend to have low angular mismatches, tend to have low energy, and are believed to form paths for PWSCC relatively infrequently. Where different bundles of dendrites meet, larger angular mismatches often occur between the grains of the bundles. In this case, the resulting grain boundaries can be high energy and are believed to be more common paths for PWSCC. However, it has been found that some high-angle grain boundaries or sections of boundaries have relatively low energy since they have coincident site lattices (meaning that the crystal orientations are such that the atomic structures of the two grains have a significant level of matching); this causes those particular high-angle boundaries to be relatively more resistant to PWSCC propagation. Such low-energy, high-angle grain boundaries may be present in cases for which the crack path is kinked, connecting two planes that are offset by as much as 1–2 mm even with high-angle boundaries in close proximity that would have facilitated a straighter crack path.

The typical wavy pattern of high energy grain boundaries observed in Alloy 82 and 182 weld metals is illustrated in Figure 2-2 [9,10]. This micrograph shows columnar grains with wavy grain boundaries that separate colonies of similarly oriented dendrites. The dark particles in the intergranular regions are titanium carbonitride inclusions. The structure of the grain boundaries is further illustrated in Figure 2-3 [11], which also shows migrated grain boundaries (MGB) that develop as the result of subsequent weld passes. Visible in this figure are solidification subgrain boundaries (SSGB) formed between dendrites, solidification grain boundaries (SGB), and migrated grain boundaries. PWSCC cracks in weld metals typically follow the higher energy SGB and/or MGBs.

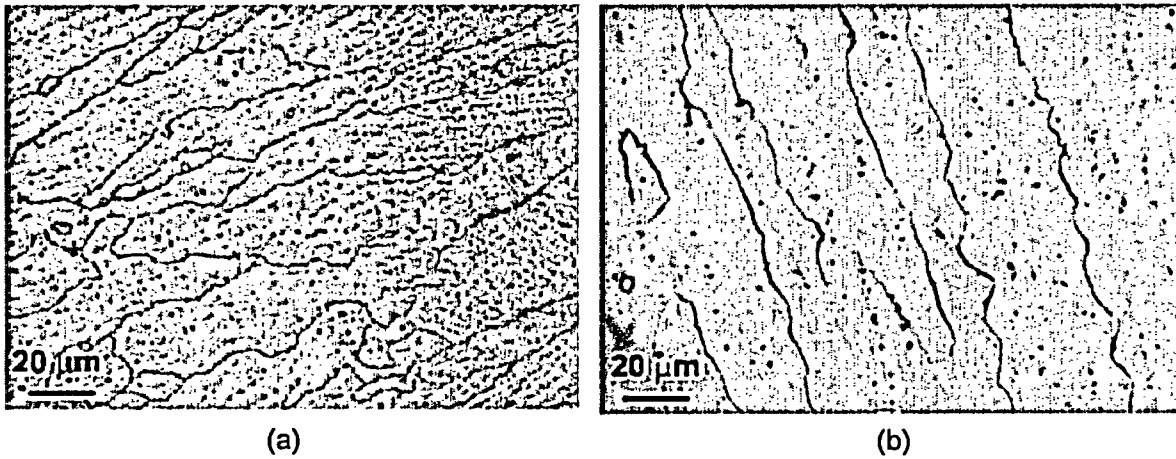


Figure 2-2
Light Optical Micrographs Showing Columnar Grains: (a) Alloy 182 Weld [9] and
(b) Alloy 82H Weld [10]

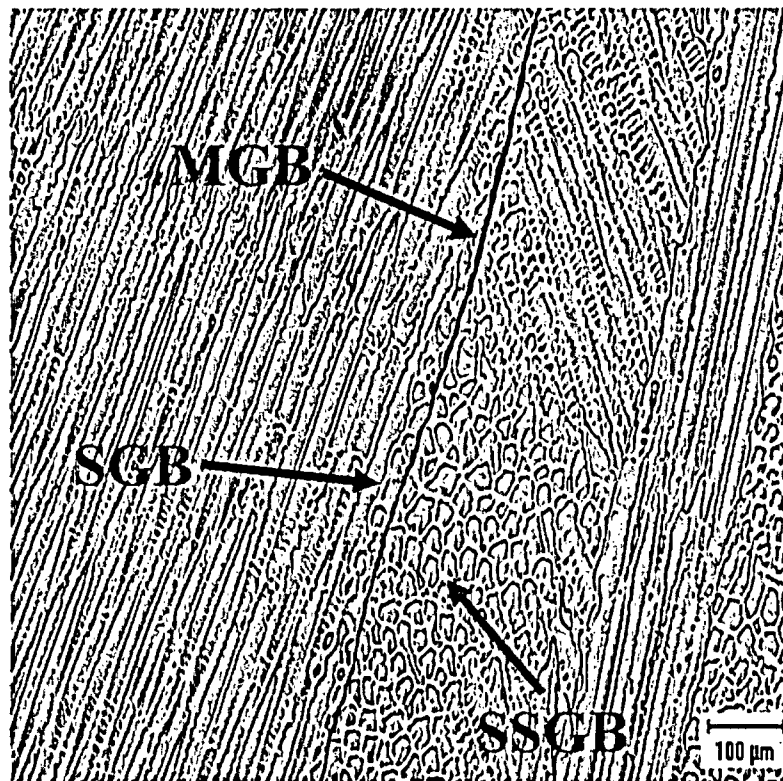


Figure 2-3
Micrograph Showing Various Kinds of Grain Boundaries in Weld Metals (Courtesy of Ohio
State University [11])

The orientation of the crack in the weld, i.e., relative to the weld's columnar microstructure, has a strong influence on the CGR. Thus, it is necessary to include the relative crack orientation (i.e., parallel or perpendicular to the direction of the weld dendrites) in the development of a CGR model. (The convention used for identifying crack orientation is shown in Figure 3-5.) Cracks grow fastest along high energy grain boundaries in the direction of grain growth, and next fastest along high energy grain boundaries perpendicular to the direction of grain growth, i.e., parallel to the welding direction. Cracks that grow perpendicular to the high energy grain boundaries, i.e., perpendicular to the columnar dendrites, grow significantly slower.

2.2 Effects of Chemical Composition on Crack Growth Rate

The nominal chemical compositions of Alloys 82, 182, and 132 are shown in Table 2-1.

Table 2-1
Nominal Chemical Composition for Alloy 82, 182, and 132 Weld Metal

Alloy	wt. %					
	Ni	Cr	Fe	Mn	Nb	Ti
82	71	20	2	3	2.5	0.5
182	67	15	8	7	1.8	0.5
132	70	15	9	1	2.5	—

The only well explored effect of the compositional differences among the weld alloys on PWSCC is the influence of chromium. Buisine, et al. evaluated the PWSCC resistance of nickel-based weld metals with various chromium contents ranging from about 15% to 30% chromium [12]. Testing was performed in doped steam and primary water. Alloy 182, with about 14.5% chromium, was the most susceptible. Alloy 82 with 18–20% chromium took three or four times longer to crack. For chromium contents between 21 and 22%, no stress corrosion crack initiation was observed, as was also the case for Alloys 52 and 152 which have about 30% chromium. These results indicated that weld metals with 30% chromium were resistant to cracking, with a threshold for PWSCC resistance being between 22 and 30% chromium. This behavior is consistent with that of mill annealed wrought Ni-Cr-Fe base alloys. Tests by Yonezawa, et al. evaluated the effect of chromium on the PWSCC susceptibility of wrought Ni-Cr-Fe alloys and showed that the susceptibility decreased as the chromium content increased from about 1% to over 15% [13]. Extensive testing has shown that Alloy 690, with about 30% chromium, is very resistant to PWSCC. MRP-111 [82] summarizes additional laboratory data collected by AREVA that support these conclusions regarding the importance of chromium content.

Exposure to sensitizing heat treatments¹ causes precipitation of chromium carbides at grain boundaries and reduces the chromium concentration adjacent to grain boundaries. Conceptually, this effect might be expected to increase the susceptibility to PWSCC of Alloy 600 type materials. However, as reviewed in the Steam Generator Reference Book [14], the opposite has been observed for wrought materials: sensitized wrought Alloy 600 has been shown by tests and operating experience to have improved resistance to PWSCC as compared to mill annealed

¹ Sensitization refers to the precipitation of chromium carbides leading to low chromium concentration at grain boundaries, making the material susceptible to rapid corrosion in acid-oxidizing environments.

material. Bruemmer and Henager [15] have studied the microchemistry and microdeformation aspect of this improved resistance and suggest that a change in microdeformation characteristics is the primary component in the improvement in steam generator tubing. Tests of weld materials regarding the effects of exposure to sensitizing heat treatment are limited, but those that are available indicate that they improve resistance to PWSCC. However, Amzallag et al. [16] report no correlation between the intrinsic material susceptibility to stress corrosion cracking (SCC) (as distinct from the benefits associated with stress relief) and the precipitation of carbides at grain boundaries based on their tests on Alloy 82/182 specimens. This apparent result for Alloy 82/182, as reported in Reference [16], is in contrast to established results for wrought Alloy 600 [17,18,19], which exhibits greater SCC resistance with increased grain boundary carbide decoration, an effect that may be related to grain boundary creep.

The impact of carbon content on the crack growth rate of Alloy 82/182/132 has not been well characterized. However, a couple of laboratory investigations using primary environments suggest that total carbon content has little effect: Cassagne et al. [20] and Foster et al. [21] both reported little change in crack growth rate for specimens of Alloy 182 and Alloy 600, respectively, that had carbon concentrations ranging between 0.02% and 0.10%.

Impurities (Si, P, and S) in nickel-based materials tend to segregate at grain boundaries [22]. A clear understanding of how each of these affects PWSCC susceptibility has not been obtained. However, these impurity elements can affect the hot cracking susceptibility of nickel-based weld metals [23,24]. As discussed in Section 3.1.7, the defects present in weld metal as the result of hot cracking could plausibly affect crack initiation and growth rates, although recent investigations provide evidence to the contrary.

In summary with regard to compositional effects: (1) increasing the average chromium concentration of the material correlates with increasing resistance to PWSCC, (2) the reduction in local chromium concentration that occurs at grain boundaries as the result of exposure to sensitizing heat treatments does not increase the material's susceptibility to PWSCC, and the reduction of residual stresses provided by the heat treatment is helpful, and (3) there are no known consistent effects of impurities on PWSCC susceptibility.

2.3 Effect of Weld Design and Fabrication on Crack Growth Rate

Weld design and fabrication can affect CGR in weld metals in several ways, such as by their effects on residual stresses, local material composition, strength level of the weld material, microstructure, and presence of micro-flaws.

Residual Stresses. It is considered that residual stresses associated with welding have a strong influence on PWSCC CGR because residual stresses often are a strong contributor to the stress intensity factor at crack tips within the welds—and laboratory tests have shown the crack-tip stress intensity factor to be a key parameter. The residual stress in a weld is a function of welding parameters such as number of passes, heat input during each pass, performance of repair welds, and the degree of restraint of the weld joint, i.e., the resistance to deformation and relief of stresses caused by weld shrinkage as the weld metal cools. Highly restrained welds generally have high levels of residual stresses. Stress relief heat treatments at about 600°C (1112°F) have been shown to relieve surface stresses, but apparently have little effect on deep-seated residual stresses in welds made with Alloy 182 [16].

Local Material Composition. Depending on welding conditions, the chemical content of regions of a weld adjacent to a base metal with lower alloy content may be significantly affected by dilution from the base metal. The extent of dilution depends upon a number of factors, such as the type of welding, heat input, amount of base metal penetration, groove shape, etc. There are no known reports of this type of dilution being important to CGR in Alloy 82/182/132.

Strength Level. Tests of wrought material indicate that the CGR increases as the strength level of the material is increased, e.g., by cold working [25,26]. It is expected that this same effect applies to weld materials, i.e., crack growth rates are expected to increase as the material's yield and tensile strength are increased. The strength level of the weld metal may be somewhat affected by the residual strain in the weld, which is controlled by the restraint level of the weld joint design. It also can be affected by dilution of carbon content from the low-alloy steel, and by grain size. These factors depend on the weld joint design and on welding conditions such as joint restraint and groove shape, heat input, and dilution. Thus, the effect of strength level on CGR of weld metals is expected to be controlled by the same array of parameters as those that control microstructure and local material composition.

Microstructure. As discussed in Section 2.1, the microstructure of Alloy 82/182/132 is complex. The major feature consists of dendritic grains, where high-angle grain boundaries separate colonies of similarly oriented dendrites. The grain structure is anisotropic with columnar grains aligned in the weld root-to-crown direction and slightly inclined in the welding direction. In the as-welded condition, grain boundaries usually have a wavy or convoluted shape that results from impingement of dendrite colonies as the weld metal solidifies. Dendrites within the grains, which form parallel to the direction of heat flow during solidification, have a cored, compositionally segregated, structure. The interdendritic regions tend to have increased concentrations of niobium and manganese and a high density of micron-size inclusions.

PWSCC in Alloy 82, 182 and 132 welds involves an intergranular (IG) cracking mechanism, whereby cracks propagate along high-angle grain boundaries [10,27,28]. Recent work [29] has shown that susceptible boundaries have to be not only high-angle, but also high-energy, i.e., even high-angle boundaries may not crack if they exhibit lattice site coincidence. Cracks in welds usually have an undulating or wavy character that reflects the wavy morphology of the grain boundaries.

Crack advance in as-welded specimens is very uneven, especially in the rapid growth direction parallel to the direction of dendrite growth. Stress corrosion cracking fingers extend out beyond the main crack as intergranular cracks initiate and propagate along the most susceptible grain boundaries. In tests, unbroken ligaments often form in the wake of advancing crack fronts because the most SCC-resistant boundaries tend not to fail, although testing techniques may be optimized to minimize this tendency. In some regions, uncracked ligaments can be massive and extend back to the fatigue precrack commonly used in CGR testing, thereby resulting in incomplete "engagement" of the stress corrosion crack to the precrack over the full width of the specimen. Such uneven crack fronts and incomplete engagement of stress corrosion cracks are sources of potential uncertainty in making laboratory measurements of CGR for welds. These issues are addressed in more detail in Section 3.4 and Appendix D.

Appendix A provides a more in depth discussion of the microstructure and SCC cracking mechanisms affecting Alloy 82, 182 and 132 welds.

Weld Defects. Micro-fissures and other weld defects such as pores and slag inclusions are often present in Alloy 82/182/132. The possibility of latent micro-fissures being present is dependent primarily upon the hot and ductility-dip cracking susceptibility of the weld metal, the weld joint design (e.g., degree of restraint), welding parameters such as heat input and number of passes, and welder skill. It can also be affected by the presence of impurities such as phosphorous, sulfur, and minor elements such as silicon. The influence of these factors on the possibility of micro-fissures being present is discussed in Appendix A.7.

The PWSCC CGR in the weld metal could plausibly be affected by these latent defects, especially micro-fissures. However, as also discussed in Appendix A.7, recent investigations indicate no discernable effect of hot or ductility-dip cracking on PWSCC. On the other hand, relatively large and sharp defects such as some lack of fusion areas could potentially promote PWSCC as a stress concentrator and source of increased stress intensity factor (see Section 3.1.7).

3

CRACK GROWTH RATE TESTING TECHNIQUES AND DATA SCREENING

3.1 Specimen Manufacture

Special purpose welds were typically fabricated to make compact tension (CT) specimens for conducting crack growth rate tests for nickel-based alloy welds used in PWR applications. The majority of the specimens included in the Alloy 82/182/132 crack growth rate database were manufactured using a single side V-shaped butt weld preparation. Weld fabrication details can affect the weld metal microstructure and mechanical properties, as discussed in Section 2 and Appendix A. Ideally, consideration should be given to the impact of these details on the crack growth data and careful characterization of the weld microstructure and properties should be provided, although that was not always the case with the database considered here. However, for the present purpose of establishing a generic crack growth rate equation for application to Alloy 82/182/132 weld metals, it is sufficient to note that test specimens were usually manufactured from a butt weld configuration similar to that commonly used in plants, and that the welding parameters corresponded to normal industry practice with attention given to:

- Base metal chemistry and simulated weld joint design
- Weld wire/stick chemistry
- Welding parameters including heat input, travel speed and weld bead dimensions
- Solidification direction and weld dendrite direction
- Restraint
- In process NDE
- Various types of solidification cracking or ductility-dip cracking and
- Post-welding heat treatment (PWHT)

Each of these factors is discussed in relation to the manufacture of the crack growth rate database specimens together with discussion of general considerations regarding their possible effects on the stress corrosion cracking rates determined by tests of the specimens.

3.1.1 Simulated Weld Joint Design

Alloy 182/132 welds are typically laid down using a manual metal arc process. Alloy 82 welds may be applied using either a manual or an automatic tungsten inert gas (TIG) or metal inert gas (MIG) process. Simple sketches of joint geometry used for fabricating crack growth test specimens are shown in Figures 3-1 and 3-2. The test weld block shown in Figure 3-1 is made with two plates and a backing strip. For this geometry, each plate can be clamped to add constraint to the test weld. The test weld block shown in Figure 3-2 is made from a single plate, and it is difficult to add constraint to this test weld. Weld shrinkage strains introduced during cooling may deform both the weld and base metal and induce weld residual stresses and strains.

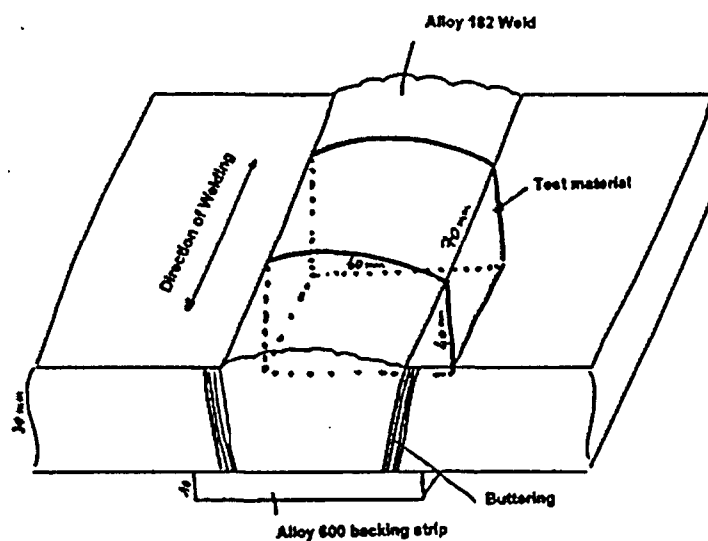


Figure 3-1
Example of an Alloy 182 Test Weld Block Made With Two Plates and a Backing Strip [6]

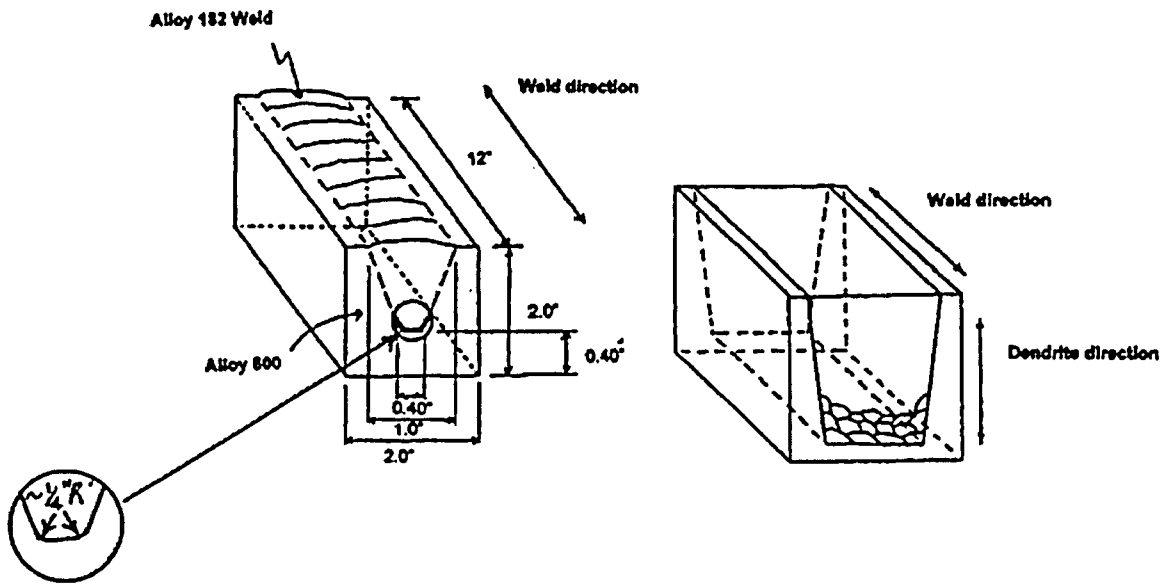


Figure 3-2
Example of an Alloy 182 Test Weld Block Made With a V-groove In a Single Plate [6]

3.1.2 Weld Chemical Composition

Table 3-1 lists as-deposited composition data for the Alloy 82/182/132 welding material test specimens directly applied in the development of the MRP-115 deterministic CGR model in Section 4.² The corresponding American Welding Society (AWS) chemical composition specification ranges are also listed in the table. Test specimen fabrication utilized typical vendor fabrication practices and ASME/AWS specified weld metals and are thus considered representative of the weld materials in operating PWRs.

3.1.3 Solidification Direction and Weld Dendrite Direction

As-welded structures in these nickel-based alloy welds have a dendritic substructure. Dendrites tend to nucleate epitaxially on the underlying solidified metal giving rise to a marked macroscopic texture from the bottom to the top of the weld, as discussed in Section 2 and in more detail in Appendix A. The grain structure is anisotropic as columnar grains form parallel to the heat flow direction, which is approximately normal to the welding direction. The dendrites tend to grow parallel to each other in packets. With time and in competition, dendrites overlap and form mainly high angle grain boundaries between dendrite packets. Stress corrosion cracks generally follow the high angle, high energy boundaries. However, as discussed in Section 2 and Appendix A, some high angle boundaries are low energy and resistant to crack propagation.

² The composition data in Table 3-1 are based on the as-deposited condition except for the weld PP751 tested by Westinghouse and for the three welds tested by Studsvik for which composition data were provided for the weld wire/stick material.

The above described situation is shown schematically in Figure 3-3 [11]. In Figure 3-3, the dendrites are growing perpendicular to the groove wall and intersecting near the middle of the weld, where they form a high energy solidification grain boundary. This situation is somewhat different than that shown in Figure 2-1 where, because of different groove geometry, the dendrite growth was more nearly vertical. The boundaries between individual dendrites are called solidification subgrain boundaries and are typically low energy boundaries. Where the dendrites intersect or overlap, solidification grain boundaries form. In multipass welds, the SGBs can migrate on cooling after solidification and during re-heating and result in a straighter, migrated grain boundary.

Despite the different geometries, in both cases high energy grain boundaries form at the locations where different packets of dendrites meet, and it is at these grain boundaries that PWSCC most readily occurs. Figure 3-4 is a micrograph of an actual weld that further illustrates the microstructure and the high energy grain boundaries where PWSCC mainly occurs.

Table 3-1
Compositions of the Test Materials Used for Crack Growth Rate Tests (MRP Database After Screening)

Test Organization	Alloy	Weld ID	Producer	Ref.	Ni	Cr	Fe	C	Mn	Cu	Si	Co	S	P	Ti	Nb+Ta
Specifications	600	Spec.	ASTM B166/B167	30	72.0 min	14.0-17.0	6.0-10.0	0.15 max	1.0 max	0.50 max	0.50 max	n/a	.015 max	—	—	—
	600	Typical	—	—	73.07	15.69	9.65	0.033	0.78	0.02	0.29	0.18	0.001	0.009	—	—
	182	Spec.	AWS ENiCrFe-3	31	59.0 min	13.0-17.0	10.0 max	0.10 max	5.0-9.5	0.50 max	1.0 max	0.12 max	.015 max	0.03 max	1.0 max	1.0-2.5
	132	Spec.	MHI	28	68.0 min	13.0-17.0	11.0 max	0.08 max	2.0-3.5	0.50 max	0.50 max	n/a	.015 max	.015 max	—	1.5-4.0
	132	Spec.	AWS ENiCrFe-1	31	62.0 min	13.0-17.0	11.0 max	0.08 max	3.5 max	0.50 max	0.75 max	n/a	.015 max	.03 max	—	1.5-4.0
	82	Spec.	AWS ERNiCr-3	32	67.0 min	18.0-22.0	3.0 max	0.10 max	2.5-3.5	0.50 max	0.50 max	n/a	.015 max	0.03 max	0.75 max	2.0-3.0
	82H	Spec.	AWS ERNiCr-3	32	67.0 min	18.0-22.0	3.0 max	0.03-0.10	2.3-3.5	0.50 max	0.50 max	n/a	.015 max	0.03 max	0.75 max	2.0-3.0

Content Deleted – MRP/EPRI Proprietary Material

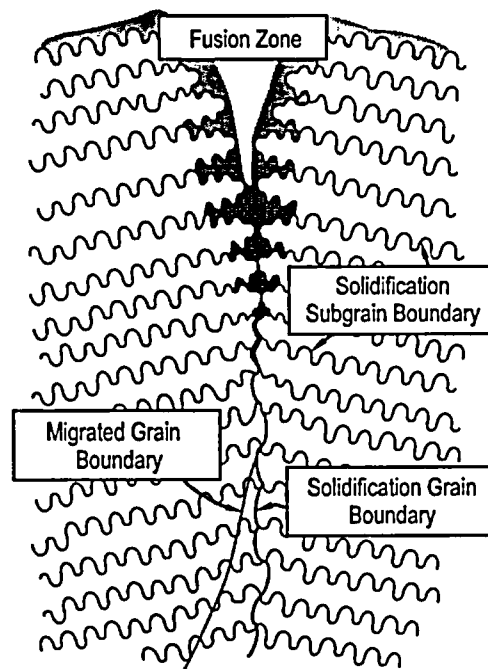


Figure 3-3
Sketch Showing Various Kinds of Grain Boundaries in Weld Metals [11]

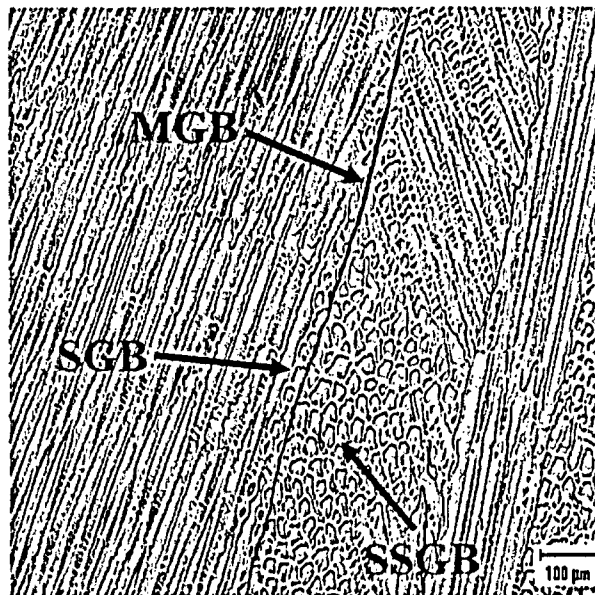


Figure 3-4
Micrograph Showing Various Kinds of Grain Boundaries in Weld Metals (Courtesy of Ohio State University [11])

3.1.4 Convention Used for Identifying Crack Orientation

Because CGR is strongly affected by the direction of crack orientation relative to the microstructure, it is important during tests to identify and control the direction of crack growth relative to the microstructure. The convention used for identifying crack orientation relative to weld fabrication, and thus relative to weld microstructure, is illustrated in Figure 3-5 [6].

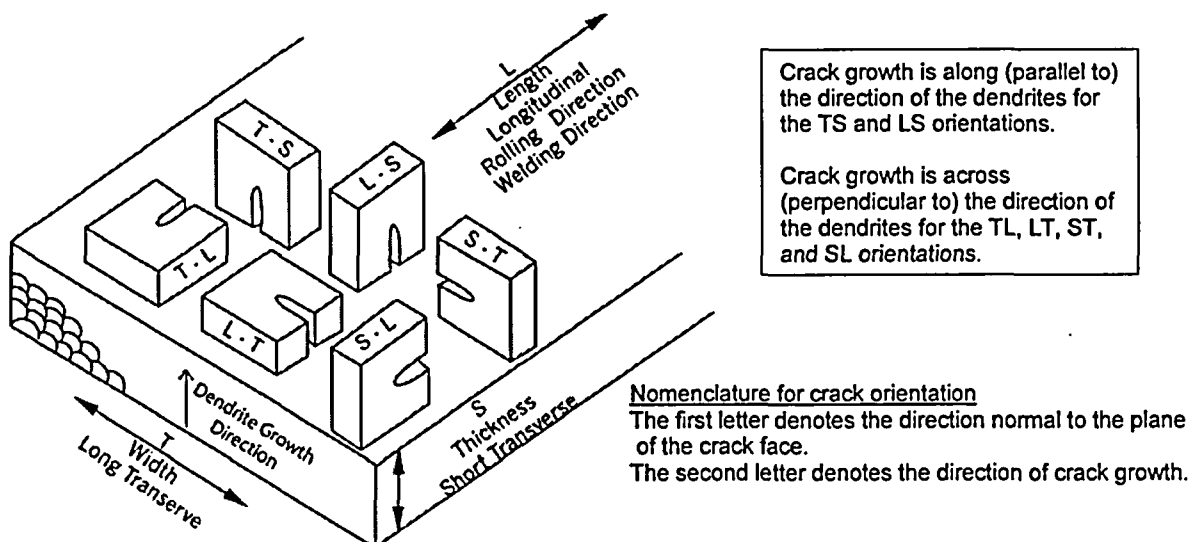


Figure 3-5
Terminology Used for Orientations of Cracks in Test Specimen With Respect to Welds [6]

3.1.5 Restraint

Nickel-based alloys and the other structural materials used with these welding materials start to liquefy when heated in the range from approximately 1350 to 1450°C. When welds start to cool from these elevated temperatures, significant levels of thermal displacements are involved which can lead to considerable stresses and strains. These stresses and strains depend on the degree of mechanical constraint in the weld and are usually sufficient to plastically deform the underlying weld metal as well as the base metal. A J-groove weld will normally be much more constrained than a butt weld. The resulting solidification-strain-induced stresses are considered likely to make the material more susceptible to stress corrosion cracking, and it is also possible that the weld shrinkage strains increase the strength of the weld metal somewhat and thereby have some effect on CGR. Estimates of the residual stresses present in and adjacent to the weld can be determined by various techniques such as X-ray diffraction or finite element analyses, and estimates of material strengthening can be determined by mechanical tests, such as hardness and tensile tests.

The stresses and strains induced during the welding process take the form of macroscopic, local residual stresses and strains as well as microscopic strains at the grain boundaries. Accounting for effects of restraint induced stresses and strains on CGR in test specimens and in plants is normally addressed as follows.

Content Deleted – MRP/EPRI Proprietary Material

3.1.6 In-Process NDE

The ASME Boiler and Pressure Vessel Code set requirements for in-process NDE of PWR pressure boundary welds. Typically, pressure boundary full penetration plant welds (ASME Division III, Class 1 components) required radiography and surface examination, and then repair as necessary. Typically, pressure boundary partial penetration plant welds (ASME Division III, Class 1 components) required progressive surface examination during welding and surface examination subsequent to welding as such weld geometries were typically not amenable to meaningful volumetric examination. Early ASME Code versions required progressive surface examinations in increments of weld deposit of the lesser of $\frac{1}{3}$ the weld thickness or $\frac{1}{2}$ inch, whichever was less, whereas later Code versions changed the " $\frac{1}{3}$ thickness" requirement to " $\frac{1}{2}$ thickness." Unacceptable defects were ground out as required before proceeding to deposit subsequent layers.

Because of the favorable laboratory conditions under which test specimens are fabricated, and because there is better access for NDE and for repair of test specimens, it is considered that the typical quality of welds in test specimens may in general be better than that of typical plant welds. However, even under ideal welding conditions some defects are expected, and test laboratories have reported the presence of defects in some laboratory test welds. There are currently no universal standards for in-process NDE of test welds although many test laboratories use test welds produced according to standard plant welding procedures.

3.1.7 Weld Defects

As discussed in Section A.7 in Appendix A, nickel-based welds made with Alloys 82/182/132 can be affected by various forms of solidification cracking, liquation cracking, and ductility-dip cracking during manufacture. The first two occur when low melting point phases form during the last stages of solidification or during reheating due to elemental segregation. Solidification cracking and liquation cracking are often collectively known as hot cracking since these types of cracking occur near the completion of solidification. By contrast, ductility-dip cracks are solid-state intergranular defects that form in heavily restrained welds due to a high-temperature ductility loss, and as such are distinct from "hot cracks."

Modifications in welding consumables and procedures have very much improved resistance to solidification and liquation cracking. Ductility-dip cracking is different in that no low melting point phases seem to be involved and it is sufficient to apply strain above a given threshold in specific temperature ranges during cooling for high angle, high energy grain boundaries to separate [11,43]. Ductility-dip cracking is thus a practical problem in welds with high mechanical constraint. In the case of butt welds made with low constraint and in the absence of excessive dilution with stainless or low-alloy steels, the risk of macroscopic ductility-dip cracking occurring is considered low.

In summary, processes such as ductility-dip cracking can be expected to produce subsurface weld defects or surface defects small enough to be accepted for service during pre-service NDE. It is seemingly plausible that weld defects such as hot cracking or ductility-dip cracking could affect the CGR in those welds. However, recent investigations appear to provide convincing evidence that such weld defects do not play a significant role in PWSCC initiation and propagation. Thomas, et al. [27] have performed detailed microscopic characterization work on cracked Alloy 182 samples from the Ringhals Unit 4 plant in Sweden showing no significant interaction between stress corrosion cracks and hot or ductility-dip cracks. In a recent MRP-sponsored experimental program using Alloy 182 weld material formed into pressurized test capsules [29], there was also reported no significant effect of hot or ductility-dip cracks on the PWSCC process. These results are not surprising if one considers the fundamental differences in the current mechanistic understanding of PWSCC (see for example Scott and Combrade [44]) compared to the mechanisms of hot cracking and ductility-dip cracking.

Finally, it should be mentioned that relatively large and sharp weld defects such as some weld lack of fusion regions may have the potential to promote PWSCC by creating a local stress concentrator and a high local crack tip stress intensity factor. Lack of fusion areas at the weld wetted surface would be expected to be detected during pre-service NDE. Such subsurface defects would necessarily have to become wetted by the primary coolant through some cracking

process before they could grow via PWSCC. Potential types of cracking to cause a subsurface lack of fusion region to become wetted include ductile tearing, environmental or mechanical fatigue, and PWSCC (from the wetted surface). Although there is not universal agreement among experts, it is possible that at least some of the cracking observed in Bottom Mounted Instrumentation nozzles at South Texas Project Unit 1 in 2003 may have been promoted through the wetting of subsurface weld lack of fusion areas [45,46,47].

3.1.8 Post-Welding Heat Treatment

Post-weld heat treatment of the buttering used in primary weld preparations is standard practice, and PWHT is in some cases also performed on the filler metal following final welding. In addition, PWHT of some nickel-based weld metals often occurs indirectly as a consequence of stress relief heat treatments performed on adjacent low-alloy steel components per ASME Code requirements. In these latter cases, the stress relief temperature is well below that which would be optimum for nickel-based alloys.

Investigations of welded mock-ups have shown that surface strains and stresses of (surface ground) Alloy 182 welds seem to be relaxed significantly but not in the bulk weld metal [16].³ The same study indicated that such heat treatments can sometimes improve the stress corrosion resistance of Alloy 182, particularly for batches with high carbon contents—although the effect is limited to the reduction in stress and has no apparent impact on the intrinsic stress corrosion resistance of the material. Another study examined this issue and reported that there was a slightly beneficial effect of PWHT (by a factor between two and four) on CGRs measured for four weld metals with various carbon and silicon contents [20]. Based primarily on these data, Le Hong et al. [9] recommend that CGRs be reduced by a factor of 2.0 for stress relieved specimens compared to otherwise similar as-received specimens.

The influence of various post-weld heat treatments on the intergranular stress corrosion cracking (IGSCC) behavior of Alloy 182 under boiling water reactor (BWR) normal water chemistry (NWC) conditions was examined in an extensive program, carried out by Ljungberg et al., which also examined many other variables such as alloy composition and water impurities. No clear conclusions were drawn from CGR measurements with regard to this factor [48], but long term exposure of blunt-notched compact tension specimens in an operating reactor revealed a higher susceptibility to crack initiation in the as-welded condition than after PWHT [49].

For all of the test specimen crack growth rate data directly applied in the development of the deterministic CGR model for Alloy 82/182/132 welds in Section 4, no stress relief was applied to the test welds.

³ Briant and Hall [41] have reported that PWHT produced more precipitation of gamma prime in the Alloy 182 weld metal, and caused chromium depletion in some cases.

3.1.9 Crack Front Patterns

CGR specimens for Alloy 82/182/132 weld metals often exhibit irregular crack fronts, with regions of non-engagement (no SCC crack initiation) and with large differences in the extent of SCC crack growth. Photomicrographs of example fracture surfaces that illustrate the variety of crack front types that can occur are shown in Figures 3-6, 3-7 and 3-8 (taken from Appendix D). These figures reflect test specimens that are included in the MRP database (Table 4-1).

Figure 3-6 illustrates a case where the crack front is moderately well behaved, i.e., it is not very irregular. Figure 3-7 represents a more typical case where the crack front is irregular, with some large areas exhibiting no SCC crack growth. Figure 3-8 illustrates a case with a highly irregular crack front. Other examples are included in Appendix D, and approaches for evaluating CGRs in the context of irregular crack growth behavior are discussed in Section 3.4 and Appendix D.

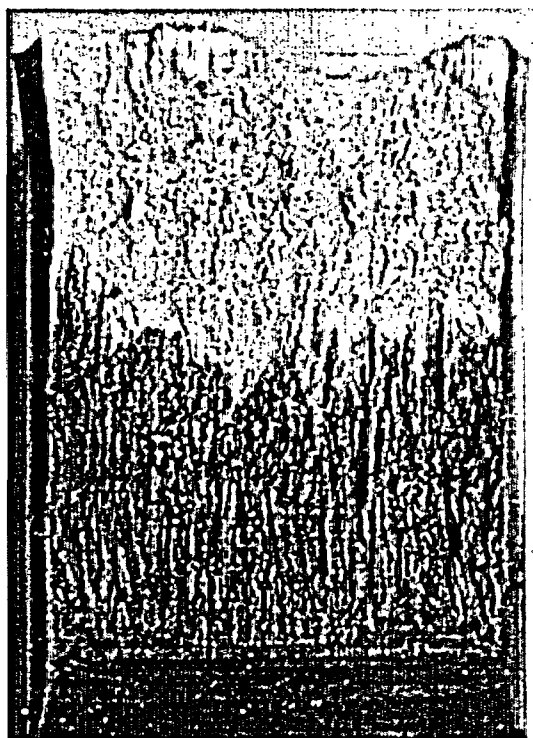


Figure 3-6
Example of a Fracture Surface of Alloy 182 Weld Metal With Moderately Uniform Crack Front

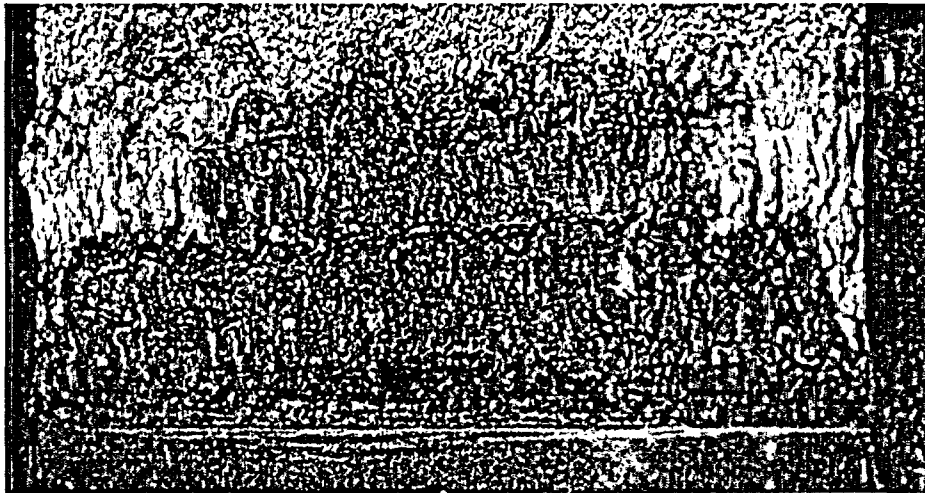


Figure 3-7
Example of a Fracture Surface of Alloy 182 Weld Metal With Irregular Crack Front



Figure 3-8
Example of a Fracture Surface of Alloy 182 Weld Metal With Highly Irregular Crack Front

3.2 Specimen Loading

The welding specimens applied directly in Section 4 to develop the MRP-115 CGR model (Table 4-2) reflect a number of loading variables, including stress intensity factor, cyclic loading parameters, and weld orientation. As shown in Table 4-2, test results in the database reflect the following:

- Stress intensity factors ranging from 19.7 to 60.0 MPa√m for Alloy 182/132 specimens and from 28.0 to 56.8 MPa√m for Alloy 82 specimens (see Figures 4-3 and 4-4).
- A combination of constant loading and cyclic loading. Cyclic loading parameters include load ratios, R , between 0.65 and 0.75 and hold times between 6000 and 100,000 s.
- Three of the six possible weld orientations (TS, LS, and TL). TS and LS represent orientations where crack growth is parallel to the direction of the weld dendrites, and TL represents an orientation where crack growth is across (perpendicular to) the direction of the dendrites.

Sections 3.2.1 through 3.2.3 below identify key issues associated with controlling specimen loading parameters during CGR testing. Further details and testing recommendations are provided in Appendix B.

3.2.1 Specimen Loading Considerations

During CGR testing, addressing the following issues can yield more consistent and meaningful test results:

- Application of a stress intensity factor within accepted limits. All of the laboratories that contributed CGR data to the MRP database in Section 4 applied linear elastic fracture mechanics (LEFM) validity criteria to their data (e.g., ASTM E399 and E647).
- Use of side grooving to maintain the crack plane
- Limiting variation in the stress intensity factor during “constant load” testing
- Use of cyclic loading to maintain a straight crack front

3.2.2 Fatigue Precracking

In order to facilitate accurate PWSCC CGR measurements, a transgranular fatigue precrack is generated first in order to provide an initiation line for the PWSCC growth mechanism. Precracking issues which must be considered include:

- The length of the precrack
- The stress intensity factor generated during precracking
- The loading details associated with the precrack, including load ratio (R) and environment (air vs. *in situ*)

3.2.3 On-line Crack Monitoring

Continuous crack monitoring is a valuable tool which can: 1) aid in determining when SCC initiated from the fatigue precrack, and 2) assist in estimating CGRs during different phases of multi-condition testing. The most commonly used technique for such monitoring is reversed DC potential drop. Some of the issues that affect how, and whether, the results of on-line monitoring are used in developing CGR data include:

- The straightness of the crack front
- Crack front unevenness (often significant with Alloy 82/182 weld metal)
- The degree of disagreement between the online monitoring results and post-test fractography
- Minimum acceptable crack increments

3.2.4 Other Testing Factors

There are other testing factors that must also be considered, including:

- Careful control and documentation of machining, surface condition (e.g., to obtain proper corrosion potentials), and pre-oxidation in high temperature water
- Control of test temperature, with stability ideally within $\pm 0.5^\circ\text{C}$.
- Control and monitoring of water purity and dissolved gas chemistry.
- Measurement of the corrosion potential of the CT specimen and a platinum electrode.

3.3 Test Environment

The environments for the tests that developed the data used in this report are shown in Table 3-2. As shown in Table 3-2, all of the environments were hydrogenated high-temperature water, often with lithium and boric acid additions to simulate the PWR primary coolant environment. Concentrations of impurities such as chlorides and sulfates were limited to low levels. The temperature range covered was 280 to 360°C. Because of the sensitivity of PWSCC CGRs to the hydrogen concentration, special care was taken to screen out data from tests where careful control of hydrogen was not ensured.

Table 3-2
Environments Used for Crack Growth Rate Tests (MRP Database After Screening)

Test Org.	Weld ID	Temp. (°C)	LI (ppm)	B (ppm)	Dissolved Hydrogen (cc(STP)/kg H ₂ O) ³	Ref.
Westinghouse	D545/D582, 33644, PP751	323–342	2.0	1200	25	[6]
Studsvik	26B2	343, 345	2.0, 2.2	1202–1273	28.8–30.4	[33]
Studsvik	6892	343	2.2	1212	29.5	[34]
Studsvik	WC05F8	319	2.28	1297	29.6	[34]
Bechtel Bettis	A-1, C-1, C-2, C-3, C-4	338	Note 1	Note 1	50	[10]
LM KAPL	LM 182-1	328	Note 2	Note 2	35	[37]
LM KAPL	LM 182-2	338	Note 2	Note 2	40	[37]
LM KAPL	LM 82-1	360	Note 2	Note 2	40	[37]
LM KAPL	LM 82-2	338	Note 2	Note 2	20, 40	[37]
LM KAPL	LM 82-3	316–360	Note 2	Note 2	30–40	[37]
MHI	MG-7, 132 Heat	325	3.5	1800	30	[28]

Notes:

- 1) High temperature hydrogenated water with a room temperature pH of 10.1 to 10.3
- 2) High temperature hydrogenated water with a high temperature pH of 6.6
- 3) The unit for dissolved hydrogen of cc(standard temperature and pressure (STP))/kg H₂O is abbreviated as cc/kg in the text

3.4 Derivation of Crack Growth Rate Considering Uneven Crack Fronts

Alloy 82/182/132 weld specimens tend to exhibit uneven stress corrosion cracks, which introduce uncertainty into crack growth rate measurements. For specimens with small to intermediate amounts of SCC, it is common for intergranular cracking in these materials to incubate along the transgranular (TG) fatigue precrack front nonuniformly versus test time, so that only portions of the crack front may exhibit IG cracking in limited duration tests. Even when intergranular cracks are almost fully engaged, fingers of SCC often jut out beyond the overall crack front, thereby demonstrating the heterogeneous nature of SCC in these weld metals.

The incomplete engagement and uneven crack front issues are important because they can introduce a bias in CGR measurements. Because these issues are complex, there is no single approach for assuring that the bias is removed from the CGR database. Specific analysis methods designed to account for incomplete engagement and uneven crack fronts were proposed and debated in detail at the EPRI-MRP CGR Expert Panel meetings. Two points of view concerning this issue are provided in Sections D.1 and D.2 of Appendix D. The fundamental difference in these views involves the underlying cause of the absence of crack incubation in some regions. At present, it is not known if the non-incubated regions are associated with “pinned” transgranular fatigue precracks, with regions with enhanced SCC resistance, or with a combination of both effects. These differences are important because they govern how the unengaged and shallow crack extension regions are treated when calculating average CGR. It is noteworthy, however, that the issue of engagement is quantitatively less important for average crack lengths of more than about 2 mm as discussed in Appendix H.

While no consensus was reached concerning computational methods that address the incomplete engagement and uneven crack front issues for future testing, a consensus was reached on how to address this issue in the existing CGR database. Specifically, there was agreement that including the zero-crack extension values within the unengaged portion of the precrack produces non-conservative CGR estimates. To address this problem, the EPRI-MRP CGR Expert Panel agreed that it is appropriate that the average crack extension used to compute CGR be based solely on the engaged segments of the stress corrosion crack (i.e., a simple average of all non-zero crack extension values). In addition, data points with less than 50 percent engagement and less than 0.5 millimeters of average crack extension were excluded from the screened database. See Section D.3 for additional discussion.

3.5 Screening Criteria

The starting point for screening the available stress corrosion crack growth database for nickel-based welds Alloy 82/182/132 was the same as that adopted for the earlier MRP-55 [3] study of Alloy 600. The EPRI expert panel for PWSCC revised those screening criteria in consideration of the issues that are particularly relevant to weld metals, and Table 3-3 lists the key factors that were considered during the screening process for the Alloy 82/182/132 weld CGR data.

Table 3-3
Key Factors for Consideration in CGR Testing and Data Reporting

1	Material within specifications including composition/condition/heat treatment
2	Mechanical strength properties
3	ASTM specimen size criteria and degree of plastic constraint
4	Pre-cracking technique (including straightness criteria, plastic zone size, crack morphology)
5	Special requirements for testing welds (e.g. pre-crack location, residual stresses/strains)
6	Environment (chemistry, temperature, electrochemical potential (ECP), flow rate at specimen, neutron/gamma flux)
7	Loop configuration (e.g., once-through, refreshed, static autoclave)
8	Water chemistry confirmation by analysis (e.g., Cl, SO ₄ , O ₂ , Cr, total organic carbon (TOC), conductivity)
9	Active constant or cyclic loading versus constant displacement loading (e.g., using wedge)
10	On-line measurement of crack length versus time during test (including precision)
11	Actual crack length confirmed by destructive examination (assessment method/mapping)
12	Appropriateness of crack characteristics (fraction SCC along crack front, uniformity, adequate SCC increment, transgranular portions within IGSCC fracture surface, etc.)
13	Possible effects of changes in loading or chemistry conditions during a test (including heat up and cool down)
14	Calculation and reporting of K or ΔK values
15	Reporting of raw a vs. t data and derivation of da/dt values
16	Reproducibility of data under nominally identical test conditions

It should be noted that the main reasons leading to exclusion of Alloy 600 data from further consideration in the MRP-55 study were:

- No measurable growth
- Less than 50% of crack front with IGSCC initiated (called hereafter “engagement”) or lack of crack front mapping to enable this feature to be assessed and average growth rates to be calculated in addition to the maximum rates supplied
- Out of specification PWR primary water chemistry (particularly hydrogen)
- Cyclic or ripple loading with less than 1 hour hold time at constant load during each cycle.

A similar pattern emerged for the nickel-based weld metal Alloys 82/182/132 with the addition of a few instances of data rejected because of loading beyond LEFM criteria. However, the second criterion listed above relating to crack engagement assumed much increased importance for the weld metals. Due to difficulties with lack of uniform crack initiation from starter fatigue cracks and the development of irregular crack fronts discussed in detail in Appendix D, an additional requirement to that of greater than 50% engagement used here was a minimum crack growth increment averaged across the specimen width (Δa_{ave}) of at least 0.5 millimeters. A sensitivity study established that the precise choice of the Δa_{ave} cutoff used as the screening criterion did not have an arbitrary influence on the acceptable screened data set and the eventual outcome of the data analysis (see Appendices G and H). Appendix F shows a summary table of the available worldwide database for the nickel-based welds including the main reasons why certain data points in each set were screened out from direct use in the development of the MRP

crack growth equation. The excluded data are compared with the MRP-115 recommended CGR in Section 5.1.4.

A detailed treatment of hydrogen effects, which are known to be potentially significant for crack growth in nickel-based weld metals, was not possible with the limited number of results contained in the screened database. It was noted, however, that one set of KAPL data which apparently illustrates a significant K_I dependency actually resulted more from testing at two distinct H_2 levels. This topic is addressed in detail in Appendix C.

4

MRP DATABASE AND DERIVATION OF CGR CURVES

4.1 Development of MRP Database for Alloy 82/182/132

The set of available worldwide data for Alloy 82/182/132 CGRs measured under PWR primary water conditions using controlled fracture mechanics specimens is summarized in Table 4-1. This table identifies the test organizations, weld IDs, alloy type, reasons for screening points out of the MRP database, type of loading used, and range of reported percentage engagement to IGSCC. Table 4-1 also summarizes the practice used by each test laboratory to calculate the CGR based on the crack increment averaged across the test specimen or based on the maximum crack increment. In Section 3, Table 3-1 identifies the weld compositions, and Table 3-2 lists the chemical environments including test temperature.

The complete MRP database of CGR data for Alloys 82, 182, and 132 after application of the screening process discussed in Section 3.5 is presented in Table 4-2. The data that were excluded from consideration in the development of the MRP-115 deterministic CGR model are documented in Appendix F, including listing of the reason or reasons that each data point was excluded. Note that the MRP expert panel concluded that Alloy 182 and Alloy 132 should be regarded as sufficiently similar to be described by one CGR curve.

Figure 4-1 is a CGR versus stress intensity factor plot showing the complete set of available data for which average CGRs were reported, adjusted to a common reference temperature of 325°C assuming a thermal activation energy of 130 kJ/mole (31.0 kcal/mole). This is the same activation energy that was applied to the CGR data for Alloy 600 in MRP-55 [3]. The expert panel judged that there were insufficient data to develop reliable activation energy values for Alloy 182/132 and for Alloy 82, so the reliable activation energy value for Alloy 600, which has a similar composition, was recommended for use with Alloys 82, 182, and 132. Multiple independent studies of Alloy 600 have resulted in thermal activation energy values within about 10–15% of the value of 130 kJ/mole (31.0 kcal/mole) [3]. (See Appendix C.2 for a discussion of the sensitivity to temperature of the CGR data for Alloys 82, 182, and 132 in the context of the effect of dissolved hydrogen concentration.)

Figure 4-2 is the corresponding plot for the available data for which CGRs based on the maximum crack increment across the specimen width were reported. Finally, Figures 4-3 and 4-4 show the average CGR data in the MRP database following the screening process; Figure 4-3 shows the data for Alloys 182 and 132, and Figure 4-4 shows the data for Alloy 82. Note that for reference purposes, two previously applied CGR curves are shown in Figures 4-1 through 4-4. The MRP-21 [6] curve for Alloy 182, published in 2000, was based on the smaller set of data available at the time it was developed, and it did not result from a systematic statistical assessment. The MRP-55 [3] curve for Alloy 600 thick-wall material was published in 2002 and

is currently being used to disposition in-service flaws and in safety assessments of hypothetical flaws.

4.2 Data Reduction

The statistical methodology for developing the deterministic CGR equation for Alloy 82/182/132 weld metal is described below. The procedure is similar to that presented in MRP-55 [3] for Alloy 600 wrought material, but includes a linearized multiple regression model in order to determine a best-fit stress intensity factor exponent, β , while still treating the data on a weld-by-weld basis:

1. Collect data including reported initial or average K , CGR based on the crack increment averaged across the entire specimen width, average crack increment, test temperature, and percentage engagement of the crack front to IGSCC (%eng).

As discussed in Appendix H, average CGR data were used rather than the maximum measured CGR across the specimen width because it is believed that the average CGR is a better measure of the fundamental material behavior, whereas the maximum CGR is more dependent on the spatial variability in resistance to PWSCC. In addition, the maximum CGR appears to be more dependent on test duration than the average CGR; Figure H-1 in Appendix H shows that crack depth unevenness is usually not greater than 2 mm beyond the average depth and very occasionally up to 4 mm. Finally, it is standard practice in fatigue testing of CT specimens to average the crack extension across the specimen width [63].

2. Perform data screening using the key factors listed in Table 3-3.
3. Modify the reported CGR to account for the effect of incomplete initiation of PWSCC across the crack front by dividing by the fraction engagement as discussed in Appendix D:

$$CGR' = \frac{CGR}{\left(\frac{\%eng}{100}\right)} \quad \text{Equation 4-1}$$

4. Adjust the data to a common reference temperature of 325°C using an activation energy of 130 kJ/mole (31.0 kcal/mole).
5. Assume no stress intensity factor threshold for PWSCC of the weld metals (i.e., $K_{th} = 0$). The EPRI expert panel for PWSCC concluded that, for the weld metal materials, there were insufficient data to justify a stress intensity factor threshold other than zero (see Appendix E).
6. Assume the following form to model the set of screened average CGR data:

$$\frac{CGR'}{f_{temp}} = \alpha f_{weld} f_{alloy} f_{orient} K^\beta \quad \text{Equation 4-2}$$

where

α = power-law constant

f_{temp} = factor adjusting CGR to common reference temperature of 325°C

- f_{weld} = common factor applied to all specimens fabricated from the same weld to account for weld wire/stick heat processing and for weld fabrication (serves the same function as the heat factor (f_{heat}) applied in MRP-55 [3] to all specimens fabricated from the same heat of Alloy 600 wrought material to account for the effect material processing differences on the CGR)
 f_{alloy} = factor accounting for effect of composition difference between Alloy 182/132 and Alloy 82 (taken as 1.0 for Alloy 182/132)
 f_{orient} = factor accounting for difference in CGR resulting from crack growth perpendicular to the direction of the weld dendrites versus parallel to the direction of the dendrites (taken as 1.0 for the "parallel" case)
 K = crack tip stress intensity factor
 β = power-law exponent
7. Linearize the assumed form of the CGR equation by taking the natural logarithm of the adjusted CGR.
 8. Perform a least-squares multiple linear regression fit treating the weld factor (f_{weld}) as a normally distributed random variable.
 9. Choose the alloy factor (f_{alloy}) for Alloy 82 based on the value that makes the log-mean for the set of weld factors for Alloy 182/132 welds equal to the log-mean for the set of weld factors for the Alloy 82 weld.
 10. Determine the orientation factor (f_{orient}) for crack growth in the direction perpendicular to the weld dendrites (TL, LT, ST, SL) versus growth parallel to the dendrites (TS, LS) based on the best-fit from the regression model.
 11. Similar to the procedure in MRP-55, base the deterministic CGR equation on the 75th percentile of the log-normal distribution for the 19 weld factors.

The linearized multiple regression model fit to the set of 77 points in the screened MRP database resulted in the following:

- the set of 19 weld factors (f_{weld}) tabulated in Table 4-3 and plotted in Figure 4-5
- an alloy factor (f_{alloy}) of $1/2.6 = 0.385$ for Alloy 82
- an orientation factor (f_{orient}) of 0.5 for crack growth perpendicular to the direction of the dendrites
- a stress intensity factor exponent (β) of 1.6
- a constant factor of 9.82×10^{-13}

Figure 4-5 shows the log-normal distribution fit to the set of 19 weld factors.⁴ Because it is fit to the weld factors, this distribution describes the variability in CGR due to difference in weld wire/stick material heat processing and weld fabrication. The 75th percentile value of this distribution is a weld factor of 1.49. For the purpose of producing a single deterministic CGR model, the 75th percentile weld factor is absorbed into the constant factor, resulting in a value of α of 1.5×10^{-12} .

4.3 MRP Disposition Curves

The deterministic CGR curves for Alloy 182/132 and Alloy 82 are shown in Figure 4-6. The MRP database indicates that the CGR for Alloy 82 is on average 2.6 times lower than that for Alloy 182/132, so the MRP-115 curve for Alloy 82 is 2.6 times lower than the curve for Alloy 182/132. For crack propagation that is clearly perpendicular to the dendrite solidification direction, a factor of 2.0 lowering the CGR may be applied to the curves for Alloy 182/132 and Alloy 82.

Figures 4-7 and 4-8 show the results of the statistical analysis in comparison with the MRP screened database for Alloys 182/132 and 82, respectively. Note that, unlike for Figures 4-3 and 4-4, the data in Figures 4-7 and 4-8 have been normalized for the effect of crack orientation. The raw CGRs for points for which the crack growth was perpendicular to the dendrite direction have been increased by a factor of 2.0.

The mathematical form of the MRP-115 CGR curve for Alloy 182/132 at 325°C (617°F) is:

$$CGR \text{ (in m/s)} = 1.5 \times 10^{-12} K^{1.6} \quad (\text{for } K \text{ in MPa}\sqrt{\text{m}}) \quad \text{Equation 4-3}$$

$$CGR \text{ (in inches/hr)} = 2.47 \times 10^{-7} K^{1.6} \quad (\text{for } K \text{ in ksi}\sqrt{\text{in}}) \quad \text{Equation 4-4}$$

The general form of the MRP-115 equation is as follows:

$$\dot{a} = \exp \left[-\frac{Q_g}{R} \left(\frac{1}{T} - \frac{1}{T_{ref}} \right) \right] \alpha f_{alloy} f_{orient} K^B \quad \text{Equation 4-5}$$

where:

- \dot{a} = crack growth rate at temperature T in m/s (or in/h)
- Q_g = thermal activation energy for crack growth
= 130 kJ/mole (31.0 kcal/mole)
- R = universal gas constant
= 8.314×10^{-3} kJ/mole-K (1.103×10^{-3} kcal/mole-°R)

⁴ As was the case for the heat factor distribution in MRP-55 [2], the most likely estimator fit was applied in Figure 4-5. This standard type of statistical fit is appropriate for cases in which random samples are taken from a population.

T	=	absolute operating temperature at location of crack, K (or °R)
T_{ref}	=	absolute reference temperature used to normalize data
	=	598.15 K (1076.67°R)
α	=	power-law constant
	=	1.5×10^{-12} at 325°C for \dot{a} in units of m/s and K in units of MPa√m (2.47×10^{-7} at 617°F for \dot{a} in units of in/h and K in units of ksi√in)
f_{alloy}	=	1.0 for Alloy 182 or 132 and $1/2.6 = 0.385$ for Alloy 82
f_{orient}	=	1.0 except 0.5 for crack propagation that is clearly perpendicular to the dendrite solidification direction
K	=	crack tip stress intensity factor, MPa√m (or ksi√in)
β	=	exponent
	=	1.6

The MRP curve may be interpreted as the mean of the upper half of the distribution describing the variability in CGR due to material “heat,” or—in this case—individual weld. Therefore, the MRP curve addresses the concern that welds that are more susceptible than average to crack initiation tend to have higher CGRs than average. Cracking detected in operating plants would tend to be located in components using such susceptible welds.

It is noted that all of the data points in Table 4-2 which were derived from 1 inch CT specimens fall on or below the MRP-115 line for Alloy 182—even after correction for dendrite orientation. This is in contrast to data points derived from 0.5–0.6 inch CT specimens, some of which are above the MRP-115 line. However, it is judged that insufficiently diverse data are available to discern whether specimen size in fact has a significant impact on measured CGRs because only the two sets of Studsvik data reflect 1 inch CT specimens (while all others reflect CT specimens of 0.5–0.6 inches in width).

Table 4-1
Summary of Data Sources for CGR Testing of Alloy 82, 182, and 132 Welds

Test Lab	Ref.	Welds Tested		Number CGR Points																				Loading	Percentage Engagement to IGSCC (For Points After Screening)													
		Before Screen	After Screen (Avg Data)	Before Screen								Screened Out Points (20 points with 2 reasons)										After Screen																
				All Pts		Avg CGR Data		Max CGR Data		Both Avg & Max		No CGR Reported	A _{max} < 0.5 mm	Hold Time < 1 h	Engag. < 50%	H ₁ = 150 cc/kg	Outside LEFM	Flutter Load	Temp. Change	Loading Changes	Max CGR Only ¹	Total	Avg CGR Data			Max CGR Data		Both Avg & Max										
				by weld	by Lab	by weld	by Lab	by weld	by Lab	by weld	by Lab												by weld			by Lab	by weld	by Lab	by weld	by Lab	by weld	by Lab	by weld	by Lab	by weld	by Lab	by weld	by Lab
Content Deleted – MRP/EPRI Proprietary Material																																						

Table 4-2
Laboratory Alloy 82/182/132 CGR Data in the Screened MRP Database¹

Point No.	Specimen Parameters								Water Chemistry				Loading Parameters				Average CGR					Maximum CGR							
	Test Lab ²	Specimen	Alloy	Producer ³	Weld ID	Weld Orientation ⁴	Specimen Type ⁵	Applied Cold Work (%) & Stress Relief ⁶	Li (ppm)	B (ppm)	H ₂ (cc/kg)	H ₂ (ppm)	Calculated H ₂ Partial Press. (atm)	Test Duration (h)	Type of Loading	Holdtime (s)	R Min. Load to Max. Load	% Engagement	K (MPa√m)	Test Temperature (°C)	Average Δa (mm)	Measured (m/h)	Temp. Adjusted (m/h)	Temp. & % Eng. Adjusted (m/h)	(CGR _{meas} /CGR _{adj}) ^{7,8}	Maximum Δa (mm)	Measured (m/h)	Temp. Adjusted (m/h)	CGR _{meas} /CGR _{adj} ⁹
1																													
2																													
3																													
4																													
5																													
6																													
7																													
8																													
9																													
10																													
11																													
12																													
13																													
14																													
15																													
16																													
17																													
18																													
19																													
20																													
21																													
22																													
23																													
24																													
25																													

Content Deleted – MRP/EPRI Proprietary Material

Table 4-2 (continued)
Laboratory Alloy 82/182/132 CGR Data in the Screened MRP Database¹

Point No.	Specimen Parameters							Water Chemistry				Loading Parameters				Average CGR					Maximum CGR									
	Test Lab ²	Specimen	Alloy	Producer ³	Weld ID	Weld Orientation ⁴	Specimen Type ⁵	Applied Cold Work (%) & Stress Relief ⁶	LI (ppm)	B (ppm)	H ₂ (cc/g)	H ₂ (ppm)	Calculated H ₂ Partial Press. (atm)	Test Duration (h)	Type of Loading	Holdtime (t)	R Min. Load to Max. Load	% Engagement	K (MPa√in)	Test Temperature (°C)	Average Δa (mm)	Measured (m/h)	Temp. Adjusted (m/h)	Temp. & % Eng. Adjusted (m/h)	(CGR _{meas} × Temp.) / CTR _{ref}	Maximum Δa (mm)	Measured (m/h)	Temp. Adjusted (m/h)	CGR _{meas} / CTR _{ref}	
26																														
27																														
28																														
29																														
30																														
31																														
32																														
33																														
34																														
35																														
36																														
37																														
38																														
39																														
40																														
41																														
42																														
43																														
44																														
45																														
46																														
47																														
48																														
49																														
50																														

Content Deleted – MRP/EPRI Proprietary Material

Table 4-2 (continued)
Laboratory Alloy 82/182/132 CGR Data in the Screened MRP Database¹

Point No.	Specimen Parameters								Water Chemistry				Loading Parameters				Test Temperature (°C)	Average CGR					Maximum CGR						
	Test Lab ⁷	Specimen	Alloy	Product ²	Weld ID	Weld Orientation ⁸	Specimen Type ²	Applied Cold Work (%) & Stress Relief ⁹	LI (ppm)	B (ppm)	H ₂ (cc/kg)	H ₂ (ppm)	Calculated H ₂ Partial Press (atm)	Test Duration (h)	Type of Loading	Holdtime (t)		R Min. Load to Max. Load	% Engagement	K (MPa√m)	Average Δa (mm)	Measured (m/y)	Temp. Adjusted (m/y)	Temp. & % Eng. Adjusted (m/y)	(CGR _{meas}) ¹⁰ × (CGR _{red}) ¹¹	Maximum Δa (mm)	Measured (m/y)	Temp. Adjusted (m/y)	CGR _{meas} /CGR _{red}
51																													
52																													
53																													
54																													
55																													
56																													
57																													
58																													
59																													
60																													
61																													
62																													
63																													
64																													
65																													
66																													
67																													
68																													
69																													
70																													
71																													
72																													
73																													
74																													
75																													

Content Deleted – MRP/EPRI Proprietary Material

Table 4-2 (continued)
Laboratory Alloy 82/182/132 CGR Data In the Screened MRP Database¹

Point No.	Specimen Parameters								Water Chemistry					Loading Parameters				Test Temperature (°C)	Average CGR					Maximum CGR				
	Test Lab ²	Specimen	Alloy	Product ³	Weld ID	Weld Orientation ⁴	Specimen Type ⁵	Applied Cold Work (%) & Stress Relief ⁶	Li (ppm)	B (ppm)	H ₂ (cc/kg)	H ₂ (ppm)	Calculated H ₂ Partial Press. (atm)	Test Duration (h)	Type of Loading	Holdtime (t)	R Min. Load to Max. Load		% Engagement	K (MPa√m)	Average Δa (mm)	Measured (m/y)	Temp. Adjusted (m/y)	Temp. & % Eng. Adjusted (m/y)	(CGR _{meas}) ⁷ × Temp/M/CGR _{meas} ⁸	Maximum Δa (mm)	Measured (m/y)	Temp. Adjusted (m/y)
76	Content Deleted – MRP/EPRI Proprietary Material																											
77																												

Table 4-3
Calculated Normalization Factors for Alloy Type (82/182/132) and Weld Heat/Processing

Weld Rank	Weld ID	Alloy	Producer	Testing Lab	No. of Data Points		Alloy Factor f_{alloy} (Note 1)	Weld Factor f_{weld} (Note 1)	$f_{alloy}f_{weld}$
					Before Screen	After Screen			
1	Content Deleted – MRP/EPRI Proprietary Material	182	Content Deleted – MRP/EPRI Proprietary Material				1.00	2.17	2.17
2		182					1.00	2.12	2.12
3		132					1.00	1.70	1.70
4		182					1.00	1.25	1.25
5		182					1.00	1.15	1.15
6		182					1.00	0.91	0.91
7		132					1.00	0.89	0.89
8		82H					0.38	2.04	0.78
9		82H					0.38	2.03	0.78
10		182					1.00	0.76	0.76
11		182					1.00	0.74	0.74
12		82H					0.38	1.54	0.59
13		82					0.38	1.32	0.51
14		82H					0.38	1.32	0.51
15		182					1.00	0.51	0.51
16		182					1.00	0.38	0.38
17		82					0.38	0.61	0.24
18		82H					0.38	0.47	0.18
19		82					0.38	0.31	0.12
–		182					0.38	0.31	0.12
–		82					0.38	0.31	0.12
–		82H					0.38	0.31	0.12
–		82H					0.38	0.31	0.12
–		82					0.38	0.31	0.12
–		82					0.38	0.31	0.12
–		182					0.38	0.31	0.12
–		182					0.38	0.31	0.12
–		182					0.38	0.31	0.12

Notes:

¹ Assuming form $CGR = \alpha f_{temp} f_{alloy} f_{weld} K^{1.6}$

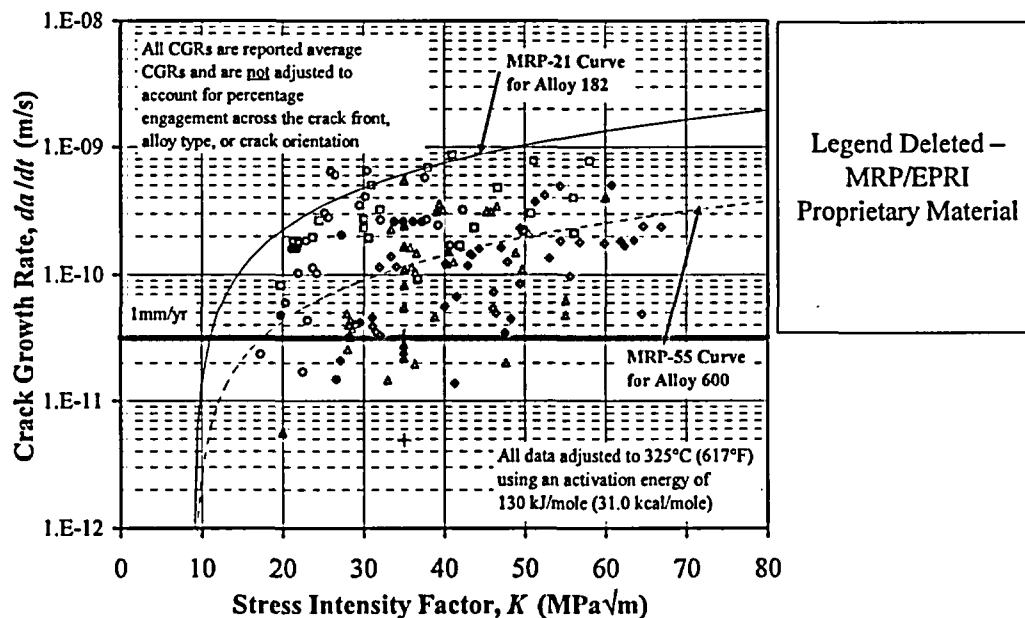


Figure 4-1
Complete Set of Worldwide Alloy 82/182/132 Average CGR Data Before Screening Process (144 points)

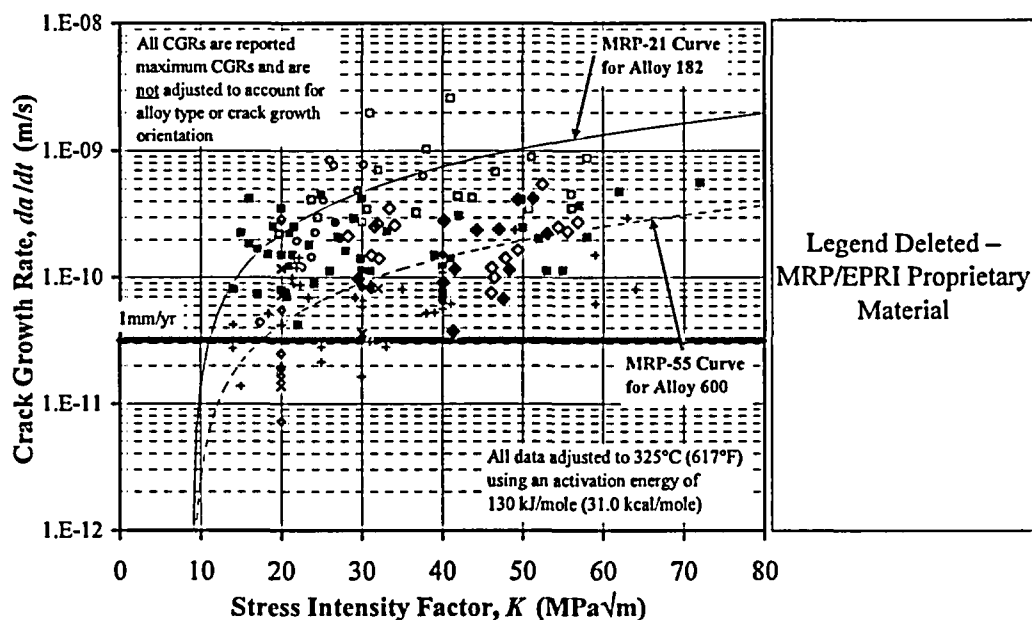


Figure 4-2
Complete Set of Worldwide Alloy 82/182/132 Maximum CGR Data Before Screening Process (158 points)

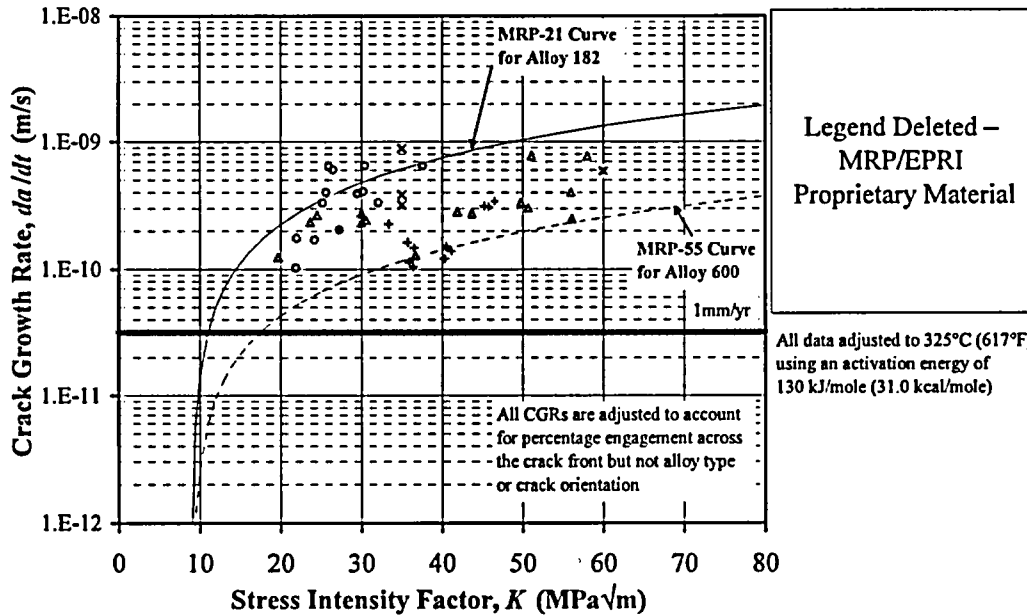


Figure 4-3
Average CGR Data for Alloys 182 and 132 After MRP Screening (43 Points)

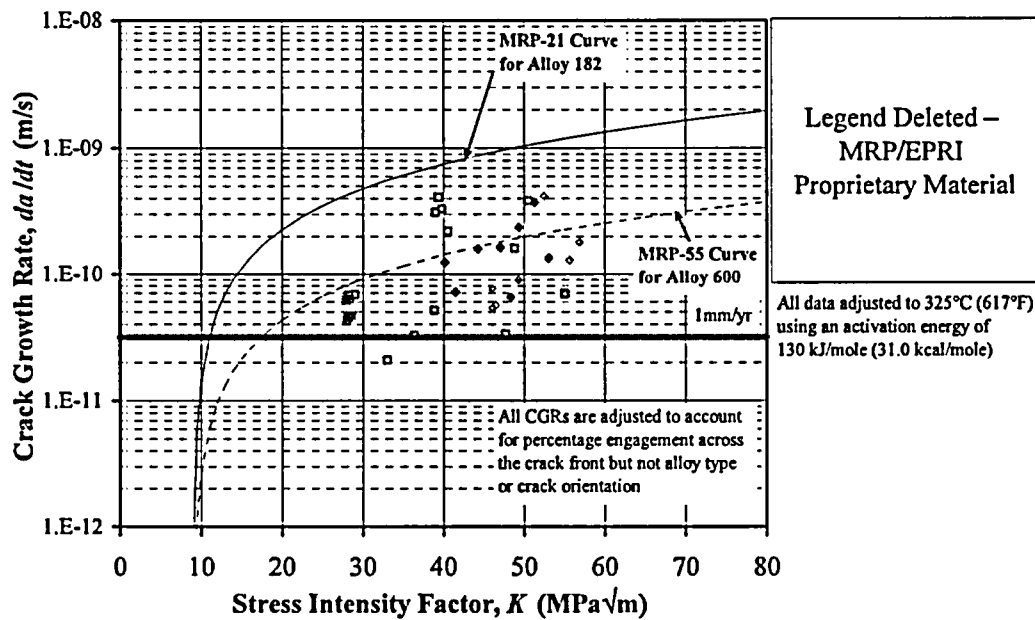


Figure 4-4
Average CGR Data for Alloy 82 After MRP Screening (34 Points)

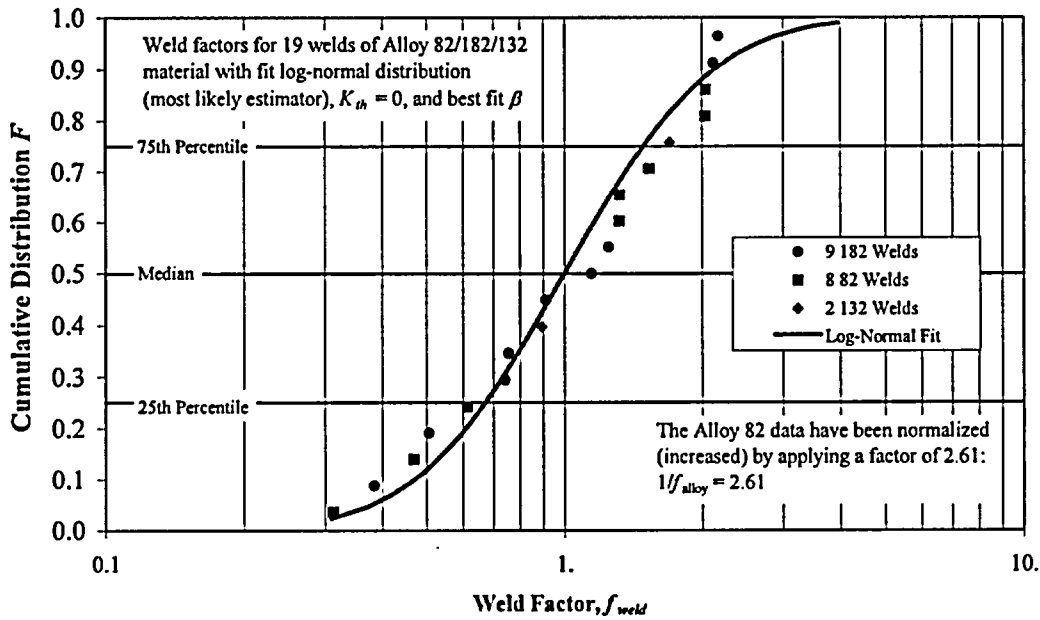


Figure 4-5
Log-Normal Fit to 19 Weld Factors for Screened MRP Database of CGR Data for Alloy 82/182/132

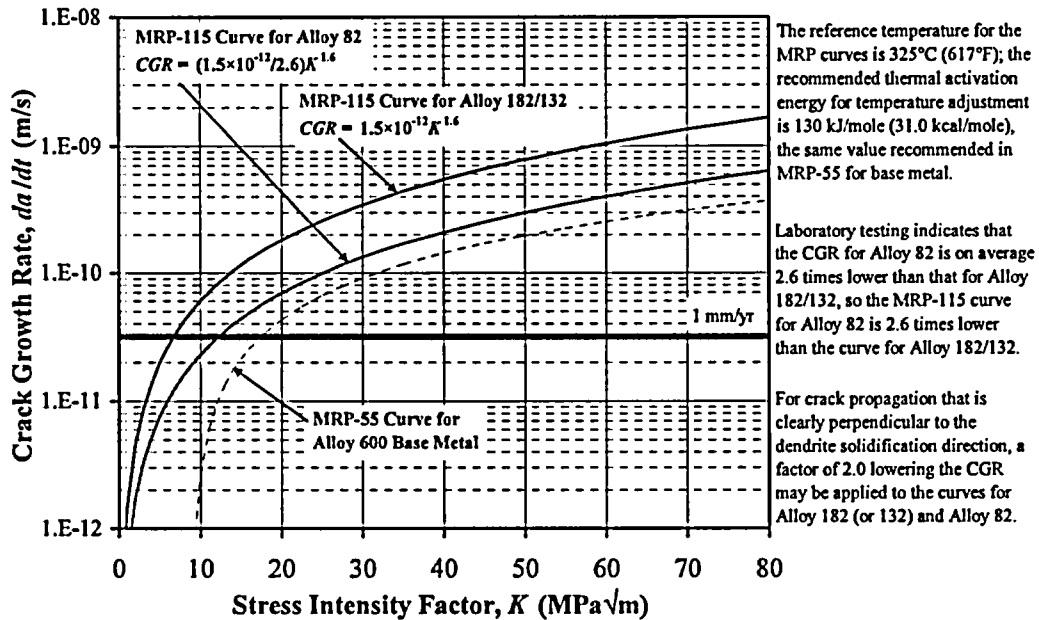


Figure 4-6
MRP-115 Deterministic Curves for Alloy 182/132 and Alloy 82 Weld Materials

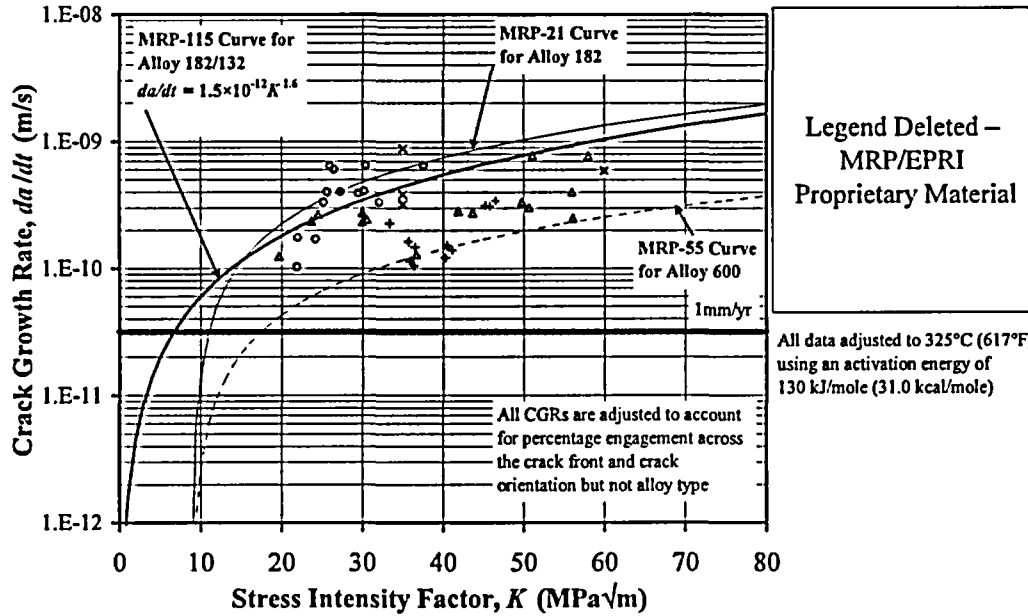


Figure 4-7
Average CGR Data for Alloys 182 and 132 After MRP Screening (43 Points) Normalized to a Crack Orientation Parallel to the Weld Dendrites with MRP-115 Curve for Alloy 182/132

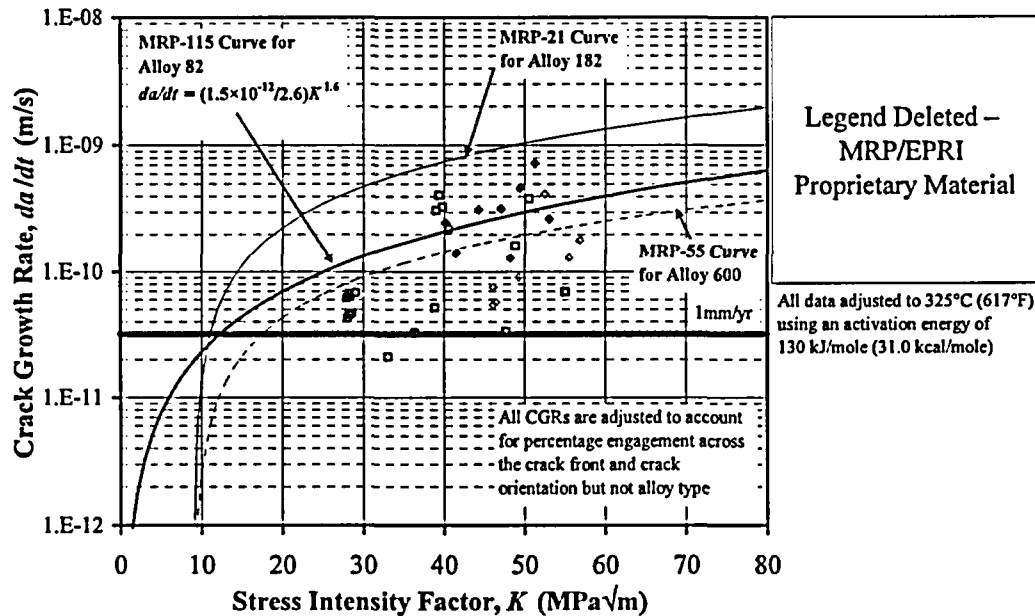


Figure 4-8
Average CGR Data for Alloy 82 After MRP Screening (34 Points) Normalized to a Crack Orientation Parallel to the Weld Dendrites with MRP-115 Curve for Alloy 82

5

COMPARISON OF MRP DISPOSITION CURVES WITH OTHER DATA

5.1 Comparison With Other Laboratory Data

As described below, several comparisons were made of the MRP-115 deterministic equation to the data that were not included in the final screened MRP database of average CGR data. These comparisons were made in order to verify the robustness of the MRP-115 multiple linear regression model given the manner in which the data screening process was implemented. These comparisons were also performed to verify the absence of any hidden effects in the overall set of CGR data collected.

5.1.1 Comparison With Laboratory Data Generated for Removed Plant Weld Material

As described in more detail in MRP-113 [64], boric acid crystal deposits led to the discovery of a small hole in the Alloy 82/182 butt weld between the low-alloy steel reactor vessel outlet nozzle and the stainless steel primary coolant pipe during the October 2000 refueling outage at VC Summer. Destructive examinations revealed the presence of several axial cracks, including a through-wall axial crack extending essentially the full weld width, as well as a short, shallow circumferential crack in the Alloy 182 cladding that arrested when it reached the low-alloy steel nozzle.

Samples of both Alloy 182 and Alloy 82 material taken from this hot leg safe end weld were used in a series of crack growth rate tests completed by Westinghouse [52,65]. The samples were 0.5T-compact tension specimens with thicknesses ranging from 2.4 to 3.2 mm. In all four cases, the entire sample was taken from weld material, perhaps reducing the residual stresses further than would have occurred if base metal were also part of the specimens. The test conditions included a test temperature of 325°C; a simulated primary water environment with 3.5 ppm Li, 1800 ppm B, and 30–35 cc/kg dissolved hydrogen; fatigue pre-cracking in air at a stress intensity factor below 15 MPa√m; and a nominal test stress intensity factor of either 20 or 35 MPa√m. Further details are provided as Point Nos. 6 through 21 of Table F-1 in Appendix F.

The specimens were periodically unloaded to a load equal to 70% of the full applied load ($R = 0.7$) in order break any oxides that might affect the accuracy of the crack growth measurements. Side grooves were included in the specimens in an attempt to keep cracking in the intended plane. For the Alloy 82 specimens (Nos. 14 through 21 in Table F-1), testing was in the TS direction (meaning that the crack plane was parallel to the dendrites) while for the Alloy 182 specimens (Nos. 6 through 13 in Table F-1), testing was in the TL direction (meaning that crack

growth was perpendicular to the dendrites). Per Reference [53], the 16 entries in Table F-1 (Nos. 6 through 21) reflect the results of four-phase tests conducted on each of the two Alloy 182 and two Alloy 82 specimens.

Content Deleted – MRP/EPRI Proprietary Material

For each of the four samples, post-test fractography was used to determine the overall crack increment, and this increment was divided into four parts on the basis of DC potential drop measurements taken during the test, thereby facilitating four separate data points for each sample corresponding to the above four test phases.

The crack growth rate data produced from these tests are plotted on Figure 5-1 along with the MRP-115 curves for Alloy 182 and Alloy 82. As noted on the figure, two sets of data points are included for the Alloy 182 specimens: the as-measured CGRs, and CGRs increased by a factor of 2.0 to account for the crack orientation (perpendicular to the dendrites).

The following observations concerning Figure 5-1 are noted:

- The VC Summer data were screened from the database used to develop the MRP-115 deterministic model because these laboratory data were generated during multi-condition tests in which the loading type was changed.
- These data are still in reasonable agreement with the MRP-115 lines for both Alloy 182/132 and Alloy 82, given the crack orientation correction of the CGRs for the two Alloy 182 weld samples.

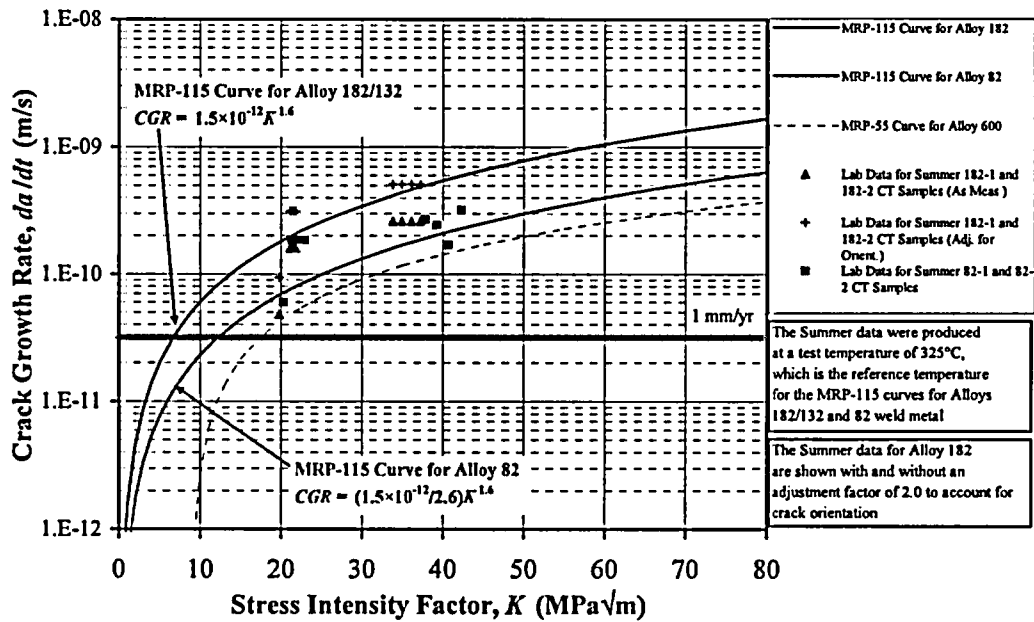


Figure 5-1

Comparison of MRP-115 Curves for Alloys 182/132 and 82 With Westinghouse CGR Data for Weld Material Removed From VC Summer Reactor Hot Leg Safe End Butt Weld [52,65]

5.1.2 Comparison With Additional Westinghouse Data Investigating the Potential Effect of pH

In 2003, Westinghouse conducted a program that examined the crack growth rate of many primary system materials including Alloy 182 welds as a function of primary water pH [66].

Content Deleted – MRP/EPRI Proprietary Material

Content Deleted – MRP/EPRI Proprietary Material

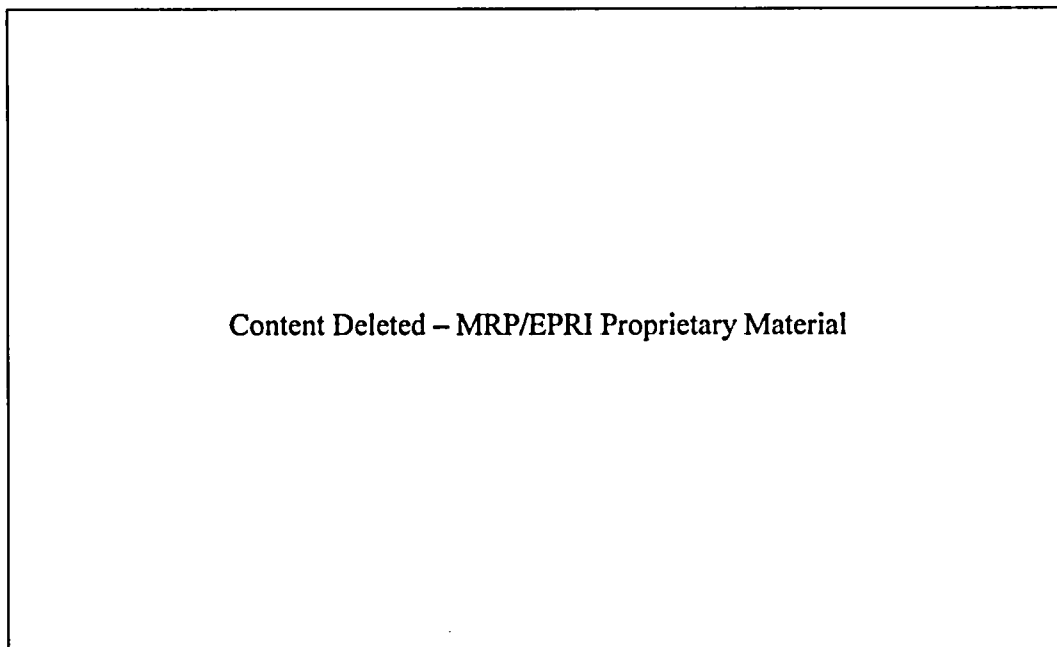


Figure 5-2
Additional Westinghouse Crack Growth Data Gathered to Investigate the Potential Effect of pH for Alloy 182

5.1.3 Comparison With Average Crack Growth Data That Were Screened Out from the MRP Database

For the purpose of comparison with the MRP-115 curve, the figures in Appendix G show the average crack growth rate versus stress intensity factor for the data that were excluded during development of the MRP-115 deterministic equation. These plots reveal that relatively few of the screened out data points lie above the MRP-115 curve, regardless of the reason for exclusion (short crack extension, small cyclic loading hold time, high dissolved hydrogen, violation of LEFM criteria, or low crack engagement). As an example, consider Figure G-1 (repeated as Figure 5-3 for convenience), which shows the data points excluded due to an average crack increment smaller than 0.5 mm. Only three of the more than 20 points lie above the MRP-115 curve, indicating that no systematic, non-conservative biases have been introduced during the present evaluation. Similar conclusions hold for all of the remaining data excluded for the appropriate reasons discussed in Section 3.5.

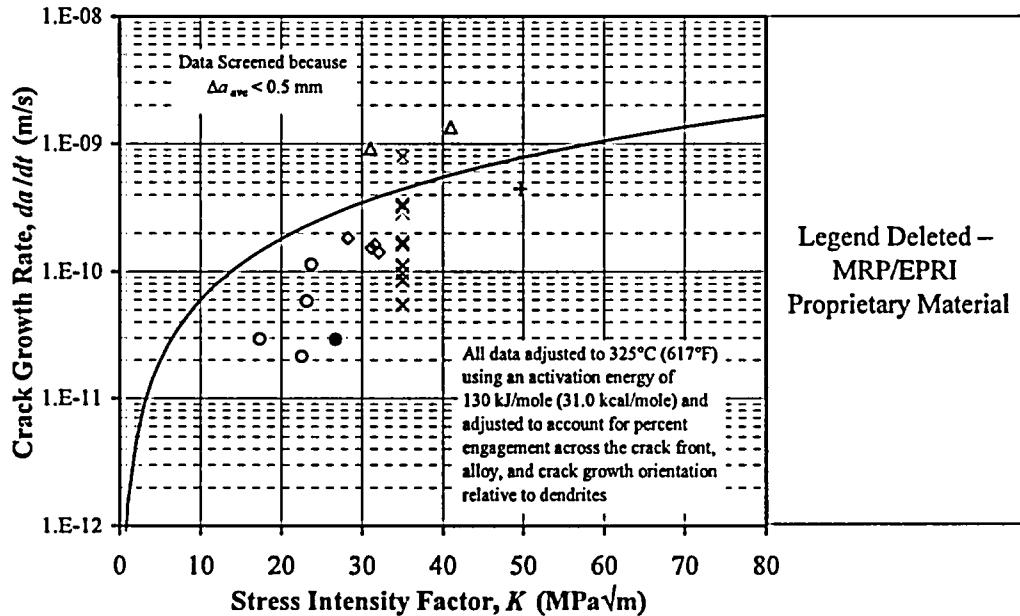


Figure 5-3
Average Crack Growth Rate Versus Stress Intensity Factor for Data Screened Out Because $\Delta a_{ave} < 0.5$ mm

5.1.4 Comparison With Maximum Crack Growth Data That Were Screened Out From the MRP Database

The evaluations in Appendix H led to the following conclusions:

- After about 2 mm of crack extension, the maximum and average crack advances tend to increase at the same rate. Because the average CGR would be expected to exhibit less scatter than the maximum, it would be a better measure of fundamental material behavior.
- Available maximum CGRs corresponding to the average CGRs included in the MRP database are, on average, higher than the maximum CGRs for specimens which were excluded from the MRP database. This trend was quantified in Appendix H (see Figure H-7, repeated as Figure 5-4, and Table H-1).
- Based on the above, hypothetical inclusion of the data that were screened out because the average CGR was not reported would result in a decrease in the MRP-115 deterministic curve. In other words, the exclusion of these data from the MRP database did not introduce any significant non-conservative bias to the MRP-115 curve.

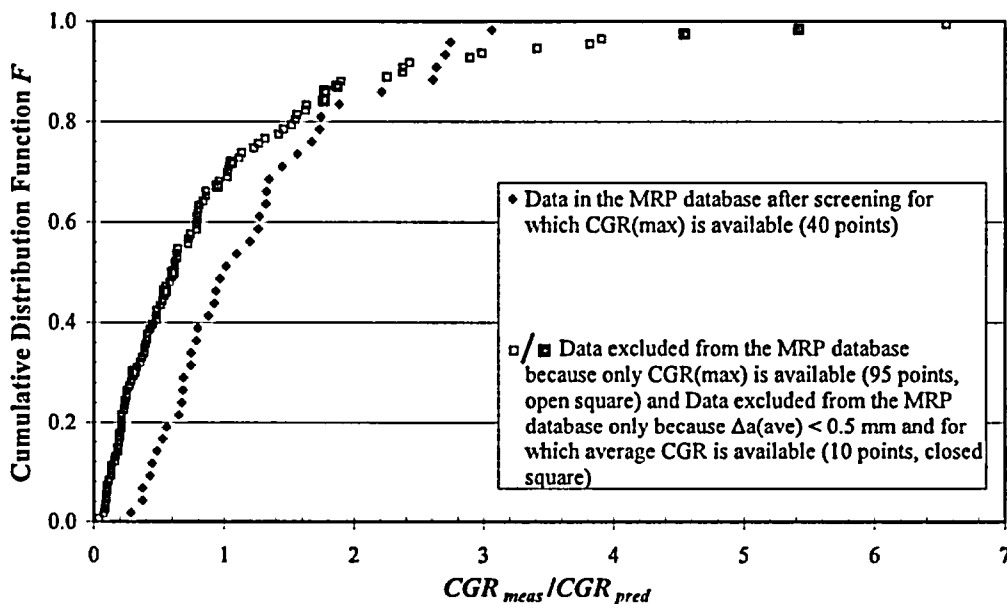


Figure 5-4
Comparison of Cumulative Distribution Function for Maximum Measured CGR Normalized by the CGR Predicted by the MRP-115 Deterministic Model

5.1.5 Investigation of Effect of Periodic Unloading and Hold Time

As described in detail in Appendix I, an investigation of cyclic loading and the associated hold time revealed the following:

- Normalized average CGRs taken from the MRP database exhibit at most a weak dependence on cyclic hold time. Scatter in the data for constant load tests covered a wider range of CGRs than the range spanned by cyclic tests, regardless of hold time.
- For the CGRs in the MRP database taken as a whole, and for several data subsets, there is no significant difference in CGR for tests with hold times of about 6000 s or larger (including constant load tests). This is illustrated for a specific heat of material tested by Bettis as shown in Figure 5-5.
- For tests with shorter hold times (e.g., 600 s), the difference in CGR appears to be limited to approximately a factor of 2 (e.g., see Figure 5-5), in agreement with models and experiments reported in the literature (e.g., Reference [62]).

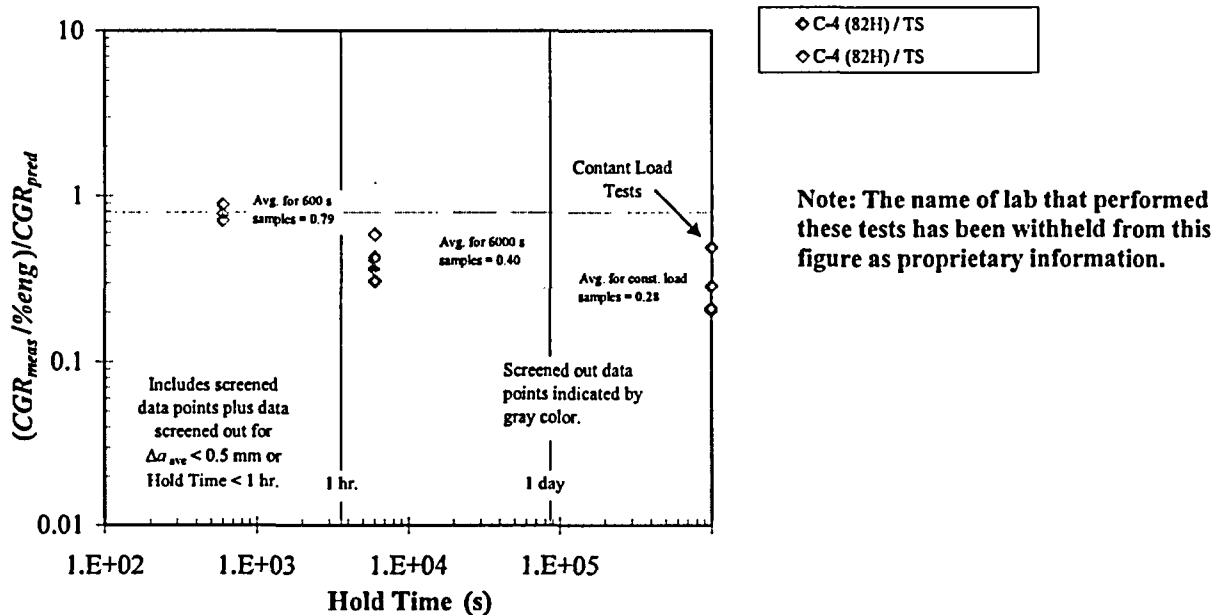


Figure 5-5
Average Crack Growth Rates Normalized by the CGR Predicted by the MRP-115
Deterministic Model Plotted as a Function of Hold Time (Data from Single Lab—Heat C-4)

5.2 Comparison With Other Field Data

During the Ringhals Unit 3 refueling outage in 2000, two axially oriented defects were detected in one of the reactor vessel outlet nozzle-to-safe-end Alloy 182 butt welds using a qualified eddy current technique [67,68,69,70].⁶ During the 2000 outage, the depth of each defect was measured to be 9 ± 3 mm and the length 16 ± 10 mm with ultrasonic testing (UT). As shown in Table 5-1, after additional operation for approximately 8000 effective full power hours, the first defect (Crack 1) had grown to a depth of 13 ± 3 mm while the second defect (Crack 2) measured 16 ± 3 mm.

Table 5-1
Data Reported for Ringhals Unit 3 Hot Leg Safe End Nozzle Weld Cracks

Crack	Statistical Case	Initial Depth	Final Depth	Extension	Average CGR (m/s)		Stress Intensity Factor (MPa√m)		
		a_1 (mm)	a_2 (mm)	Δa (mm)	Oper. At 319°C	Adj. To 325°C	Initial K_1	Final K_2	Mean K_{ave}
1	Stat. Lower Bound	11.12	10.88	No Growth	No Growth		32.2	32.2	32.2
	Best Estimate	9.0	13.0	4.0	1.4E-10	1.8E-10	29.5	33.5	31.5
	Stat. Upper Bound	6.88	15.12	8.24	2.9E-10	3.7E-10	24.0	35.5	29.7
	Worst Case	6.0	16.0	10.0	3.5E-10	4.5E-10	21.0	36.5	28.8
2	Stat. Lower Bound	11.12	13.88	2.76	9.6E-11	1.3E-10	32.3	34.6	33.5
	Best Estimate	9.0	16.0	7.0	2.4E-10	3.2E-10	29.5	36.5	33.0
	Stat. Upper Bound	6.88	18.12	11.24	3.9E-10	5.1E-10	24.0	38.3	31.2
	Worst Case	6.0	19.0	13.0	4.5E-10	5.9E-10	21.0	39.5	30.3

The left portion of Table 5-1 lists the initial and final crack depths and corresponding crack extensions associated with best-estimate, statistical upper- and lower-bound, and worst case crack growth. The best-estimate case assumes that the initial and final crack depths are subject to no error (or, more properly, that each is subject to the same error). For example, for Crack 1, the best-estimate initial depth, final depth, and extension are 9, 13, and 4 mm, respectively. The worst-case crack growth assumes that the initial and final depths are at the extreme values implied by the measurement uncertainty (e.g., for Crack 1, the initial depth would have been $9 - 3 = 6$ mm, the final depth $13 + 3 = 16$ mm, and the extension $16 - 6 = 10$ mm). The upper and lower statistical bounds assume that the initial and final depth measurements are independent (i.e., that the measurement errors in each case are not subject to a common bias). Based on standard engineering tolerance stack-up assumptions, this implies that the uncertainty in the measurement difference is equal to $\pm 3\sqrt{2} = \pm 4.24$ mm. If half of this uncertainty tolerance is assigned to both the initial and final depth measurements, the values in Table 5-1 for "Stat. Lower Bound" and "Stat. Upper Bound" are obtained (e.g., initial depth of $9 - 2.12 = 6.88$ mm,

⁶ Note that the root pass of each of the double-V type welds at Ringhals is reported to have been produced using Alloy 82 weld metal. However, the reported cracks did not extend to the root region. Hence, both cracks were located exclusively in Alloy 182 material.

final depth of $13+2.12 = 15.12$ mm, and extension of $15.12-6.88 = 8.24$ mm for the statistical upper bound for Crack 1).

The stress intensity factors that apply at the locations of the Ringhals Unit 3 defects were calculated by Efsing and Lagerström [67]—based on stresses (including welding residual stresses) calculated using the finite-element method and fracture mechanics calculations assuming standard superposition assumptions—for different crack lengths and are reported in the rightmost portion of Table 5-1.

Figure 5-6 shows the Ringhals Unit 3 field data plotted with the deterministic MRP-115 curve for Alloy 182 weld metal. The solid and open squares in Figure 5-6 represent the best-estimate crack growth rates for the depth increase of the two Ringhals Unit 3 cracks. These two points have been adjusted to the reference temperature of 325°C (617°F) using the standard thermal activation energy of 130 kJ/mole (31.0 kcal/mole), and they reflect the stress intensity factors calculated by Efsing and Lagerström [67]. (The points are shown at the average of the initial and final stress intensity factors corresponding to the best-estimate initial and final measured depths.) The tolerance bars on the points illustrate the uncertainty in the average crack growth between the two UT inspections based on the statistical tolerance for the crack extension discussed above (± 4.2 mm). Note that the statistical lower bound crack growth rate for Crack 1 corresponds to no growth because the ± 4.2 millimeters tolerance is greater than the best-estimate extension for this crack.

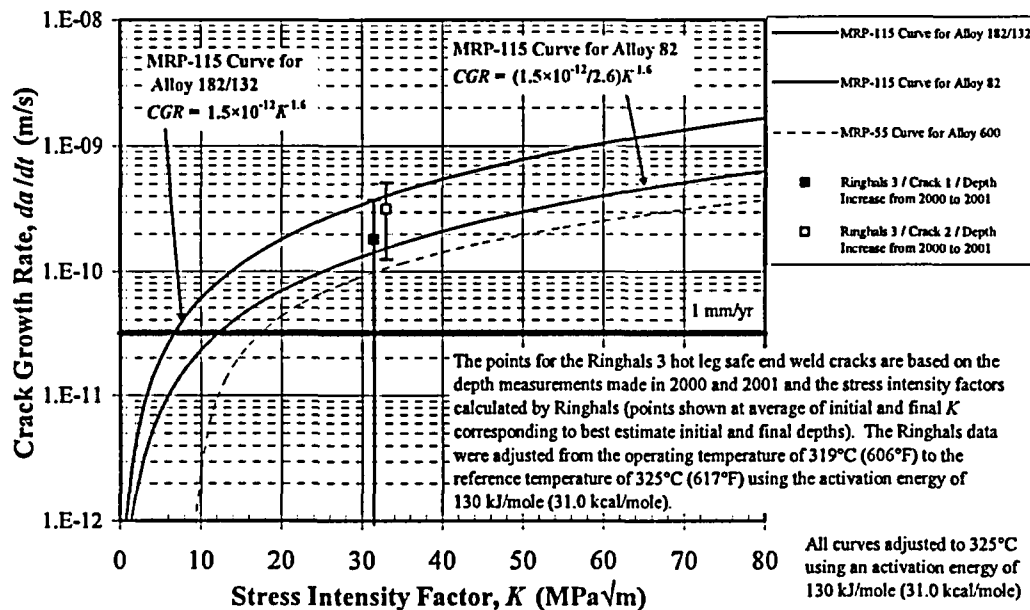


Figure 5-6
Field Crack Growth Data for Ringhals Unit 3 Hot Leg Safe End Alloy 182 Weld

5.3 Comparison With Other Deterministic Curves for Alloy 182

Figure 5-7 compares the MRP-115 curve for Alloy 182/132 with the following four deterministic curves:

- The two-part curve developed by Ringhals [68]. After adjustment from 320°C to 325°C using an activation energy of 130 kJ/mol, the equation developed by Ringhals may be written as follows (shown as the red curve in Figure 5-7), where K is the stress intensity factor:

$$CGR \text{ (m/s)} = \begin{cases} 7.22 \times 10^{-23} K^{9.3}, & K < 25.1 \text{ MPa}\sqrt{\text{m}} \\ 6.0 \times 10^{-10}, & K > 25.1 \text{ MPa}\sqrt{\text{m}} \end{cases} \quad \text{Equation 5-1}$$

This curve was developed as a reasonable bound to the maximum CGR data (roughly 50 points) gathered and screened by Ringhals, including their own testing as well as that from other laboratories.⁷ It also reflects the observation that the CGR appeared to be independent of stress intensity factor for values above about 28–30 MPa√m (plateau behavior). Note that the plateau value of 6.0×10^{-10} m/s in Eq. [5-1]—reflecting maximum CGRs—is about three times larger than the plateau for average CGRs (2.0×10^{-10} m/s) found in recent Ringhals tests [68].

- The plateau curve published by EDF based on laboratory test data [9]. This curve is described by the following general equation:

$$CGR = 175 \times 10^9 (K - K_{th})^\beta \exp\left(-\frac{Q}{RT}\right) \left(1 + \frac{CW}{10}\right) C_{HT} C_{orient} C_{ldg} \quad \text{Equation 5-2}$$

where:

CGR = crack growth rate ($\mu\text{m/h}$)

K = stress intensity factor ($\text{MPa}\sqrt{\text{m}}$)

K_{th} = threshold stress intensity factor = 9 MPa√m

β = stress intensity exponent = 0.1

Q = activation energy = 130 kJ/mol

T = absolute temperature (K)

CW = percent cold work

R = universal gas constant = 8.314 kJ/mol-K

⁷ The screening criteria used by Ringhals are similar to those used in developing the MRP-115 database in Table 4-2; see Reference [71] for additional details on the Ringhals procedure as applied to Alloy 600.

$$C_{HT} = \text{stress relief factor} = \left\langle \begin{array}{c} 1 \\ 0.5 \end{array} \middle| \begin{array}{c} \text{as welded} \\ \text{stress relieved} \end{array} \right\rangle$$

$$C_{orient} = \text{dendrite orientation factor} = \left\langle \begin{array}{c} 1 \\ 0.5 \end{array} \middle| \begin{array}{c} \text{parallel} \\ \text{perp.} \end{array} \right\rangle$$

$$C_{ldg} = \text{loading factor} = \left\langle \begin{array}{c} 1 \\ 2 \end{array} \middle| \begin{array}{c} \text{constant} \\ \text{cyclic} \end{array} \right\rangle$$

The specific curve shown in Figure 5-7 is for an as-welded specimen at 325°C with no cold work, constant loading, and cracking parallel to the dendrite orientation:

$$\begin{aligned} CGR &= 0.791 (K-9)^{0.1} \text{ } [\mu\text{m/h}] \\ &= 2.2 \times 10^{-10} (K-9)^{0.1} \text{ } [\text{m/s}] \end{aligned} \quad \text{Equation 5-3}$$

The EDF equation was developed by the authors of References [9] and [62] based on the results of CGR testing carried out by EDF, ETH, and CEA on nearly 100 Alloy 182 specimens as well as a review of other published CGR data for Alloy 182. The small value for β (0.1) reflects their observation that the stress intensity factor appeared to have a limited effect on CGR for values above 15 MPa $\sqrt{\text{m}}$ [62], creating a plateau effect.

- The MRP-21 curve that has previously been applied in the U.S. [6]. This curve is described by the following equation (see Figure 5-7):

$$CGR = 1.4 \times 10^{-11} (K-9)^{1.16} \text{ } [\text{m/s}] \quad \text{Equation 5-4}$$

where K is the stress intensity factor in units of MPa $\sqrt{\text{m}}$. This curve was intended to bound the bulk of the CGR data available at the time (2000) and was derived by multiplying the Scott curve, developed based on field data for steam generator PWSCC in the early 1990s [7], by a constant factor. It was not the result of a systematic statistical assessment.

- The MRP-55 curve for thick-wall Alloy 600 material [3]:

$$CGR = \exp \left[-\frac{Q_R}{R} \left(\frac{1}{T} - \frac{1}{T_{ref}} \right) \right] \alpha (K - K_{th})^\beta \quad \text{Equation 5-5}$$

where all variables are as defined above or are given by:

CGR = crack growth rate (m/s)

K = stress intensity factor ($\text{MPa}\sqrt{\text{m}}$)

K_{th} = threshold stress intensity factor = $9 \text{ MPa}\sqrt{\text{m}}$

β = stress intensity exponent = 1.16

T_{ref} = absolute reference temperature (598.15 K)

α = crack growth amplitude

$= 2.67 \times 10^{-12}$ at 325°C

For a temperature of 325°C , this equation simplifies to:

$$CGR \text{ (m/s)} = 2.67 \times 10^{-12} (K - 9)^{1.16} \quad \text{Equation 5-6}$$

Like the MRP-115 curve, this equation was derived using a multiple regression statistical fit (based on a heat-by-heat treatment of the data). Unlike the MRP-115 curve, however, the MRP-55 curve assumes a threshold stress intensity value of $9 \text{ MPa}\sqrt{\text{m}}$ (see Appendix E) and also uses Scott's value for the exponent β (1.16) rather than letting the exponent be determined by the statistics associated with the Alloy 182 CGR data as for the MRP-115 curve.

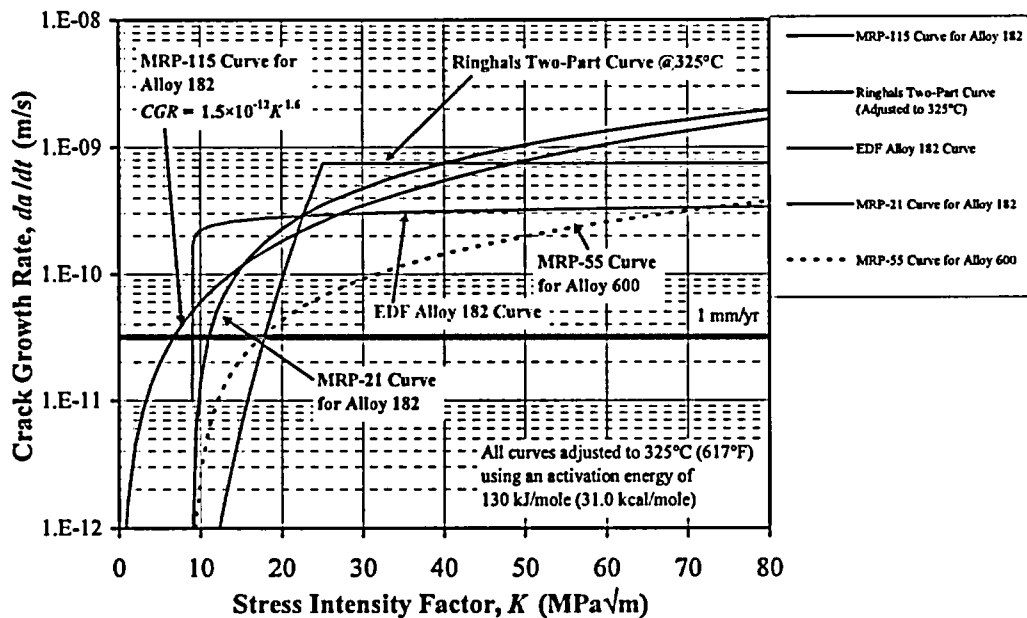


Figure 5-7
Comparison of MRP-115 Curve for Alloy 182 Weld Metal With Other Disposition Curves

Examination of the five curves in Figure 5-7 and the underlying data leads to the following observations:

- The MRP-115 curve is based on a worldwide database of CGR measurements for both Alloy 182 and Alloy 82 from numerous laboratories. In addition, these measurements reflect average CGRs, which are believed to be a better description of material behavior than maximum CGRs.
- The MRP-115 curve is about 30% lower than the MRP-21 curve for stress intensity factors greater than about 20 MPa√m. At smaller stress intensity factors, the MRP-115 curve is higher.
- The MRP-115 curve is nearly parallel to, and about four times higher than, the MRP-55 curve for stress intensity factors greater than 20 MPa√m.
- The MRP-115 curve crosses the Ringhals curve at about 22 MPa√m and again at 40 MPa√m; for stress intensity factors outside this range, the MRP-115 curve is higher (by well over an order of magnitude below 10 MPa√m and by a modest 25% at 60 MPa√m). On the other hand, for stress intensities within the range of 22–40 MPa√m, the Ringhals curve is higher (by up to a factor of two at about 25 MPa√m).
- Similarly, the MRP-115 curve crosses the EDF curve at about 9 MPa√m and again at 28 MPa√m. For stress intensity factors outside this range, the MRP-115 curve is higher (by a factor of 10 at 60 MPa√m), while for stress intensities within this range (9–28), the EDF curve is higher (by up to a factor of five at about 9 MPa√m).

6

EXAMPLE APPLICATION

Now that the crack growth model has been developed, it is helpful to illustrate its application to typical geometries where flaws have been found in the field. Subsequently, a second series of examples will be presented to illustrate the effect of the new MRP-115 model with no stress intensity factor threshold, compared to the previous model of MRP-21 [6], which had a threshold.

Before proceeding to the example calculations, the following general steps constitute a deterministic crack growth evaluation (additional guidance on the overall approach is provided in Section XI of the ASME Code [72]):

- Calculate the stress field in the region of interest including the effect of welding residual stresses and normal operating stresses. Either a conventional strength-of-materials approach (as used in Section 6.1) or, alternatively, finite element analysis (FEA) can be used to determine the stresses. Use of FEA is normally required if there are weld repairs to the inside and/or outside weld surfaces (see, e.g., MRP-106 [73]).
- Determine the stress intensity factor K that corresponds to the postulated weld geometry as a function of crack size. References [74], [75], and [76] provide standard K expressions from LEFM that are often applied to calculate stress intensity factors from the corresponding stress field. These standard K expressions are based on LEFM superposition assumptions, so they do not take any credit for relaxation of the residual stress field as the crack grows.
- Choose an initial flaw size based on the size crack that is detected in the field, the detectability limit for a particular type of inspection, or another criterion such as the size crack that results in a CGR of engineering significance. Choose a final crack size based on criteria such as the size crack that produces coolant leakage, the allowable crack size for continued service, or the critical crack size for pressure boundary rupture. Typically, an assumption also is made regarding the flaw aspect ratio (length vs. depth) during the growth process.
- Calculate the time for crack growth by integrating a deterministic CGR equation such as the MRP-115 equation (Eq. [4-5]) for the variable K as a function of crack size. Typically, the normal operating temperature is assumed, and the number of points in the numerical integration is selected to be large enough so that the result is insensitive to the step size.

6.1 Example Application: PWR Piping Butt Welds

6.1.1 Example Geometry

The locations chosen for the calculations in the first series of examples are the reactor vessel outlet nozzle-to-safe-end weld and the pressurizer safety and relief nozzle-to-safe-end weld. Both of these particular examples are for a plant designed by Westinghouse, where the nozzle is low-alloy steel, and the piping is stainless steel. The stainless steel safe end is welded to the pipe in the field in most applications, and is connected to the nozzle with an Alloy 182 weld, as shown in Figure 6-1.

6.1.2 Loadings

In this example, a flaw is postulated in the Alloy 182 weld material, oriented circumferentially, with a range of aspect ratios. The calculations discussed here have considered all the appropriate loadings, including dead weight, thermal expansion, welding residual stress, and pressure. Since PWSCC is a long term phenomenon controlled by steady state stresses, seismic loads and thermal transient loads are not included.

6.1.3 Welding Residual Stresses

For these example cases, the standard residual stress distributions shown in Figure 6-2 [77] were assumed. These expressions were developed in the 1980s based on residual stress measurements for test mockups of BWR piping butt welds.

6.1.4 Operating Stresses

Using a strength-of-materials approach, the operating stress values were calculated using the following equations:

$$\sigma_m = \frac{F_x}{A} \quad \text{Equation 6-1}$$

$$\sigma_b = \frac{1}{Z} \sqrt{M_y^2 + M_z^2} \quad \text{Equation 6-2}$$

where:

F_x	=	axial force component (membrane)
M_y, M_z	=	moment components (bending)
A	=	cross-section area
Z	=	section modulus

The section properties A and Z at the weld location were determined based on the nominal pipe dimensions. Details regarding how the strength-of-materials approach may be applied to determine stresses for piping butt welds are provided in MRP-109 [78] and MRP-112 [79].

MRP-109 is the Westinghouse deterministic butt weld safety assessment, which covers PWRs designed by Westinghouse and Combustion Engineering, and MRP-112 is the corresponding AREVA assessment, which covers PWRs designed by Babcock & Wilcox.

6.1.5 Results

Results were generated for the two example locations using the MRP-115 CGR model (Eq. [4-5]) to determine the time for an assumed initial part-depth, circumferential flaw to grow in the through-wall direction to a depth of 75% of the wall thickness. The results of the calculation for the reactor vessel outlet nozzle are shown in Figure 6-3 for a range of aspect ratios. The nominal outside diameter of the pipe is 30 inches, and the wall thickness is 2.6 inches. The temperature used for the example was 617°F (325°C), so no temperature adjustment was required when applying Eq. [4-5]. Similar results are shown in Figure 6-4 for the pressurizer safety and relief nozzle, where the piping outside diameter (OD) is 6 inches, and the temperature of operation is 653°F (345°C). The temperature factor corresponding to this temperature is 2.33 per Eq. [4-5], meaning that it is predicted that the pressurizer location is subject to 2.3 times the CGR compared to the hot leg location, all other factors being equal.

Note that the crack growth is most rapid for the largest aspect ratio, 10, which corresponds to a flaw with length 10 times its depth. For Figure 6-3, the assumed initial flaw depth was about 2% of the wall thickness, or 0.05 inches. For Figure 6-4, the assumed initial flaw depth was about 4% of the wall thickness. The assumption of a shallower flaw would have resulted in a longer growth time, but the goal here was to illustrate how a realistic flaw would grow. As can be seen in these figures, the assumed initial flaw size can have a significant effect on the result.

6.2 Effects of a Stress Intensity Factor Threshold Assumption

The MRP-115 model developed in this report contains no stress intensity factor threshold for crack growth because, as discussed in Appendix E, no basis could be found for the existence of one in the MRP database, which includes no data for crack tip stress intensity factors less than 19.7 MPa√m. As such, it differs from the previous work reported in MRP-21 [6], where a threshold for Alloy 600 was assumed to apply to the weld metal as well (see Eq. [5-4]).

Several calculations were carried out to examine the effect of the stress intensity factor threshold assumption, for four different locations:

- Pressurizer Safety and Relief Nozzle Safe End
- Pressurizer Surge Nozzle Safe End
- Core Flood Nozzle Safe End
- Decay Heat Nozzle Safe End

In each of these examples, both part-through- and through-wall flaws were evaluated, and the results plotted using the two CGR models. Westinghouse performed the calculations for the first two examples, and AREVA performed the calculations for the last two examples, which are for plants designed by Babcock & Wilcox. The geometry of the locations chosen for evaluation is given in a text box in each of Figures 6-5 through 6-8, and the applied loads are also shown in

Example Application

the same location. It will be useful to discuss the results of these calculations, which are consistent for each of these examples.

The effect of the elimination of the stress intensity factor threshold on crack growth through the thickness of the weld is in each case detrimental, in that the time for a flaw to propagate through the wall is shorter. Once a flaw is through the wall and leaking, the time required for it to reach a critical circumferential length is actually somewhat longer with the MRP-115 model, although the difference is sometimes small, as seen in Figure 6-6.

The explanation for this behavior is related to the value of the applied stress intensity factor. As shown in Figure 5-7, for stress intensity factors below about 15 ksi $\sqrt{\text{in}}$ the MRP-115 model gives a higher rate than the threshold model, while for higher values of K the MRP-115 curve is typically about 30% lower than the MRP-21 curve. The impact is also affected by the residual stresses, which typically become negative (compressive) near the center wall region of a thick weldment. When this effect comes into play, the stress intensity factor drops as the flaw propagates through the weld, and often will drop to the so-called threshold value. If a threshold is assumed, this implies that the crack would stop. If it is not, the crack slows down but continues to grow.

On balance, it may be concluded that the use of a model with no stress intensity factor threshold value is conservative for the applications discussed here. In addition to this advantage, this approach is more strongly based technically, as discussed in Appendix E.

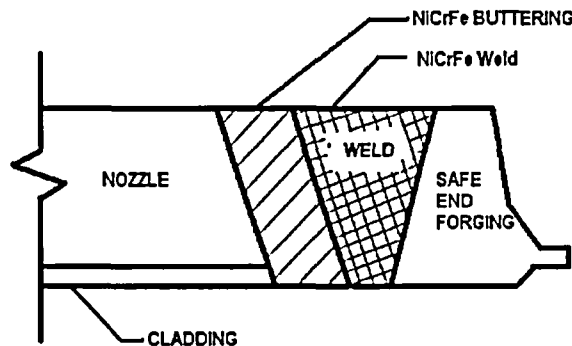
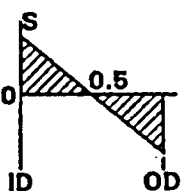
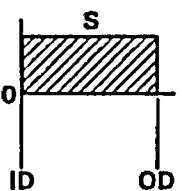
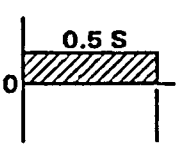


Figure 6-1
Geometry of the Weld Region Used for the Crack Growth Illustrations (Reactor Vessel Outlet Nozzle and Pressurizer Safety and Relief Nozzle-to-Safe-End Welds)

Wall Thickness	Through-Wall Residual Stress ¹	
	Axial	Circumferential ²
< 1 inch		
≥ 1 inch	See Note 3	

¹S = 30 ksi

²Considerable variation with weld heat input.

$$\sigma = \sigma_i [1.0 - 6.91(a/t) + 8.69(a/t)^2 - 0.48(a/t)^3 - 2.03(a/t)^4]$$

σ_i = stress at inner surface (a = 0)

Figure 6-2
Standard Residual Stress Distributions Applied to Piping Butt Welds [77]

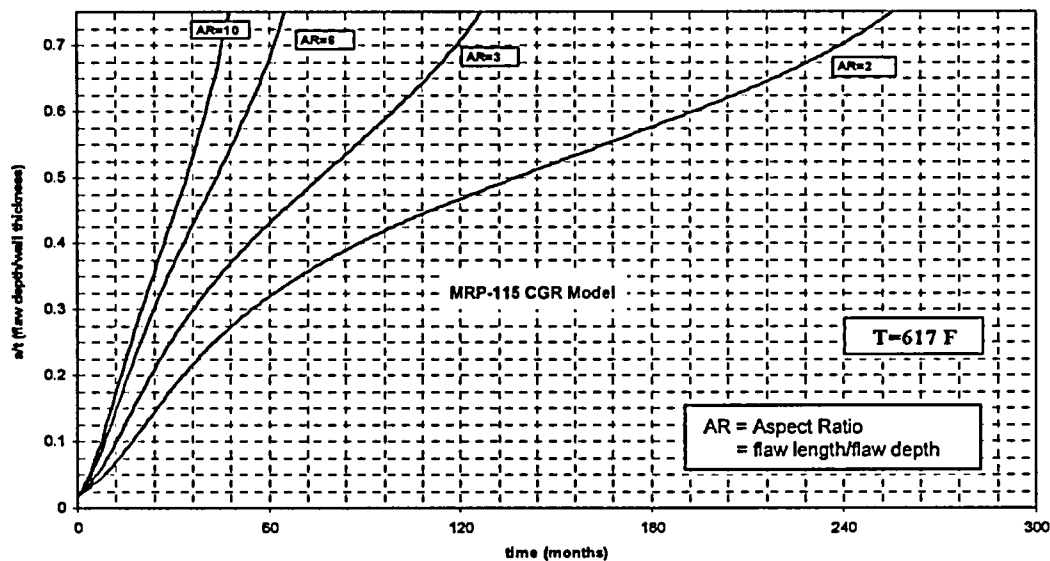


Figure 6-3
Results of Sample Calculations for a Range of Flaw Shapes: Time for Through-Wall Growth for a Part-Depth Circumferential Flaw at a Reactor Vessel Outlet Nozzle (RVON) Safe End Region (Incl. Residual Stress)

Example Application

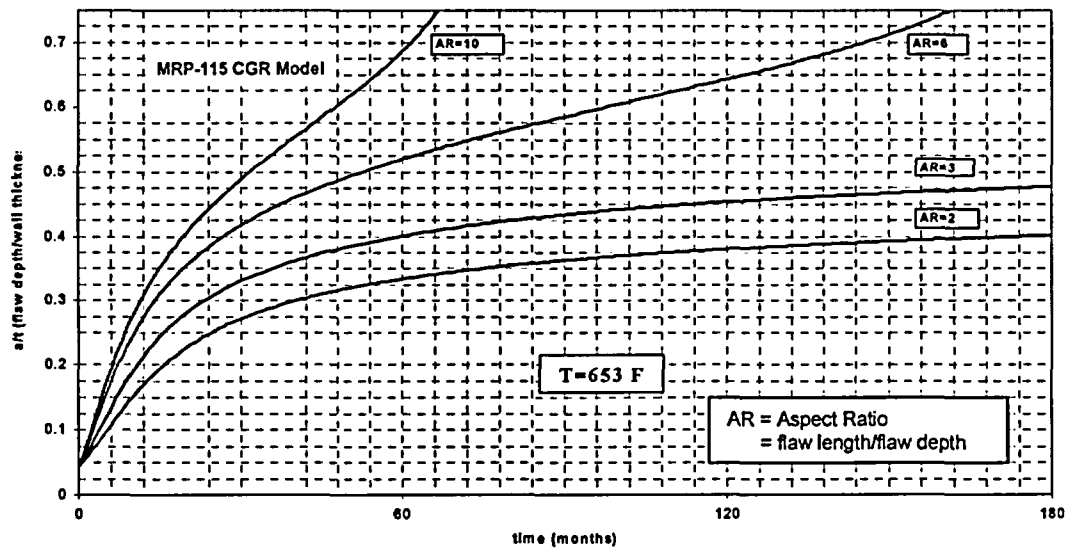


Figure 6-4
Results of Sample Calculations for a Range of Flaw Shapes: Time for Through-Wall Growth for a Part-Depth Circumferential Flaw at a Pressurizer (PZR) Safety and Relief Nozzle Safe End Region (Incl. Residual Stress)

Content Deleted – MRP/EPRI Proprietary Material

Content Deleted – MRP/EPRI Proprietary Material

Figure 6-5
Results of Sample Calculations Showing the Effect of a Stress Intensity Factor Threshold:
Circumferential Flaw at a Pressurizer Safety and Relief Nozzle Safe End Region; Time for
Through-Wall Growth for a Part-Depth Circumferential Flaw (top) and Subsequent Time for
Growth in the Circumferential Direction of a Through-Wall Circumferential Flaw (Bottom)

Content Deleted – MRP/EPRI Proprietary Material

Content Deleted – MRP/EPRI Proprietary Material

Figure 6-6
Results of Sample Calculations Showing the Effect of a Stress Intensity Factor Threshold:
Circumferential Flaw at a Pressurizer Surge Nozzle Safe End Region; Time for Through-
Wall Growth for a Part-Depth Circumferential Flaw (top) and Subsequent Time for Growth
In the Circumferential Direction of a Through-Wall Circumferential Flaw (Bottom)

Content Deleted – MRP/EPRI Proprietary Material

Content Deleted – MRP/EPRI Proprietary Material

Figure 6-7
Results of Sample Calculations Showing the Effect of a Stress Intensity Factor Threshold:
Circumferential Flaw at a Core Flood Nozzle Safe End Region; Time for Through-Wall
Growth for a Part-Depth Circumferential Flaw (top) and Subsequent Time for Growth in the
Circumferential Direction of a Through-Wall Circumferential Flaw (Bottom)

Content Deleted – MRP/EPRI Proprietary Material

Content Deleted – MRP/EPRI Proprietary Material

Figure 6-8
Results of Sample Calculations Showing the Effect of a Stress Intensity Factor Threshold:
Circumferential Flaw at a Decay Heat Nozzle Safe End Region; Time for Through-Wall
Growth for a Part-Depth Circumferential Flaw (top) and Subsequent Time for Growth in the
Circumferential Direction of a Through-Wall Circumferential Flaw (Bottom)

7

CONCLUSIONS

The following are the key conclusions regarding the present MRP study of stress corrosion CGRs of Alloy 82/182/132 nickel-based weld metals under PWR primary water conditions:

- An international expert panel was formed and collected detailed laboratory test data for the relevant set of worldwide laboratory CGR tests using pre-cracked fracture mechanics specimens.
- The expert panel developed screening criteria to qualify data for use in the development of a deterministic CGR model for Alloy 82, 182, and 132 weld metals. The screening criteria were based upon the criteria previously applied to Alloy 600 wrought material in MRP-55 [3], but were necessarily extended to cover the special test considerations associated with the weld metal materials.
- Based on a literature review and the laboratory experience of the expert panel members, a methodology was developed for considering the potentially non-conservative effect of incomplete “engagement” to intergranular SCC across the specimen width and over test duration. Engagement fractions were estimated for all the specimens in the screened database, and, in the case of incomplete engagement, the reported CGRs were adjusted by dividing by the respective engagement fractions. This approach is appropriate regardless of whether the incomplete engagement is caused by isolated islands of more crack-resistant material or is a testing artifact due to the difficulty of the crack transitioning from the transgranular fatigue pre-crack to the intergranular stress corrosion crack—or a combination of the two.
- The expert panel concluded that there are currently insufficient data available to include a stress intensity factor threshold in the deterministic CGR model for the nickel-based weld metals. Analyses of weld metal cracking that involve the existence of pre-existing defects (either real or postulated) could be strongly influenced by assuming an arbitrary stress intensity factor threshold value.
- A linearized, multiple regression statistical model was fitted to the screened database including an Arrhenius temperature correction, an alloy factor (Alloy 182/132 or Alloy 82), a crack orientation factor (parallel or perpendicular to the weld dendrites), a crack tip stress intensity factor exponent, and a weld factor that accounts for the randomness associated with the heat of weld wire/stick material and welding process. Insufficient data were available to include dissolved hydrogen concentration (i.e., electrochemical potential), cold working, post-weld heat treatment stress relief, or loading type (constant or periodic unloading) in the model.

Conclusions

- For the purpose of producing a single deterministic CGR model, the 75th percentile weld factor was absorbed into the statistical model, resulting in the recommended CGR equation for Alloy 182/132 and Alloy 82 as listed on page 4-4. The MRP recommends that this equation be applied for the disposition of PWSCC flaws detected in these materials in PWR primary circuits (similar to [4,80]) and used in safety case calculations that assume hypothetical PWSCC flaws [78,79]. Furthermore, the data in this report may be used to determine statistical CGR distributions for use in probabilistic fracture mechanics models of the growth of PWSCC flaws in the weld metal materials.
- Detailed comparisons with the available worldwide laboratory CGR data that were not included in the final screened database used to produce the MRP-115 deterministic model were performed. These comparisons verified the robustness of the MRP-115 multiple linear regression model given the manner in which the data screening process was implemented and verified the absence of any hidden effects in the overall set of CGR data collected.

Evaluation of the only known set of repeat PWSCC crack sizing data for nickel-based weld metals in an operating PWR plant (2 cracks in Alloy 182 reactor vessel outlet nozzle-to-safe-end weld at the Swedish plant Ringhals Unit 3) produced best-estimate CGRs bounded by the MRP-115 curve for Alloy 182/132 as shown in Figure 5-6.

In other countries, different approaches have been applied to develop CGR disposition curves for the nickel-based weld metals, resulting as would be expected in CGR curves somewhat different than the MRP-115 model as shown in Figure 5-7.

- Section 6 provides examples of how the previous MRP-21 [6] and the new MRP-115 deterministic models may be applied to calculate the time for flaws in piping butt weldments to grow to larger sizes. As expected, the assumption of no stress intensity factor threshold has a significant effect for relatively small part-depth flaws.
- Finally, this report also documents the recommendations of the expert panel with regard to best practices for performing future CGR tests with pre-cracked nickel-based weld metal specimens.

8

REFERENCES

-
1. *Materials Reliability Program: PWSCC of Alloy 600 Type Materials in Non-Steam Generator Tubing Applications—Survey Report Through June 2002: Part 1: PWSCC in Components Other than CRDM/CEDM Penetrations (MRP-87)*, EPRI, Palo Alto, CA: 2003. 1007832.
 2. "Inspection Experience," Chapter 4 in *Materials Reliability Program Reactor Vessel Closure Head Penetration Safety Assessment for U.S. PWR Plants (MRP-110): Evaluations Supporting the MRP Inspection Plan*, EPRI, Palo Alto, CA: 2004. 1009807.
 3. *Materials Reliability Program (MRP) Crack Growth Rates for Evaluating Primary Water Stress Corrosion Cracking (PWSCC) of Thick-Wall Alloy 600 Materials (MRP-55) Revision 1*, EPRI, Palo Alto, CA: 2002. 1006695.
 4. Paragraph IWB-3660, "Evaluation Procedure and Acceptance Criteria for PWR Reactor Vessel Upper Head Penetration Nozzles," *ASME Boiler & Pressure Vessel Code, Section XI*, ASME International, July 2004 Edition.
 5. R. S. Pathania, A. R. McIlree, and J. Hickling, "Overview of Primary Water Cracking of Alloys 182/82 in PWRs," *Fontevraud 5 International Symposium: Contribution of Materials Investigation to the Resolution of Problems Encountered in Pressurized Water Reactors*, SFEN, France, September 23–27, 2002, pp. 13–27.
 6. *Crack Growth of Alloy 182 Weld Metal in PWR Environments (PWRMRP-21)*, EPRI, Palo Alto, CA: 2000. 1000037.
 7. P. M. Scott, "An Analysis of Primary Water Stress Corrosion Cracking in PWR Steam Generators," *Presented at NEA/CSNI Specialist Meeting on Operating Experience with Steam Generators*, Brussels, Belgium, September 16–20, 1991.
 8. W. J. Mills and C. M. Brown, *Fracture Toughness of Alloy 82H Welds*, Bettis Atomic Power Laboratory, Report B-T-3501, April 2003.
 9. S. Le Hong, J. M. Boursier, C. Amzallag, and J. Daret, "Measurements of Stress Corrosion Cracking Growth Rates in Weld Alloy 182 in Primary Water of PWR," *Proceedings of 10th International Conference on Environmental Degradation of Materials in Nuclear Power Systems—Water Reactors*, NACE International, 2002.
 10. W. J. Mills and C. M. Brown, "Stress Corrosion Crack Growth Rates for Alloy 82H Welds in High Temperature Water," *Proceedings of 11th International Conference on Environmental Degradation of Materials in Nuclear Power Systems—Water Reactors*, ANS, 2003, pp. 1240–1254.

References

11. J. C. Lippold and A. J. Ramirez, "Elevated Temperature Grain Boundary Embrittlement and Ductility-Dip Cracking of Nickel-Base Weld Metals," *USNRC-ANL Conference on Vessel Penetration Inspection, Cracking, and Repairs*, September 29–October 2, 2003, Gaithersburg, Maryland.
12. D. Buisine, et al., "PWSCC Resistance of Nickel Based Weld Metals with Various Chromium Contents," *Proceedings: 1994 EPRI Workshop on PWSCC of Alloy 600 in PWRs*, EPRI, Palo Alto, CA: 1995. TR-105406, Paper D5.
13. T. Yonezawa, N. Sasaguri, and K. Onimura, "Effects of Metallurgical Factors on Stress Corrosion Cracking of Ni-base Alloys in High Temperature Water," *Proceedings of the 1988 JAIF International Conference on Water Chemistry in Nuclear Power Plants*, 1988, pp. 490–495.
14. "Primary Water Stress Corrosion Cracking," Chapter 7 in *Steam Generator Reference Book, Revision 1*, EPRI, Palo Alto, CA: 1994. TR-103824.
15. S. M. Bruemmer, and C. H. Henager, Jr., "Microstructure, Microchemistry and Microdeformation of Alloy 600 Tubing," *Proceedings of 2nd International Conference on Environmental Degradation of Materials in Nuclear Systems—Water Reactors*, ANS International, 1985, pp. 293–300.
16. C. Amzallag, J.-M. Boursier, C. Pagès, and C. Gimond, "Stress Corrosion Life Assessment of 182 and 82 Welds Used in PWR Components," *Proceedings of 10th International Conference on Environmental Degradation of Materials in Nuclear Power Systems—Water Reactors*, NACE International, 2002.
17. F. Cattant, D. Garriga-Majo, F. de Keroulas, P. Todeschini, and J. Van Duysen, "Effectiveness of 700°C Thermal Treatment on Primary Water Stress Corrosion Sensitivity of Alloy 600 Steam Generator Tubes: Laboratory Tests and Field Experience," *Proceedings of 5th International Symposium on Environmental Degradation of Materials in Nuclear Power Systems—Water Reactors*, ANS, 1991, pp. 901–913.
18. C. Amzallag, S. Le Hong, C. Pagès, and A. Gelpi, "Stress Corrosion Life Assessment of Alloy 600 PWR Components," *Proceedings of 9th International Symposium on Environmental Degradation of Materials in Nuclear Systems—Water Reactors*, The Minerals, Metals & Materials Society, Warrendale, PA, 1999, pp. 243–250.
19. C. Amzallag, S. Le Hong, C. Benhamou, and A. Gelpi, "Methodology Used to Rank the Stress Corrosion Susceptibility of Alloy PWR Components," *Proceedings: 2000 EPRI Workshop on PWSCC of Alloy 600 in PWRs (PWRMRP-27)*, EPRI, Palo Alto, CA: 2000. 1000873, Paper E1.
20. T. Cassagne, D. Caron, J. Daret, and Y. Lefèvre, "Stress Corrosion Crack Growth Rate Measurements in Alloys 600 and 182 in Primary Water Loops under Constant Load," *Proceedings of 9th International Symposium on Environmental Degradation of Materials in Nuclear Systems—Water Reactors*, The Minerals, Metals & Materials Society, Warrendale, PA, 1999, pp. 217–224.
21. J. P. Foster, W. H. Bamford, and R. S. Pathania, "Effect of Materials Variables on Alloy 600 Crack Growth Rates," *Proceedings of 8th International Symposium on Environmental Degradation of Materials in Nuclear Power Systems—Water Reactors*, ANS, 1997, pp. 340–348.

22. G. S. Was, "Grain-Boundary Chemistry and Intergranular Fracture in Austenitic Nickel-base Alloys—A Review," *Corrosion*, Vol. 46, No. 4, 1990, pp. 319–330.
23. S. Kou, "Solidification and Liquation Cracking Issues in Welding," *Journal of Metals*, June 2003, p. 37.
24. L. Li and R. W. Messler, Jr., "Segregation of Phosphorus and Sulfur in Heat-Affected Zone Hot Cracking of Type 308 Stainless Steel," *Welding Journal*, Vol. 81, No. 5, 2002, p. 78.
25. R. Magdowski, F. Vaillant, C. Amzallag, and M. O. Speidel, "Stress Corrosion Crack Growth Rates of Alloy 600 in Simulated PWR Coolant," *Proceedings of 8th International Symposium on Environmental Degradation of Materials in Nuclear Power Systems—Water Reactors*, ANS, 1997, pp. 333–339.
26. P. L. Andresen, "Similarity of Cold Work and Radiation Hardening in Enhancing Yield Strength and SCC Growth of Stainless Steel in Hot Water," *Corrosion 2002*, NACE International, 2002, Paper 02509.
27. L. E. Thomas, J. S. Vetrano, S. M. Bruemmer, P. Efsing, B. Forssgren, G. Embring, and K. Gott, "High-Resolution Analytical Electron Microscopy Characterization of Environmentally Assisted Cracks in Alloy 182 Weldments," *Proceedings of 11th International Conference on Environmental Degradation of Materials in Nuclear Power Systems—Water Reactors*, ANS, 2003, pp. 1212–1225.
28. K. Tsutsumi, H. Kanasaki, K. Yoshimoto, Y. Nomura, S. Asada, and T. Yonezawa, "SCC Growth Rate of Nickel Based Alloy 132 Weld Metal in PWR Primary Water," *Proceedings of 11th International Conference on Environmental Degradation of Materials in Nuclear Power Systems—Water Reactors*, ANS, 2003, pp. 1255–1265.
29. *Analysis of Stress Corrosion Cracks in Alloy 182 Weld Metal After Exposure to PWR Primary Water (MRP-107)*, EPRI, Palo Alto, CA: 2004. 1009399.
30. "Standard Specification for Nickel-Chromium-Iron Alloys (UNS N06600, N06601, N06603, N06690, N06025, and N06045) and Nickel-Chromium-Cobalt-Molybdenum Alloy (UNS N06617) Rod, Bar and Wire," ASME/ASTM SB/B 166.
31. "Specification for Nickel and Nickel-Alloy Welding Electrodes for Shielded Metal Arc Welding," ASME SFA-5.11 and AWS A5.11/5.11M-97.
32. "Specification for Nickel and Nickel Alloy Bare Welding Electrodes and Rods," ASME SFA-5.14 and AWS A5.14/A5.14M-97.
33. R. Lindström, P. Lidar, and J. Lagerström, "Crack Growth of Alloy 182 in a Simulated Primary Side PWR Environment," *Proceedings of 8th International Symposium on Environmental Degradation of Materials in Nuclear Power Systems—Water Reactors*, ANS, 1997, pp. 422–429.
34. Private communication from A. Jenssen (Studsvik Nuclear AB) to G. White (Dominion Engineering, Inc.), October 3, 2001.
35. Private communication from A. Jenssen (Studsvik Nuclear AB) to G. White (Dominion Engineering, Inc.), March 11, 2004.
36. Private communication from R. Jacko (Westinghouse) to G. White (Dominion Engineering, Inc.), March 9, 2004.

References

37. S. A. Attanasio, J. V. Mullen, J. W. Wuthrich, W. W. Wilkening, and D. S. Morton, "Stress Corrosion Crack Growth Rates (SCCGRs) for Alloy 182 and 82 Welds," *USNRC-ANL Conference on Vessel Penetration Inspection, Cracking, and Repairs*, September 29–October 2, 2003, Gaithersburg, Maryland.
38. Private Communication from T. Yonezawa to G. White, June 17, 2004.
39. T. R. Gurney, "The Effect of Residual Stresses," Chapter 10 in *Fatigue of Welded Structures, Second Edition*, Cambridge University Press, New York, 1979.
40. A. P. L. Turner, J. E. Broussard, and E. S. Hunt, "Analytical Prediction of Residual Stresses in BWR Shroud Support Structure Welds," Appendix D in *BWR Vessel and Internals Project: Evaluation of Crack Growth in BWR Nickel Base Austenitic Alloys in RPV Internals (BWRVIP-59)*, EPRI, Palo Alto, CA: 1998. TR-108710.
41. C. L. Briant and E. L. Hall, "The Microstructural Causes of Intergranular Corrosion of Alloys 82 and 182," *Corrosion*, Vol. 43, September 1987, pp. 539–548.
42. J. O. Nilsson, et al., "The Effect of Heat Treatment on Toughness in Nickel-Based Weld Metal in the 600°–900°C Temperature Range," *Welding Journal*, January 1994, pp. 45–49.
43. J. C. Lippold, W. A. T. Clark, and M. Tumuluru, "An Investigation of Weld Metal Interfaces," *The Metal Science of Joining*, edited by M. J. Cieslak, J. H. Perepezko, and M. E. Glicksman, TMS, 1992, pp. 141–145.
44. P. M. Scott and P. Combrade, "On the Mechanism of Stress Corrosion Crack Initiation and Growth in Alloy 600 Exposed to PWR Primary Water," *Proceedings of 11th International Conference on Environmental Degradation of Materials in Nuclear Power Systems—Water Reactors*, ANS, 2003, pp. 29–38.
45. *Materials Reliability Program: South Texas Project Unit 1 Bottom Mounted Instrumentation Nozzles (#1 and #46) Analysis Reports and Related Documentation (MRP-102)*, EPRI, Palo Alto, CA: 2003. 1009309.
46. S. Thomas, "Bottom Mounted Instrument Penetration—Condition Resolution," *USNRC-ANL Conference on Vessel Penetration Inspection, Cracking, and Repairs*, September 29–October 2, 2003, Gaithersburg, Maryland.
47. S. Thomas, "PWSCC of Bottom Mounted Instrument Nozzles at South Texas Project," *Proceedings of Twelfth International Conference on Nuclear Engineering*, ASME International, April 25–29, 2004, Arlington, Virginia.
48. *Stress Corrosion Cracking of Alloys 600 and 182 in BWRs*, EPRI, Palo Alto, CA: 1995. TR-104972.
49. *Stress Corrosion Cracking Initiation in BWRs in the Nickel-Base Alloys 600 and 690, and their Weld Alloys 182, 82 and 72 (BWRVIP-110)*, EPRI, Palo Alto, CA: 2003. 1007535.
50. W. H. Bamford, J. P. Foster, and R. S. Pathania, "An Investigation of Alloy 182 Stress Corrosion Cracking in Simulated PWR Environment," *Proceedings of 9th International Symposium on Environmental Degradation of Materials in Nuclear Systems—Water Reactors*, The Minerals, Metals & Materials Society, Warrendale, PA, 1999, pp. 279–296.
51. J. Foster, W. Bamford, and R. Pathania, "Alloy 182 SCC Crack Growth Rates in a Simulated PWR Environment," *Proceedings: 2000 EPRI Workshop on PWSCC of Alloy 600 in PWRs (PWRMRP-27)*, EPRI, Palo Alto, CA: 2000. 1000873, Paper D7.

52. R. J. Jacko, R. E. Gold, G. V. Rao, K. Koyama, and A. Kroes, "Results of Accelerated SCC Testing of Alloy 82, Alloy 182 and Alloy 52M Weld Metals," *USNRC-ANL Conference on Vessel Penetration Inspection, Cracking, and Repairs*, September 29–October 2, 2003, Gaithersburg, Maryland.
53. R. Jacko, (Westinghouse Electric Company), e-mail transmittal to Glenn White (Dominion Engineering, Inc.), July 14, 2004 (stamped 3:06 PM EDT)
54. Private communication from A. Jenssen (Studsvik Nuclear AB) to G. White (Dominion Engineering, Inc.), September 10, 2003.
55. Private communication from A. Jenssen (Studsvik Nuclear AB) to G. White (Dominion Engineering, Inc.), March 28, 2003.
56. Private communication from A. Jenssen (Studsvik Nuclear AB) to G. White (Dominion Engineering, Inc.), August 14, 2003 and August 6, 2004.
57. C. M. Brown and W. J. Mills, "Effect of Water on Mechanical Properties and Stress Corrosion Behavior of Alloy 600, Alloy 690, EN82H Welds, and EN52 Welds," *Corrosion*, Vol. 55, No. 2, 1999, pp. 173–186.
58. Private communication from W. J. Mills (Bettis Atomic Power Laboratory) to G. White (Dominion Engineering, Inc.), September 11, 2003.
59. Private communication from S. A. Attanasio (Lockheed Martin) to G. White (Dominion Engineering, Inc.), September 25, 2003.
60. Private communication from T. Yonezawa (Mitsubishi Heavy Industries) to J. Hickling (EPRI), August 2003.
61. F. Vaillant, P. Moulart, J. M. Boursier, C. Amzallag, and J. Daret, "Crack Growth Rates in Thick Materials of Alloy 600 and Weld Metals of Alloy 182 in Laboratory Primary Water: Comparison with Field Experience," *Fontevraud 5 International Symposium: Contribution of Materials Investigation to the Resolution of Problems Encountered in Pressurized Water Reactors*, SFEN, France, September 23–27, 2002, pp. 107–116.
62. S. Le Hong, *Stress Corrosion Crack Growth Rates Measurements on Alloy 182 in Primary Water of PWR—Final Report*, EDF, June 2000. HT-44/00/027/A.
63. "Standard Test Method for Constant Load Amplitude Fatigue Crack Growth Rates," E647-95a, *1997 Annual Book of ASTM Standards, Volume 03.01*, ASTM, 1997.
64. Material Reliability Program: Alloy 82/182 Pipe Butt Weld Safety Assessment for US PWR Plant Designs (MRP-113), EPRI, Palo Alto, CA: 2004. 1009549.
65. G. Moffat, W. H. Bamford, D. Seeger, K. R. Hsu, and D. C. Bhomick, "Development of the Technical Basis for Plant Startup for the V. C. Summer Nuclear Plant," *Proceedings of ASME 2001 Pressure Vessels and Piping Conference*, Atlanta, GA, 2001.
66. R. J. Jacko, et al., *Evaluation of the Impact of High pH on Primary System Materials Corrosion*, Westinghouse, March 2004. WCAP-16247-NP (Class 3).
67. P. Efsing and J. Lagerström, "Analysis of a Defected Dissimilar Metal Weld in a PWR Power Plant," *Proceedings of 10th International Conference on Nuclear Engineering (ICONE-10)*, ASME International, Arlington, VA, April 14–18, 2002.

References

68. A. Jenssen, K. Norrgård, C. Jansson, J. Lagerström, G. Embring, and P. Efsing, "Structural Assessment of Defected Nozzle to Safe-End Welds in Ringhals 3 and 4," *Fontevraud V International Symposium on Contribution of Materials Investigation to the Resolution of Problems Encountered in Pressurized Water Reactors*, SFEN, 2002, pp. 43–54.
69. Private communication from P. Efsing (Ringhals) to G. White (Dominion Engineering, Inc.), January 23, 2004.
70. A. Jenssen, K. Norrgård, J. Lagerström, G. Embring, and D. R. Tice, "Assessment of Cracking in Dissimilar Metal Welds," *Proceedings of 10th International Conference on Environmental Degradation of Materials in Nuclear Power Systems—Water Reactors*, NACE International, 2002.
71. P. Efsing and C. Jansson, "Screening of Crack Growth Data and the Relevance from an End-Users Perspective," *Proceedings of 11th International Conference on Environmental Degradation of Materials in Nuclear Power Systems—Water Reactors*, ANS, 2003, pp. 180–188.
72. Appendix A-3320, *ASME Boiler & Pressure Vessel Code, Section XI*, July 2003 Addenda.
73. *Materials Reliability Program: Welding Residual and Operating Stresses in PWR Plant Alloy 182 Butt Welds (MRP-106)*, EPRI, Palo Alto, CA: 2004. 1009378.
74. T. L. Anderson, *Fracture Mechanics: Fundamentals and Applications*, Second Edition, CRC Press, 1995, p. 632.
75. I. S. Raju and J. C. Newman, "Stress Intensity Factor Influence Coefficients for Internal and External Surface Cracks in Cylindrical Vessels," *Aspects of Fracture Mechanics in Pressure Vessels and Piping*, ASME PVP Vol. 58, 1982, pp. 37–48.
76. A. Zahoor, "Section 1.5, Internal Flaw, Arbitrary Stress Distribution, $1 \leq R/t \leq 10$," in Chapter 8, "Finite Length, Axial Part-Throughwall Flaw," in Volume 3 of *Ductile Fracture Handbook*, EPRI, Palo Alto, CA: 1989. NP-6301-D.
77. Section XI Task Group for Piping Flaw Evaluation, ASME Code, "Evaluation of Flaws in Austenitic Steel Piping," *Transactions of the ASME, Journal of Pressure Vessel Technology*, Vol. 108, August 1986, pp. 352–366.
78. *Materials Reliability Program: Alloy 82/182 Pipe Butt Weld Safety Evaluation for US PWR Plant Designs: Westinghouse and CE Plant Designs (MRP-109)*, EPRI, Palo Alto, CA: 2004. 1003203.
79. *Materials Reliability Program (MRP): Alloy 82/182 Pipe Butt Weld Safety Assessment for US PWR Plant Designs: Babcock & Wilcox Design Plants (MRP-112)*, EPRI, Palo Alto, CA: 2004. 1009805.
80. Case N-694, "Evaluation Procedure and Acceptance Criteria for PWR Reactor Vessel Upper Head Penetration Nozzles, Section XI, Division 1," *Cases of ASME Boiler and Pressure Vessel Code*, Approved June 17, 2003.
81. W. J. Mills, C. M. Brown, and M. G. Burke, "Effect of Microstructure on Low Temperature Cracking Behavior of EN82H Welds," *Proceedings of 10th International Conference on Environmental Degradation of Materials in Nuclear Power Systems—Water Reactors*, NACE International, 2002.

82. *Materials Reliability Program (MRP): Resistance to Primary Water Stress Corrosion Cracking of Alloys 690, 52, and 152 in Pressurized Water Reactors (MRP-111)*, EPRI, Palo Alto, CA: 2004. 1009801.
83. G. J. Theus, "Stress Corrosion Cracking Tests of Alloy 600," *Workshop Proceedings: U-Bend Tube Cracking in Steam Generators*, EPRI, Palo Alto, CA: 1981. WS-80-136, Paper 15.
84. S. M. Bruemmer, et al., "Microstructure and Microdeformation Effects on IGSCC of Alloy 600 Steam Generator Tubing," *Corrosion*, Vol. 44, No. 11, November 1988, pp. 782-788.
85. W. F. Savage, E. F. Nippes, and G. M. Goodwin, "Effect of Minor Elements on Hot-Cracking Tendencies of Inconel 600," *Welding Journal*, Vol. 56, No. 4, 1977, p. 245.
86. T. Yonezawa and K. Onimura, "Effect of Chemical Compositions and Microstructure on the Stress Corrosion Cracking Resistance of Nickel Base Alloys in High Temperature Water," *Proceedings of EVALMAT 89*, Vol. 1, 1989, p. 235.
87. R. Thamburaj, et al., "Post-Weld Heat-Treatment Cracking in Superalloys," *International Metals Reviews*, Vol. 28, 1983, p. 1.
88. M. H. Haafkens and J. H. G. Matthey, "A New Approach to the Weldability of Nickel-base as Cast and Power Metallurgy Superalloys," *Welding Journal*, Vol. 61, No. 11, 1982, p. 25.
89. T. E. Kihlgren and C. E. Lacy, "The Control of Weld Hot Cracking in Nickel-Chromium-Iron Alloys," *Welding Journal*, Vol. 25, No. 11, 1946, p. 770.
90. M. Adachi and R. Miki, "A Study of Weld Cracking in Nickel and Nickel Alloys (Report 2)," *Journal of the Japan Welding Society*, Vol. 44, No. 12, 1975, p. 31.
91. J. N. Dupont, S. W. Banovic, and A. R. Marder, "Microstructural Evaluation and Weldability of Dissimilar Welds Between a Super Austenitic Stainless Steel and Nickel-Based Alloy," *Welding Journal*, Vol. 82, No. 6, 2003, p. 125.
92. L. Li and R. W. Messler, Jr., "The Effects of Phosphorus and Sulfur on Susceptibility to Weld Hot Cracking in Austenitic Stainless Steels," *Welding Journal*, Vol. 78, No. 12, 1999, p. 387.
93. X. Luo, K. Shinozaki, S. Yoshihara, H. Kuroki, and M. Shirai, "Theoretical Analysis of Grain Boundary Liquation at HAZ of Inconel 718 Alloy," *Quarterly Journal of the Japan Welding Society*, Vol. 18, No. 1, 2000, p. 102.
94. F. N. Rhines and P. J. Wray, "Investigation of the Intermediate Temperature Ductility Minimum in Metals," *Transactions of the ASM*, Vol. 54, 1961, pp. 117-128.
95. J. M. Kikel and D. M. Parker, "Ductility Dip Cracking Susceptibility of Filler Metal 52 and Alloy 690," *Trends in Welding Research: Proceedings of the 5th International Conference*, Pine Mountain, Georgia, June 1-5, 1988.
96. Y. Nakao, K. Shinozaki, T. Ogawa, and H. Sakurai, "Effects of Cr and S on Ductility-Dip Cracking Susceptibility in Reheated Weld Metals of Ni-Cr-Fe Ternary Alloys," *Quarterly Journal of the Japan Welding Society*, Vol. 11, No. 1, 1993, p. 108.
97. L. Li and R. W. Messler, Jr., "Stress Relaxation Study of HAZ Reheat Cracking in Type 347 Stainless Steel," *Welding Journal*, Vol. 79, No. 6, 2000, p. 137.

References

98. P. L. Andresen, "K / Size Effects on SCC in Irradiated, Cold Worked and Unirradiated Stainless Steel," *Proceedings of 11th International Conference on Environmental Degradation of Materials in Nuclear Power Systems—Water Reactors*, ANS, 2003, pp. 870–886.
99. "Standard Test for Plane-Strain Fracture Toughness of Metallic Materials," E399-90, *1997 Annual Book of ASTM Standards, Volume 03.01*, ASTM, 1997.
100. "Standard Test Method for Determining a Threshold Stress Intensity Factor for Environment-Assisted Cracking of Metallic Materials Under Constant Load," E1681-95, *1997 Annual Book of ASTM Standards, Volume 03.01*, ASTM, 1997.
101. "Critical Assessment of the Standard ASTM E 399," *Fatigue and Fracture Mechanics*, Vol. 34, ASTM, ASTM-STP 1461, 2004.
102. *Use of Pourbaix Diagrams to Infer Local Pitting Conditions*, EPRI, Palo Alto, CA: 1986. NP-4831.
103. B. Beverskog and I. Puigdomenech, "Pourbaix Diagrams for the Ternary System of Iron-Chromium-Nickel," *Corrosion*, Vol. 55, No. 11, November 1999, pp. 1077–1087.
104. J. Alvarez, R. Crovetto, and R. Fernandez-Prini, "The Dissolution of N₂ and H₂ in Water from Room Temperature to 640 K," *Ber. Bunsenges. Phys. Chem.*, Vol. 92, 1988, pp. 935–940.
105. S. Attanasio, D. Morton, and M. Ando, "Measurement and Calculation of Electrode Potential in Hydrogenated High Temperature Water, Including an Evaluation of the Yttria-stabilized ZrO₂/Fe/Fe₃O₄ as a Reference Electrode," *Corrosion 2002*, NACE International, 2002, Paper 02517.
106. S. A. Attanasio and D. S. Morton, "Measurement of the Nickel/Nickel Oxide Transition in Ni-Cr-Fe Alloys and Updated Data and Correlations to Quantify the Effect of Aqueous Hydrogen on Primary Water SCC," *Proceedings of 11th International Conference on Environmental Degradation of Materials in Nuclear Power Systems—Water Reactors*, ANS, 2003, pp. 143–155.
107. S. A. Attanasio, D. S. Morton, M. A. Ando, N. F. Panayotou, and C. D. Thompson, "Measurement of the Nickel/Nickel Oxide Phase Transition in High Temperature Hydrogenated Water Using the Contact Electric Resistance (CER) Technique," *Proceedings of 10th International Conference on Environmental Degradation of Materials in Nuclear Power Systems—Water Reactors*, NACE International, 2002.
108. D. S. Morton, S. A. Attanasio, and G. A. Young, "Primary Water SCC Understanding and Characterization Through Fundamental Testing in the Vicinity of the Nickel/Nickel Oxide Phase Transition," *Proceedings of 10th International Conference on Environmental Degradation of Materials in Nuclear Power Systems—Water Reactors*, NACE International, 2002.
109. G. A. Young, N. Lewis, and D. S. Morton, "The Stress Corrosion Crack Growth Rate of Alloy 600 Heat Affected Zones Exposed to High Purity Water," *USNRC-ANL Conference on Vessel Penetration Inspection, Cracking, and Repairs*, September 29–October 2, 2003, Gaithersburg, Maryland.

110. T. M. Angeliu, P. L. Andresen, E. Hall, J. A. Sutliff, S. Sitzman, and R. M. Horn, "Intergranular Stress Corrosion Cracking of Unsensitized Stainless Steels in BWR Environments," *Proceedings of 9th International Symposium on Environmental Degradation of Materials in Nuclear Systems—Water Reactors*, The Minerals, Metals & Materials Society, Warrendale, PA, 1999, pp. 311–318.
111. T. M. Angeliu, P. L. Andresen, E. Hall, J. A. Sutliff, and S. Sitzman, "Strain and Microstructure Characterization of Austenitic Stainless Steel Weld HAZs," *Corrosion 2000*, NACE International, 2000, Paper 00186.
112. P. L. Andresen, T. M. Angeliu, L. M. Young, W. R. Catlin, and R. M. Horn, "Mechanisms and Kinetics of SCC in Stainless Steels," *Proceedings of 10th International Conference on Environmental Degradation of Materials in Nuclear Power Systems—Water Reactors*, NACE International, 2002.
113. P. L. Andresen, P. W. Emigh, M. M. Morra, and R. M. Horn, "Effects of Yield Strength, Corrosion Potential, Stress Intensity Factor, Silicon and Grain Boundary Character on the SCC of Stainless Steels," *Corrosion 2004*, NACE International, 2004, Paper 72293.
114. "Corrosion of Metals and Alloys—Stress Corrosion Testing—Part 6: Preparation and Use of Pre-Cracked Specimens for Tests Under Constant Load or Constant Displacement," ISO 7539-6, 2nd Edition, 2003.
115. P. L. Andresen, T. M. Angeliu, and L. M. Young, "Immunity, Thresholds, and Other SCC Fiction," *Proceedings Staehle Symposium on Chemistry and Electrochemistry of Corrosion and SCC*, TMS, 2001.
116. P. L. Andresen, et al., "Effects of Yield Strength, Corrosion Potential, Stress Intensity Factor, Silicon and Grain Boundary Character on the SCC of Stainless Steels," *Proceedings of 11th International Conference on Environmental Degradation of Materials in Nuclear Power Systems—Water Reactors*, ANS, 2003, pp. 816–833.
117. P. L. Andresen, L. M. Young, and G. M. Gordon, "SCC Growth Rate Response of Alloy 22 (UNS N06022) in Concentrated Groundwater," *Proceedings of 11th International Conference on Environmental Degradation of Materials in Nuclear Power Systems—Water Reactors*, ANS, 2003, pp. 280–298.
118. R. N. Parkins, "Strain Rate Effects in Stress Corrosion Cracking," *Corrosion*, Vol. 46, No. 3, March 1990, p. 178.
119. P. M. Scott, "Prediction of Alloy 600 Component Failures in PWR Systems," *Proceedings of Corrosion'96 Research Topical Symposia, Part 1—Life Prediction of Structures Subject to Environmental Degradation*, Denver, CO, NACE, 1996, p. 135.
120. W. Bamford and G. DeBoo, "Background and Technical Basis for the Evaluation of Flaws in PWR Reactor Vessel Upper Head Penetration Regions," ASME PVP Conference, July 2004.
121. J. P. Foster et al., "Effects of Loading on Alloy 600 Crack Growth Rate Behavior," *Proceedings of 10th International Conference on Environmental Degradation of Materials in Nuclear Power Systems—Water Reactors*, NACE International, 2002.
122. S. Le Hong, F. Vaillant, and C. Amzallag, "Synthesis and Comparison of Crack Growth Rate Measurements on Tubes and Plates in Alloy 600 in High Temperature

References

- Hydrogenated Primary Water,” *Euromat 2000 Conference on Advances in Mechanical Behavior, Plasticity, and Damage*, Tours, France, November 7–9, 2000.
123. C. Amzallag and F. Vaillant, “Stress Corrosion Crack Propagation Rates in Reactor Vessel Head Penetrations in Alloy 600,” *Proceedings of 9th International Symposium on Environmental Degradation of Materials in Nuclear Systems—Water Reactors*, The Minerals, Metals & Materials Society, Warrendale, PA, 1999, pp. 235–241.
124. F. Vaillant et al., “Influence of a Cyclic Loading on Crack Growth Rates of Alloy 600 in Primary Water Environment: An Overview,” *Proceedings of 11th International Conference on Environmental Degradation of Materials in Nuclear Power Systems—Water Reactors*, ANS, 2003, pp. 189–198.
125. W. J. Mills and C. M. Brown, *Stress Corrosion Crack Growth Rates for Alloy 82H Welds*, Bettis Atomic Power Laboratory, Report B-T-3435, February 2002.

A

METALLURGICAL ASPECTS OF NICKEL-BASED WELD MATERIALS AND THEIR EFFECTS ON CRACK GROWTH RATES

Content Deleted – MRP/EPRI Proprietary Material

Content Deleted – MRP/EPRI Proprietary Material

Content Deleted – MRP/EPRI Proprietary Material

Content Deleted – MRP/EPRI Proprietary Material

Content Deleted – MRP/EPRI Proprietary Material

Content Deleted – MRP/EPRI Proprietary Material

Content Deleted – MRP/EPRI Proprietary Material

Content Deleted – MRP/EPRI Proprietary Material

Content Deleted – MRP/EPRI Proprietary Material

Content Deleted – MRP/EPRI Proprietary Material

Content Deleted – MRP/EPRI Proprietary Material

Content Deleted – MRP/EPRI Proprietary Material

Content Deleted – MRP/EPRI Proprietary Material

Content Deleted – MRP/EPRI Proprietary Material

Content Deleted – MRP/EPRI Proprietary Material

Content Deleted – MRP/EPRI Proprietary Material

B

RECOMMENDATIONS REGARDING SPECIMEN LOADING PROCEDURE

Content Deleted – MRP/EPRI Proprietary Material

Recommendations Regarding Specimen Loading Procedure

Content Deleted – MRP/EPRI Proprietary Material

Recommendations Regarding Specimen Loading Procedure

Content Deleted – MRP/EPRI Proprietary Material

Recommendations Regarding Specimen Loading Procedure

Content Deleted – MRP/EPRI Proprietary Material

C

EFFECTS OF DISSOLVED HYDROGEN CONCENTRATION AND TEMPERATURE

Content Deleted – MRP/EPRI Proprietary Material

Content Deleted – MRP/EPRI Proprietary Material

Content Deleted – MRP/EPRI Proprietary Material

Content Deleted – MRP/EPRI Proprietary Material

Content Deleted – MRP/EPRI Proprietary Material

Content Deleted – MRP/EPRI Proprietary Material

Content Deleted – MRP/EPRI Proprietary Material

Content Deleted – MRP/EPRI Proprietary Material

Content Deleted – MRP/EPRI Proprietary Material

Content Deleted – MRP/EPRI Proprietary Material

Content Deleted – MRP/EPRI Proprietary Material

Content Deleted – MRP/EPRI Proprietary Material

Content Deleted – MRP/EPRI Proprietary Material

Content Deleted – MRP/EPRI Proprietary Material

D

DERIVATION OF CRACK GROWTH RATES GIVEN INCOMPLETE ENGAGEMENT TO INTERGRANULAR CRACKING

Content Deleted – MRP/EPRI Proprietary Material

Derivation of Crack Growth Rates Given Incomplete Engagement to Intergranular Cracking

Content Deleted – MRP/EPRI Proprietary Material

Derivation of Crack Growth Rates Given Incomplete Engagement to Intergranular Cracking

Content Deleted – MRP/EPRI Proprietary Material

Content Deleted – MRP/EPRI Proprietary Material

Content Deleted – MRP/EPRI Proprietary Material

Content Deleted – MRP/EPRI Proprietary Material

Content Deleted – MRP/EPRI Proprietary Material

Content Deleted – MRP/EPRI Proprietary Material

Content Deleted – MRP/EPRI Proprietary Material

Content Deleted – MRP/EPRI Proprietary Material

Derivation of Crack Growth Rates Given Incomplete Engagement to Intergranular Cracking

Content Deleted – MRP/EPRI Proprietary Material

Content Deleted – MRP/EPRI Proprietary Material

E

CONCEPT AND SIGNIFICANCE OF A STRESS INTENSITY FACTOR THRESHOLD FOR PWSCC

Content Deleted – MRP/EPRI Proprietary Material

Content Deleted – MRP/EPRI Proprietary Material

Content Deleted – MRP/EPRI Proprietary Material

Content Deleted – MRP/EPRI Proprietary Material

Content Deleted – MRP/EPRI Proprietary Material

F

**LABORATORY ALLOY 82/182 CGR DATA EXCLUDED
IN THE DEVELOPMENT OF MRP CGR DISPOSITION
CURVES**

Content Deleted – MRP/EPRI Proprietary Material

Laboratory Alloy 82/182 CGR Data Excluded in the Development of MRP CGR Disposition Curves

Content Deleted – MRP/EPRI Proprietary Material

Laboratory Alloy 82/182 CGR Data Excluded in the Development of MRP CGR Disposition Curves

Content Deleted – MRP/EPRI Proprietary Material

Laboratory Alloy 82/182 CGR Data Excluded in the Development of MRP CGR Disposition Curves

Content Deleted – MRP/EPRI Proprietary Material

Laboratory Alloy 82/182 CGR Data Excluded in the Development of MRP CGR Disposition Curves

Content Deleted – MRP/EPRI Proprietary Material

Laboratory Alloy 82/182 CGR Data Excluded in the Development of MRP CGR Disposition Curves

Content Deleted – MRP/EPRI Proprietary Material

Laboratory Alloy 82/182 CGR Data Excluded in the Development of MRP CGR Disposition Curves

Content Deleted – MRP/EPRI Proprietary Material

G

**COMPARISON WITH EXCLUDED DATA FOR WHICH
AVERAGE CGRS WERE REPORTED**

Content Deleted – MRP/EPRI Proprietary Material

Comparison With Excluded Data for Which Average CGRs Were Reported

Content Deleted – MRP/EPRI Proprietary Material

Comparison With Excluded Data for Which Average CGRs Were Reported

Content Deleted – MRP/EPRI Proprietary Material

Comparison With Excluded Data for Which Average CGRs Were Reported

Content Deleted – MRP/EPRI Proprietary Material

Comparison With Excluded Data for Which Average CGRs Were Reported

Content Deleted – MRP/EPRI Proprietary Material

H

**COMPARISON WITH EXCLUDED DATA FOR WHICH
ONLY MAXIMUM CGRS WERE REPORTED**

Content Deleted – MRP/EPRI Proprietary Material

Comparison With Excluded Data for Which Only Maximum CGRs Were Reported

Content Deleted – MRP/EPRI Proprietary Material

Comparison With Excluded Data for Which Only Maximum CGRs Were Reported

Content Deleted – MRP/EPRI Proprietary Material

Comparison With Excluded Data for Which Only Maximum CGRs Were Reported

Content Deleted – MRP/EPRI Proprietary Material

Comparison With Excluded Data for Which Only Maximum CGRs Were Reported

Content Deleted – MRP/EPRI Proprietary Material

Comparison With Excluded Data for Which Only Maximum CGRs Were Reported

Content Deleted – MRP/EPRI Proprietary Material

Comparison With Excluded Data for Which Only Maximum CGRs Were Reported

Content Deleted – MRP/EPRI Proprietary Material

Comparison With Excluded Data for Which Only Maximum CGRs Were Reported

Content Deleted – MRP/EPRI Proprietary Material

/ **EVALUATION OF EFFECT OF PERIODIC UNLOADING AND HOLD TIME**

Content Deleted – MRP/EPRI Proprietary Material

Content Deleted – MRP/EPRI Proprietary Material

Content Deleted – MRP/EPRI Proprietary Material

Content Deleted – MRP/EPRI Proprietary Material

Content Deleted – MRP/EPRI Proprietary Material

Content Deleted – MRP/EPRI Proprietary Material